NASA Technical Memorandum 85971

N84-31215

Fuel Conservative Guidance Concept for Shipboard Landing of Powered-Lift Aircraft

David N. Warner, Jr., Leonard A. McGee,
John D. McLean and Gregory K. Schmidt

June 1984

National Aeronautics and
Space Administration

NASA Technical Memorandum 85971

Fuel Conservative Guidance Concept for Shipboard Landing of Powered-Lift Aircraft

David N. Warner, Jr
Leonard A McGee, Ames Research Center, Moffett Field, California
John D. McLean
Gregory K Schmidt, Analytical Mechanics Assoc., Inc., Mountain View, California

NASA
National Aeronautics and
Space Administration

Ames Research Center
Moffett Field. California 94035

SYMBOLS

a	speed of sound at aircraft altitude
a_0	speed of sound at sea level in the standard atmosphere
C_D	drag coefficient
C_L	lift coefficient
C_{RD}	ram drag coefficient
C_T	thrust coefficient
C_{TMAX}	maximum thrust coefficient
C_{TMIN}	minimum thrust coefficient
C_{TT}	maximum thrust coefficient which satisfies the temperature constraint
D	aerodynamic drag
E	aircraft energy
$\dot{E}_n$	normalized energy rate
EPSLN(I)	fraction of available energy rate to be used for speed change in going to the Ith waypoint
$\dot{E}_T$	total energy rate
ETMAX,ETMIN	maximum and minimum values of energy rate to be used
g	gravitational constant
HPBLC	percentage of cold-thrust air bled from the engines to be blown over the leading edge and the ailerons for boundary layer control
HR	course with respect to ship
HSH	ship heading with respect to Earth
h	altitude
$\dot{h}$	altitude rate
I	waypoint number
k_1	input normal acceleration
k_2	input longitudinal acceleration

L	aerodynamic lift
M	Mach number
MGT	measured exhaust gas temperature
m	mass
N_{TMX}	corrected engine fan speed at MGT = 920° C
N_1	engine fan speed
$N_1/\sqrt{\theta_2}$	corrected engine fan speed
N_2	engine core speed
$N_2/\sqrt{\theta_2}$	corrected engine core speed
$\bar{q}$	dynamic pressure
R(I)	turn radius at the Ith waypoint
RAMDRAG	drag from ram air through engine
SGMAX,SGMIN	sines of the maximum and minimum inertial flightpath angle
S_W	wing area
T	total gross thrust
T_{AMB}	ambient absolute temperature
T_G	gross thrust for four engines
T_{GMAX}, T_{GMIN}	maximum and minimum gross thrust
T_0	standard value of T_{AMB} at sea level
t	time
u	change in flightpath angle
V	velocity
V_a	airspeed
$\bar{V}_a$	true airspeed vector
$\dot{V}_a$	rate of change of true airspeed
VDGMAX,VDGMIN	maximum and minimum rate of change of true airspeed
V_{EQ}	equivalent airspeed
VGLS	minimum landing speed with respect to the ship

$\bar{V}_I$	velocity vector with respect to ship-fixed system
$\bar{V}_{IE}$	velocity vector with respect to Earth-fixed system
VLN	loiter speed (speed on the straight segment of the capture path)
VNOM(I),VMAX(I), VMIN(I)	nominal, maximum, and minimum indicated airspeed at the Ith waypoint
$\bar{V}_{SH}$	velocity vector of ship with respect to Earth-fixed system
VSH	ship speed relative to Earth
V_T	true airspeed
$\bar{V}_w$	velocity vector of wind with respect to ship-fixed system
$\bar{V}_{wE}$	velocity vector of wind with respect to earth-fixed system
V_{wat}	along-track component of the wind velocity
V_0	initial velocity
W	weight, mg
X(I),Y(I),Z(I)	cartesian position for the Ith waypoint with respect to the ship
XAC,YAC,ZAC,HAC	cartesian initial position and course of the aircraft with respect to the ship
α	angle of attack
α_w	wing angle of attack
γ	flightpath angle
γ_a	aerodynamic flightpath angle
γ_c	commanded flightpath angle
γ_{IE}	flightpath angle with respect to Earth-fixed system
γ_i	inertial flightpath angle
γ_m	maximum flightpath angle
γ_0	initial flightpath angle
ΔE_h	change in energy from altitude change
ΔE_v	change in energy from velocity change
Δh	altitude change
Δh_D	desired altitude change

ΔT	temperature change
δ_{AMB}	ratio of ambient pressure to the pressure at sea level
δ_F	outboard flaps
δ_{FREF}	sum of outboard and upper-surface-blowing (USB) flaps
δ_{USB}	USB flaps
ε	fraction of available energy rate to be used for speed change
θ_{AMB}	ratio of the ambient absolute temperature to the standard value at sea level
θ_2	temperature correction factor for engine core speed
ρ	actual atmospheric density
ρ_0	sea level density of the standard atmosphere
τ	time constant
σ	fraction of $\dot{E}_n$ to reserve for control
ϕ	bank (roll) angle
$(\dot{\ })$	rate of change of ( )
d( )	differentiation of ( )

Abbreviations:

DME	distance measuring equipment
ECG	energy conservative guidance
HPBLC	High-Pressure Boundary Layer Control
QSRA	Quiet Short-Haul Research Aircraft
TACAN	tactical air navigation aid
USB	upper surface blowing

FUEL CONSERVATIVE GUIDANCE CONCEPT FOR SHIPBOARD LANDING OF POWERED-LIFT AIRCRAFT

David N. Warner, Jr., Leonard A. McGee, John D. McLean,* and Gregory K. Schmidt*

Ames Research Center

SUMMARY

A simulation study was undertaken to investigate the application of Energy Conservative Guidance (ECG) software, developed at NASA Ames Research Center, to improve the time and fuel efficiency of powered-lift airplanes operating from aircraft carriers at sea. The ECG software system consists of a set of algorithms whose coefficients and parameter limits are those of the Quiet Short-Haul Research Aircraft (QSRA). When a flightpath is indicated by a set of initial conditions for the aircraft and a set of positional waypoints with associated airspeeds, the ECG software synthesizes the necessary guidance commands to optimize fuel and time along the specified path. A major feature of the ECG system is the ability to synthesize a trajectory that will allow the aircraft to capture the specified path at any waypoint with the desired heading and airspeed from an arbitrary set of initial conditions. In this study, five paths were identified and studied. The first path closely follows the manual approach procedures specified in the U.S. Navy CV NATOPS MANUAL for prop and turboprop aircraft using tactical air navigation aid (TACAN) as the major area navigation aid. Each of the four remaining paths were established to successively remove the manual restrictions from the path. These paths demonstrate the ECG system's ability to save flight time and fuel by more efficiently managing the aircraft's capabilities.

Results of this simulation study show that when restrictions on the approach flightpath imposed for manual operation are removed completely, fuel consumption during the approach was reduced by as much as 49% (610 lb fuel) and the time required to fly the flightpath was reduced by as much as 41% (5 min). When it is possible to remove only a portion of the operational constraints, somewhat lesser, but still significant, savings in both fuel and time were realized using the ECG synthesis software. Savings due to ECG were produced by (1) shortening the total flight time; (2) keeping the airspeed high as long as possible to minimize time spent flying in a regime in which more engine thrust is required for lift to aid the aerodynamic lift; (3) minimizing time spent flying at constant altitude at slow airspeeds; and (4) synthesizing a path from any location for a direct approach to landing without entering a holding pattern or other fixed approach path.

INTRODUCTION

Aircraft operating from ships at sea must constantly monitor fuel consumption to ensure a safe return to the ship and to accomplish the prescribed mission at the least cost. It has been demonstrated that energy conservation techniques managed by computer-driven displays to the pilot or by completely automatic systems are capable

*Analytical Mechanics Associates, Inc., Mountain View, California.

of substantial fuel and time savings, when operational constraints are minimized and full advantage is taken of the aircraft capabilities. In situations in which only a limited number of the operational constraints can be removed, the savings are also limited, but when summed over a large number of flights, such as in aircraft carrier operations, the fuel savings can still be substantial over a period of time.

Recent studies at NASA Ames Research Center, described in references 1, 2, and 3, have shown the effectiveness of an on-board software system designed to achieve energy conservation. The Energy Conservative Guidance (ECG) software system, which consists of a set of algorithms designed for the NASA Ames Quiet Short-Haul Research Aircraft (QSRA), synthesizes flightpaths composed of capture and reference segments that optimize fuel use along a route described by fixed waypoints. A "command table" is generated and stored in the computer which calculates a schedule of settings of the outboard flaps, the upper-surface-blown (USB) flaps, and throttle at each waypoint and at selected intermediate points. This information could be displayed to the pilot for manual actions at appropriate times or could be used by a fully automatic guidance system, thereby allowing the approach to be flown by the on-board computer system. The time to fly the synthesized flightpath is determined during the synthesis procedure and may be used for orderly and fuel-efficient control of traffic by the air controllers on the carrier.

This paper presents a simulation study of the QSRA aircraft making energy-conservative landings on an aircraft carrier deck. The feasibility of landing the QSRA on the carrier USS Kitty Hawk has been demonstrated (ref. 4). The carrier is under way at a constant speed and direction while heading its canted deck into the wind. The fuel and time used by the aircraft are computed for five different approaches, each of which is defined by a set of waypoints. In the first two approaches, the aircraft enters a standard traffic pattern, which is translating along with the ship. This pattern is described by a set of waypoints in the computer aboard the aircraft and by the initial conditions of the aircraft at the time the flightpath synthesis begins. From these initial conditions and fixed waypoints, the computer's ECG software synthesizes a reference flightpath. This flightpath consists of a capture path from the aircraft's current position and heading to a fixed path defined by the given waypoints. Time histories of various parameters are generated as are the elapsed time and the distance flown. The second flightpath was the same as the first except that the speed profile following the turn which aligns the aircraft with the centerline of the canted deck is flown at a higher speed. In the third flightpath, only two waypoints which describe the final straight-in portion of the approach are specified. The first is at 3 distance-measuring equipment (DME) n. mi., and the second is at touchdown. The fourth flightpath is the same as third except that the first waypoint is at 1 DME n. mi. The fifth flightpath differed from the fourth in that the aircraft's initial X-position is the negative of the previous initial X-positions, the heading was -90°, and the first waypoint was at 0.5 DME n. mi. from touchdown. Thus, each successive flightpath allowed the ECG software in the aircraft computer to have greater freedom to utilize the aircraft's aerodynamic capabilities by specifying flightpaths with successively longer capture paths and shorter fixed paths in order to synthesize reference paths offering improved fuel conservation as well as shorter flight times.

Navigation information is assumed to be initially supplied by a tactical air navigation air (TACAN) system aboard the aircraft carrier. This information would be used throughout the approach until visual contact with the landing deck is made by the pilot, whereupon the pilot would manually make the landing on the deck.

This study compares the fuel used and time required for a landing on the carrier for each of the five approach paths. Comparison of results will demonstrate that ECG software in an on-board computer can be effective in saving fuel in an aircraft carrier operational environment and that fuel savings increase substantially as operational restrictions are removed from the flightpath.

ENERGY CONSERVATIVE GUIDANCE SYSTEM

The ECG system is briefly described here. A detailed description is given in appendices A, B, and C. The purpose of the ECG software is to synthesize a flyable reference path from the aircraft's current position and course to a desired final position and course. The synthesized horizontal path consists of a fixed path specified by a set of input waypoints and a capture path from the aircraft's current position and course to the position and course at the capture waypoint on the fixed path. The capture path consists nominally of an initial turn, a straight segment, and a final turn. In special cases, one or both turns may become a straight line. In this study, the waypoints specifying the reference path are defined relative to a moving-ship-centered coordinate system.

In an operational situation, input data would be supplied by the pilot, or the on-board navigation system, or both. Furthermore, the pilot would have the option at any time to change the input variables and request the ECG system to synthesize a new reference path which would meet modified operational criteria. The pertinent input data used to specify the path's, the aircraft's, and the ship's initial conditions are described as follows:

X(I),Y(I),Z(I)	cartesian position for the Ith waypoint with respect to the ship
R(I)	turn radius at the Ith waypoint
VNOM(I),VMAX(I),VMIN(I)	nominal, maximum, and minimum indicated airspeed at the Ith waypoint
EPSLN(I)	ε_i, fraction of available energy rate to be used for speed change in going to the Ith waypoint (discussed in appendix A)
SGMAX,SGMIN	sines of the maximum and minimum inertial flightpath angle
VDGMAX,VDGMIN	maximum and minimum true airspeed rates
ETMAX,ETMIN	maximum and minimum values of energy rate to be used
VGLS	minimum landing speed with respect to the ship
VLN	loiter speed (speed on the straight segment of the capture path)
XAC,YAC,ZAC,HAC	cartesian initial positions and course of the aircraft with respect to ship

VSH ship speed relative to Earth

HSH ship heading relative to Earth

Indicated airspeed is specified at each fixed-path waypoint. The speed-altitude profile along the synthesized horizontal path is obtained as follows: First, the equations of motion are integrated at constant altitude forward along the first capture turn as indicated in figure 1. The speed changes at the specified maximum rate until (1) the loiter speed is achieved at A1 or (2) the turn is completed. In case (1), the distance (A1 - B) is stored and integration is continued to the end of the turn at B. In case (2), the integration continues until the loiter speed is achieved at A2 and the distance (A2 - D) is stored.

Next, integration proceeds backward along the fixed path from the final waypoint to the capture waypoint with airspeed rate and flightpath angle specified, as discussed later. If the speed and/or altitude specified for the next waypoint in the backward direction is reached before the waypoint, the distance traversed is stored and the speed and/or altitude change stops. If the waypoint is reached without achieving the waypoint speed and/or altitude, the speed and altitude actually achieved are stored and the target values are changed to those of the next waypoint in the backward direction. When the capture waypoint is reached, the target speed is set to the loiter speed and the target altitude is set to the aircraft altitude. When the backward integration reaches the end point of the forward integration (points A2 or A1), the speeds and altitudes achieved at those points by the two integrations are compared. If they are equal, the synthesis was successful. If not, capture is not feasible along the horizontal path and a "no capture" message is indicated on the pilot's display.

Assuming a successful synthesis, a command table is generated which contains the following information for each state-change location:

1. Mode flag (1 for speed and altitude changing, 2 for only speed changing, 3 for altitude only changing, 4 for a constant-speed turn, 5 for straight, constant-speed flight, and 0 for no change)

2. Index number of the next waypoint, assuming motion toward the final waypoint

3. Correction factor used for reducing integration errors

4. Time to go to the final waypoint

5. Distance to go to the final waypoint

6. Flightpath angle

7. Rate of change of airspeed

8. Flap positions

9. Bank angle

10. Altitude

11. Indicated airspeed

12. Lead distance for roll (compensates for finite roll rate)

13. Lead distance for flightpath angle (compensates for finite flightpath angle rate)

The information is used to initialize integration in real time forward along the next segment. Flight tests with NASA's Augmentor Wing powered-lift airplane using a similar strategy for the command table have shown that the aircraft can fly the trajectory defined by this table, reference 1. Modifications required to synthesize paths relative to a moving ship are described in appendix C.

The construction of the command table is performed with the help of the energy rate defined as the sum of aerodynamic flightpath angle and rate of change of true airspeed, $\dot{E}_n = \gamma_a + \dot{V}_a/g$. A detailed explanation of the technique is given in appendix A. The maximum and minimum energy rate at any flight condition characterizes the ability of the aircraft to change speed and altitude. Thus the algebraic sum of commanded values of γ_a and $\dot{V}_a/g$ must always be less than the maximum and greater than the minimum allowable energy rate.

If a change in altitude or speed is called for, the system will attempt to make the change at the maximum values of $\sin \gamma_a$ (which is found by converting SGMAX or SGMIN from inertial to aerodynamic angle) or $\dot{V}_a/g$. If the aircraft is only capable of an energy rate, $\dot{E}_n$, which is less than the desired value, the available $\dot{E}_n$ is allocated according to

$$\dot{V}_a/g = \varepsilon \dot{E}_n$$

$$\sin \gamma_a = (1 - \varepsilon)\dot{E}_n$$

For simplicity, only three values of ε are used, 0, 1, and 0.5. If $\varepsilon = 1$ or 0, priority is assigned to $(\dot{V}_a/g)$ or $\sin \gamma_a$, respectively. If $|\dot{E}_n|$ exceeds the maximum magnitude of the priority quantity, the remainder is assigned to the other. (For example, if $\varepsilon = 1$, $|\dot{V}_a/g| < 0.05$, and $\dot{E}_n = 0.07$, then $\sin \gamma_a = 0.02$.) If $\varepsilon = 0.5$, the ratios of $\dot{V}_a/g$ and $\sin \gamma_a$ to $\dot{E}_n$ are maintained the same as those of the desired values.

While the system will work with arbitrarily large magnitudes of desired $\sin \gamma_a$ and $\dot{V}_a/g$, it is more efficient to set the operational limits to correspond as closely as practical to the aircraft's capability. As the computer program is presently implemented, small anomalies in the altitude profile or arbitrary steps in γ_a may occur at onset or at the end of a speed change where the desired $|\dot{E}_n|$ exceeds aircraft capability. The system provides smoothing of γ_a, $\dot{V}_a/g$, and altitude, but small "bumps" in γ_a still appear in time histories. The values of ε for each of the fixed waypoints is input with the waypoints, and all values for the capture path are set to a prespecified value. The value of VMAX for the capture waypoint is used to restrict the speed during the final capture turn and hence minimize the turn radius.

REFERENCE FLIGHTPATHS

Five reference flightpaths were used in this study. The flightpaths were based upon a TACAN approach chart for a prop or turboprop aircraft approaching a large, canted-deck carrier which is heading due north at 20 kt with its canted deck centerlined at a heading of -11°. A 10-kt wind is blowing from -11°, or directly down the centerline of the canted deck. Initially, the aircraft is approaching the carrier along a course of 330° with respect to the canted deck (319° TACAN radial) with an airspeed of 140 kt (110 kt with respect to the ship) and at an altitude of 2000 ft (fig. 2). The distance to the touchdown point on the carrier deck is about 12 DME n. mi. along the 319° TACAN radial.

Path No. 1

A horizontal profile with waypoints is shown in figure 2 for the first flightpath, Path No. 1. This path uses a 1-n. mi. capture path to the first of the fixed waypoints that would be used by a pilot manually flying the path, which was taken from the Navy CV NATOPS MANUAL. The details of the waypoints for this path are given in table 1 wherein the position coordinates are in carrier-based coordinates in which the X-axis is positive along the magnetic north direction and the Y-axis is positive east. Each waypoint is specified by X-Y coordinates, an altitude, a turn radius, and a nominal and a maximum airspeed. This particular approach was chosen because the speed range of the Quiet Short-Haul Research Aircraft (QSRA) is more closely approximated by a prop or turboprop aircraft. From a fuel and time point of view, this flightpath is more efficient than a manually flown flightplath because the ECG software system used to produce the reference path tries to minimize the fuel used along the capture path and between each fixed waypoint, whereas a pilot flying the same path could not normally be expected to be as efficient without the workload reaching an intolerable level.

Path No. 2

A profile with waypoints is shown in figure 3 for the second flightpath, Path No. 2. Details of the waypoints are shown in table 2. It differs from Path No. 1 in that waypoint 6 of Path No. 1 has been removed. The result is that the speed following the second turn is no longer forced to an intermediate 80-kt airspeed. Thus the ECG software system is free to maintain the higher 140-kt speed as long as possible before reducing the 65-kt speed required at 3 DME (slant range) n. mi. (waypoint 6 of Path No. 2).

Path No. 3

A horizontal profile with waypoints is shown in figure 4 for Path No. 3 which takes further advantage of the energy management capabilities of the ECG software system by greatly extending the length of the capture path and shortening the fixed path. Details of the waypoints are given in table 3. It used the same starting point as the previous two flightpaths but was constrained to use only the same two final approach waypoints, that is, one waypoint at 3 DME n. mi. and 1200-ft altitude and the other at the touchdown point.

Path No. 4

A horizontal profile with waypoints is shown in figure 5 for Path No. 4 whose waypoint details are shown in table 4. It differs from Path No. 3 in that the waypoint 3 DME n. mi. from touchdown was moved to 1 DME n. mi. from touchdown. This is a point on the final descent glide slope at which the airspeed is 65 kt and the altitude is 919 ft. This flightpath saves additional fuel and time by further extending the capture portion of the flightpath into the final approach where it is most productive.

Path No. 5

A horizontal profile with waypoints is shown in figure 6 for Path No. 5 whose waypoint details are given in table 5. This flightpath illustrates the ability of the ECG system to synthesize a capture path from any location. It illustrates best the full capabilities of the ECG software which, except for the constraints on the final 0.5 DME n. mi. of the landing approach, is free to exploit the maximum capabilities of the aircraft. The 0.5 n. mi. was chosen as a minimum distance which would allow an adequate amount of time for the aircraft to become stabilized on the final approach before touchdown. The initial conditions of the flightpath are the same as in the previous flightpaths except that the initial course is -90° and the X-component of position is the negative of the previous paths. Thus, the radial distance to the touchdown point in carrier-based coordinates is the same for all flightpaths.

As for the previous paths, a knowledge of the aircraft's location and velocity relative to the ship is assumed to have been provided to a sufficient accuracy by an on-board navigation system. This particular starting point was chosen because it provided the same radial distance from the ship as the other flightpaths and thus would allow comparison.

RESULTS

Described below are the results of the ECG synthesis software for each of the five reference flightpaths in response to a given set of initial conditions and fixed waypoints. In each case a sequence of actions is defined which, if implemented either manually or automatically, would fly the QSRA aircraft along the desired reference flightpath.

Path No. 1

Referring to figures 2 and 7, the QSRA aircraft proceeds along the 330° radial (relative to the canted deck) to waypoints 1 and 2 where a left turn (indicated by the roll attitude) is begun at a distance to go of about 86,000 ft. At the end of the turn, the distance along the intended path to the touchdown point is about 79,000 ft or 13 n. mi. After level flight at an airspeed of 140 kt, the aircraft begins a constant-speed descent to an altitude of 1200 ft at a distance to go of about 59,000 ft, and the pitch angle is reduced from about 2° to -0.5° during that period. A right, 60° turn is initiated to align the flightpath of the aircraft with the canted carrier-deck. As the turn progresses, the bank angle is reduced from 11° to 8° as a result of the ECG software trying to keep the turn radius constant while the aircraft's speed with respect to the touchdown point decreases. After rolling out of the turn at a distance from touchdown of 6 DME n. mi., the aircraft resumes level flight at 1200-ft altitude along the centerline extension of the canted deck. The ECG software system then commands the deployment of the outboard flaps to a maximum of 59°, a condition required before the upper surface blowing (USB) flaps can be lowered. Later, at 28,000 ft to touchdown, the USB flaps are deployed to about 10° and the aircraft slows to 80 kt. When the aircraft has reached 19,000 ft to go, the USB flaps are lowered an additional 26° to a total of 36° and the aircraft begins to slow to the commanded airspeed of 65 kt. As the altitude continues to decrease nearly linearly with distance to touchdown, the USB flaps are further extended to 43° at 7600 ft to go, where they remain until touchdown. The touchdown speed is approximately 35 kt with respect to the deck. The aerodynamic flightpath angle is -4.5°, which is the prespecified limit during the final approach to avoid an excessive sink rate at touchdown. The total fuel used during the descent is 1148 lb and the time required from the starting point is 747 sec.

Effects of the various maneuvers on the amount of fuel used can be seen by examining the plots of engine fan speed and fuel usage rate for each flightpath.

Path No. 2

The horizontal profile of this Path was shown in figure 3 and is similar to Path No. 1. As may be seen, by comparing figure 7 with figure 8, the two paths are the same until the aircraft has rolled out of the second turn at 6 DME n. mi. from touchdown and has resumed level flight at 1200-ft altitude. Figure 8 shows that the outboard flaps are deployed to 59° at a distance of 25,000 ft to go and the speed begins to decrease. This occurs about 7000 ft farther down the path than in figure 7. At about 23,000 ft to go, the USB flaps begin deployment and are out to 34° at about 18,000 ft to go, at which time the aircraft's airspeed has been reduced to 65 kt. The pitch angle is increased to 10.5° while the flightpath angle is being maintained at 0° since rollout from the last turn. At 7500 ft to go, the USB flaps are extended to 43° as the flightpath angle is established at -4.5°, and the pitch angle is maintained at 6° where they are maintained until touchdown. The fuel used is 1080 lb and the elapsed time is 701 sec.

Path No. 3

This ECG flightpath has the same initial conditions as the previous two flightpaths, but the number of fixed waypoints is reduced to two. These are the two final approach waypoints from the set of six used in the previous path; that is, one waypoint at 3 DME n. mi. and 1200 ft altitude and the other at the touchdown point. Figure 9 shows that upon leaving the starting point, the initial course is -40°, which is held for about 3000 ft. Then a turn is made to a course of -49° and is maintained until the aircraft nears the first of the final two waypoints. At 30,000 ft to go, the throttles are retarded slightly, and at 26,000 ft to go the aircraft begins to descend as the flightpath angle is established at -4.5°. At 24,000 ft to go, the outboard flaps are fully extended to 59°, and immediately thereafter extension of the USB flaps are started. Airspeed is about 105 kt. The USB flaps are extended to 44° at 22,000 ft to go while the airspeed has decreased to about 90 kt. The aircraft reaches an airspeed of 76 kt at 20,000 ft to go at which time the throttles are slowly advanced a small amount and the USB flaps are retracted to 31° to hold this speed while the aircraft banks 5° to make a right descending turn to a course of -11°, whereupon it levels out at 1200 ft altitude. During the course change, the speed is slowed to 65 kt. At 8000 ft to go, the flightpath angle is reduced rapidly from 0° to -4.5°, and the throttles are retarded slowly after a small step-reduction. The USB flaps are extended to 43°. The aircraft then continues in this configuration to touchdown; the elapsed time is 676 sec and the fuel used is 1070 lb.

Path No. 4

The horizontal profile of Path No. 4 is the same as for Path No. 3 as may be seen by comparing figure 4 with figure 5. The only difference is that waypoint 1 in figure 5 has been moved 2 n. mi. closer to the touchdown point specified by waypoint 2. This change gives the ECG software even greater flexibility to delay the final approach, and thus to exploit the aerodynamic capabilities of the powered-lift aircraft in a portion of the flightpath where the energy payoff is highest. Locating the first waypoint at 1 DME n. mi. from touchdown rather than at 3 DME n. mi. places it on the final glide slope approach at an altitude of 919 ft. The second waypoint is the touchdown point.

Figure 10 shows that as the aircraft departs the initial position at an altitude of 2000 ft and at an airspeed of 140 kt, a small course correction is made at about 83,000 ft to go, after which the aircraft reference path is undisturbed until about 22,000 ft to go. At this point, the throttles are reduced and a slight pitch-down maneuver is executed, causing an altitude loss of about 300 ft. The airspeed then starts to decrease, followed shortly by start of the outboard flap deployment, which is complete by about 14,000 ft to go. At about 12,000 ft to go, pitch is commanded to about -5°, and the final descent begins with a flightpath angle which stabilizes at -4.5°. Also at about this time, the USB flaps are commanded to extend, stabilizing at about 40°. As the USB flaps are extended, the pitch angle comes up to 6°. At about 7500 ft to go, a 5° bank angle is commanded to change the course from -44° to -11° to align the aircraft with the carrier's canted deck. A perturbation is seen in the USB flaps, throttles, and flightpath angle as the airspeed temporarily stabilizes at 75 kt during the final turn. At the end of the turn, the throttles are then advanced slightly, the USB flaps are set at 42°, and the airspeed is stabilized at 65 kt as the aircraft continues down its descent path to touchdown on the carrier deck. Fuel used is 685 lb, which is a 385-lb reduction over the previous path. The elapsed time is 529 sec.

The fuel use reduction for Path No. 4 relative to Path No. 3 can be explained with the aid of figure 11. The synthesized data are plotted against time to compare the fuel use and time spent at each flight regime for the two approaches. Path No. 3 requires a 676-sec flight time whereas Path No. 4 requires only 529 sec, a savings of 147 sec. Figure 11 shows that the fuel rate is the same (about 1.3 lb/sec) for both paths as long as the airspeed is maintained at 140 kt. This is held for 281 sec in Path No. 3 and for 335 sec, or 54 sec longer, in Path No. 4. At these times, the engine speeds are reduced in both cases to begin decelerating with a corresponding drop in the fuel-flow rate. As the airspeed slows below approximately 100 kt, the outboard flaps are extended and the throttles reduced again. When the outboard flaps are fully extended, the USB flaps begin extension, causing the airplane to enter a powered-lift mode during which engine thrust is being used increasingly for lift, necessitating an increase in engine speed and thereby causing the fuel-flow rate to increase. Net fuel usage, however, is less than before on both paths during the deceleration and descent from the 2000-ft altitude phase. Path No. 3 then has a segment of about 165-sec duration at a constant altitude of 1200 ft which is not in Path No. 4. During this period, the fuel rate for Path No. 3 is at its highest level, between 1.8 and 2.3 lb/sec. The increase during this interval is caused by more engine thrust being required to hold both the altitude and speed constant as the USB flaps are being slowly retracted then extended again for the final approach. Thus, on Path No. 4, the final glide slope was captured while the descent from 2000 ft was still in progress, but Path No. 3 had a constant altitude and airspeed segment, which had a high fuel rate. The paths and the fuel rate are the same during the final 100 sec after the common glide slope was reached. The savings in fuel for Path No. 4

can, therefore, be traced to a combination of (1) a shorter total flight time; (2) flying 54 sec longer at 140 kt, and eliminating 165 sec spent holding altitude and airspeed in aircraft configurations in which significant engine thrust is required to enhance lift; and (3) a continuous transition from descent to final glide slope.

Path No. 5

The starting point of this path has a radial distance from the carrier which is the same as the previous paths, but the distance along the path is about 10,000 ft greater than Path No. 4. It is also different from the previous paths in that the initial course is -90° and the initial X-position is the negative of the previous paths. A horizontal profile of the path is shown in figure 6. This figure shows that the first waypoint is on the final approach at 0.5 n. mi. from touchdown. This gives the ECG software the maximum flexibility to save fuel and time while giving the aircraft adequate time to become stabilized on the final approach.

Figure 12 shows that as the aircraft departs the starting point at an altitude of 2000 ft and at an airspeed of 140 kt, a 10° left bank begins at about 94,000 ft to go. The bank angle is increased as the aircraft's speed relative to the landing point increases as a result of the ECG software trying to keep the turn radius constant. The aircraft rolls out of the turn on a course of -149° and continues at the initial speed and altitude until about 32,000 ft to go. The aircraft is pitched down slightly as the throttles are retarded slightly, causing the aircraft to reduce its airspeed and begin a descent. At about 23,000 ft to go, the outboard flaps begin to be deployed to 59°. When the aircraft has reached about 20,000 ft to go, the outboard flaps are fully extended. Then, the USB flaps begin to extend at the maximum rate while the pitch angle and angle of attack are increased positively until about 10,000 ft to go. The final turn to align the aircraft with the canted deck begins and the flightpath angle is established at its final value of -4.5° for the remainder of the approach, but the airspeed is high at about 75 kt. The USB flaps are lowered from 30° to 42° at about 3000 ft to go and the throttles are increased slightly as the airspeed is reduced to final speed of 65 kt. The fuel consumed is about 552 lb and the time is 442 sec.

CONCLUDING REMARKS

A summary of some of the more important results of the flightpath synthesis for the five approaches described in the preceding section are shown in table 6. Distance flown, flight time, and fuel used are presented for each synthesized flight. Note that, as previously described, the first four approaches started at the same location, course, and airspeed. Also, all four approaches had the same course, airspeed, horizontal profile, and glide path from 1 DME n. mi. to touchdown. The fifth path started at a different location, but flew the same horizontal profile, glide path, and airspeed as the other four from 0.5 n. mi. to touchdown. The differences between the five approaches illustrate the unique capabilities of the ECG system.

As shown in table 6, the baseline Path No. 1 approach flew 95,062 ft to touchdown in 747 sec and used 1148 lb of fuel. Although Path No. 2 flew the same predefined horizontal and vertical profiles, allowing the ECG system to fly a higher speed for a longer period shortened the flight time by 46 sec (a 6.2% reduction) and saved 68 lb of fuel (5.9%) less). When the ECG system was also allowed to exploit its horizontal and vertical flightpath synthesis capabilities to capture a waypoint nearer the touchdown point, the Path No. 3 flight was completed in a 71-sec shorter flight time (9.5%) and used 78 lb (6.8%) less fuel than the baseline approach while still providing the same stabilized final descent as the other two approaches from 3 DME n. mi. Even more fuel can be saved by capturing a waypoint which is much closer to touchdown. This is seen in Path No. 4, in which the captured waypoint was on the final glide slope only 1 n. mi. (slant range) from touchdown. This procedure saved 218 sec (29.2%) of flight time and 463 lb of fuel (40.3%) relative to Path No. 1. These savings were produced by (1) shortening the total flight time and (2) keeping airspeed high as long as possible to minimize time spent flying in a regime in which more thrust is required for lift to aid the aerodynamic lift, a less fuel efficient condition. Significant fuel savings were also shown when time spent flying at constant altitude at low airspeeds was minimized or eliminated.

The fuel savings for Paths No. 2, 3, and 4 indicate the potential of the ECG system when there is some freedom to select the horizontal, altitude, and speed profiles. More fuel could be saved in situations in which the system's path generation and flight time prediction capabilities could be used to coordinate direct landings by aircraft without spending time in holding patterns, as indicated by the results for Path No. 5. As the ECG system is allowed more freedom, fuel consumption decreases. Use of the total-path-synthesis procedure used in Paths 3, 4, and 5 may depend upon policy changes to the extent of allowing more flexibility in the selection of the approach path between the holding pattern and the final descent on the glidepath. Even if that flexibility is not allowed for operational, communications, or security reasons, this study, although limited in scope, shows that an ECG system can save flight time and fuel by more efficiently managing the aircraft's capabilities. Defining operationally acceptable limits on such parameters as minimum allowable flight time on a stabilized glide slope to touchdown and the allowable horizontal, vertical, and airspeed profiles would require experimental tests of the ECG concept.

APPENDIX A

ENERGY-RATE EQUATIONS AND SIMPLIFIED AIRCRAFT MODEL

The basic objective of the energy-management guidance system is to synthesize a flyable trajectory from the current aircraft states to some desired terminal states. The term "flyable" implies compliance with certain constraints.

The first set of constraints (which will be referred to as operational constraints) are externally imposed and are specified by input constants. Some operational constraints, including limits on inertial flightpath angle, airspeed rate, normal acceleration, bank angle, and roll rate, are dictated by passenger comfort or pilot preference. Others, determined by Air Traffic Control regulations or by terrain, take the form of specified horizontal paths together with speed and altitude restrictions.

Next are geometric constraints, which require that maneuvers meeting the operational constraints can actually be made in the space available. For example, given a maximum flightpath angle $|\gamma_m|$, a maximum rate of change of $|\gamma|$ (hence a maximum normal acceleration), and a desired change in altitude Δh_D, is it possible for $|\gamma|$ to change from its present value to $|\gamma_m|$ and then to its final value while Δh_D is being accomplished? Where should pitch-over to the final value of γ begin? These problems are solved by the system through closed-form equations which will be described in appendix B. A similar problem for the lateral case is handled by introducing step changes in the reference bank angle.

The operational and geometrical constraints are only indirectly affected by aircraft performance and do not guarantee that the aircraft can perform all maneuvers which satisfy them. The final set of constraints (which will be referred to as aircraft constraints) restrict the synthesized flightpath to flight conditions and control settings which the aircraft can achieve while meeting safety standards and reserving maneuver capability for control. Determination of the aircraft constraints requires a fast-time solution of the aircraft's equations of motion. The algorithms used for this solution depend upon energy-rate methods and are described in this appendix.

Energy-Rate Equations

The aircraft energy is defined as the sum of the kinetic and potential energies

$$E = mgh + \frac{1}{2} mV_a^2 \tag{A1}$$

where h is the altitude.

Differentiating equation (A1) with respect to time and dividing by mg gives

$$\frac{\dot{E}}{W} = \dot{h} + \frac{V_a}{g} \dot{V}_a \tag{A2}$$

Substituting $V_a \sin \gamma_a$ for $\dot{h}$ and dividing by V_a gives the normalized energy rate $\dot{E}_n$ as

$$\dot{E}_n = \frac{\dot{E}}{WV_a} = \sin \gamma_a + \frac{\dot{V}_a}{g} \tag{A3}$$

For convenience $\dot{E}_n$ will be referred to simply as the energy rate.

It can be seen from equation (A3) that $\dot{E}_n$ represents the total capability of the aircraft to change speed and altitude. Given a desired flightpath angle and airspeed rate, it is necessary to find the control settings which will produce the desired $\dot{E}_n$ in steady state.

Equations of Motion

The trajectory-synthesis algorithm requires a simple, compact method for integrating the longitudinal equations of motion while meeting all of the imposed constraints (operational, geometric, and aircraft). This is accomplished through the use of the following point-mass equations of motion:

$$mV_a = T \cos \alpha - D - \mathrm{RAMDRAG} - mg \sin \gamma_a - m\dot{V}_{wat} \cos \gamma_a \tag{A4}$$

$$mV_a\dot{\gamma}_a = (T \sin \alpha + L)\cos \phi - mg \cos \gamma_a - m\dot{V}_{wat} \sin \gamma_a \tag{A5}$$

where

T	total gross thrust
D	aerodynamic drag
RAMDRAG	drag from ram air through engine
L	aerodynamic lift
mg	aircraft weight (W)
γ_a	aerodynamic flightpath angle
ϕ	bank angle
α	angle of attack
$\dot{V}_{wat}$	along-track component of rate of change of the mean wind

It is assumed that the mean wind is a function only of altitude and has no vertical component so that

$$\dot{V}_{wat} = \frac{\partial V_{wat}}{\partial h} \dot{h} = \frac{\partial V_{wat}}{\partial h} V_a \sin \gamma_a \tag{A6}$$

where V_{wat} is the along-track component of the wind velocity and h is the altitude.

The lateral equations of motion per se need not be integrated, since the effects of bank angle are accounted for by using a fictitious aircraft weight equal to the true weight divided by $\cos \phi$.

The terms in equations (A4) and (A5) are converted to normalized coefficient form by dividing by dynamic pressure, $\bar{q}$, and wing area, S_w, to give

$$\frac{W}{\bar{q}S_w} \frac{\dot{V}_a}{g} = -(C_D + C_{RD}) - \sin \gamma_a - \dot{V}_{wat} \cos \gamma_a \tag{A7}$$

$$\frac{W}{\bar{q}S_w} \frac{V_a}{g} \dot{\gamma}_a = C_L \cos \phi - \frac{W}{\bar{q}S_w} \left(\cos \gamma_a + \frac{\dot{V}_{wat}}{g} - \sin \gamma_a\right) \tag{A8}$$

where

$$C_D = -(T \cos \alpha - D)/\bar{q}S_w$$

$$C_{RD} = \mathrm{RAMDRAG}/\bar{q}S_w$$

and

$$C_L = (L + T \sin \alpha)/\bar{q}S_w$$

Multiplying equation (A3) by $W/\bar{q}S_w$ and substituting from equation (A7) gives

$$\frac{W}{\bar{q}S_w} \dot{E}_n = -(C_D + C_{RD}) - \frac{W}{\bar{q}S_w} \frac{\dot{V}_{wat}}{g} \cos \gamma_a \tag{A9}$$

Equation (A8) requires

$$C_L = \frac{W}{\bar{q}S_w \cos \phi} \left(\frac{V}{g} \dot{\gamma}_a + \cos \gamma_a + \frac{\dot{V}_{wat}}{g} \sin \gamma_a\right)$$

or, since for trim $\dot{\gamma}_a = 0$,

$$C_L = \frac{W}{\bar{q}S_w \cos \phi} \left(\cos \gamma_a + \frac{\dot{V}_{wat}}{g} \sin \gamma_a\right) \tag{A10}$$

Solving equation (A9) for $-(C_D + C_{RD})$ gives

$$-(C_D + C_{RD}) = \frac{W}{\bar{q}S_w} \dot{E}_n + \frac{W}{\bar{q}S_w} \frac{\dot{V}_{wat}}{g} \cos \gamma_a \tag{A11}$$

Define $\dot{E}_T$ as

$$\dot{E}_T = -\left(\frac{C_D + C_{RD}}{C_L}\right)$$

or

$$\dot{E}_T = \frac{\left(\dot{E}_n + \frac{\dot{V}_{wat}}{g} \cos \gamma_a\right) \cos \phi}{\cos \gamma_a + \frac{\dot{V}_{wat}}{g} \sin \gamma_a} \tag{A12}$$

The coefficients C_D, C_{RD}, and C_L are functions only of α_w, C_T, and flaps (δ_{FREF}).

Energy-Rate Tables

The values of $\dot{E}_T$, the corresponding wing angle of attack, α_w, the thrust coefficient, C_T, and the flap parameter, δ_{FREF}, were calculated and stored in what are referred to as energy-rate tables. The values of $\dot{E}_T$ from these tables are plotted in figure A1 as a function of lift coefficient, C_L, for a set of engine parameters and weights defined in table A1. The indices in table A1 correspond to the curves in figure A1 in sequence from the uppermost curve. Note that the pressure ratios 1.0, 0.688, and 0.459 correspond to pressure altitudes of sea level, 10,000 ft, and 20,000 ft, respectively. Altitude is accounted for by linear interpolation on pressure ratio. The nominal aircraft weights listed in table A1 were used to establish airspeed, which, in turn, determines C_{TMAX}, C_{TMIN}, and the placard values of flaps. For the minimum aircraft weight (40,000 lb), C_{TMAX} and the placard flaps are the maximum value for any given value of C_L; for maximum weight (56,000 lb), C_{TMIN} is the minimum value for each C_L. The flap placards for the minimum aircraft weight were used for generating all the energy-rate table data. Curve 1 in figure A1 represents the maximum $\dot{E}_T$ atainable for any weight and altitude while curve 7 represents the minimum. Thus, those two curves represent the limits to the flight envelope over the range of C_L. The effects of spoilers and various other complications which affect the algorithms used in the program are discussed in the next section.

During synthesis, desired values of $\sin \gamma_a$ and $\dot{V}_a/g$ which satisfy the operational and geometric constraints are obtained and used to calculate the desired values of $\dot{E}_n$. The desired value of $\dot{E}_n$ together with its operational maximum and minimum are used in equation (A12) to find the desired, maximum, and minimum values of $\dot{E}_T$. Then linear interpolation on the current value of C_L is used to obtain a one-dimensional array of $\dot{E}_T$. This is equivalent to finding $\dot{E}_T$ at the intersection of a vertical line on figure A1 at the current value of C_L with C_T from the different thrust contours. Arrays of α_w, C_T, and flap settings corresponding to this value of C_L are also found. The constraints of thrust and flaps are then applied to obtain the maximum and minimum values of $\dot{E}_T$ achievable. These are stored in the first and last elements of the $\dot{E}_T$ array, respectively, and the corresponding values of α_w, C_T, and flaps are adjusted accordingly. Note that where the contours merge, the number of elements in the one-dimensional arrays is reduced. Finally, the maximum and minimum values of $\dot{E}_T$ are multiplied by a factor of σ (currently 0.9) to reserve the fraction $(1 - \sigma)$ of the available $\dot{E}_T$ for control. If the desired value of $\dot{E}_T$ computed from equation (A12) exceeds the limits on tabular values of $\dot{E}_T$ just discussed, it is set equal to the tabular limits and equation (A12) is inverted to find the resulting limit on $\dot{E}_n$.

After the desired value for $\dot{E}_n$ has been determined to be within operational and geometric limits, sin γ_a and $\dot{V}_a/g$ are recomputed using an algorithm controlled by the pilot-input parameter ε to determine the amount of $\dot{E}_n$ allocated to each. Because $\dot{E}_n$ is a function of sin γ_a, iteration is used to find the final values of $\dot{E}_n$, γ_a, $\dot{V}_a/g$, α_w, thrust coefficient, and flaps.

For a given set of α_w, C_T, and δ_{FREF}, the same value of $\dot{E}_n$ will result, independent of speed or altitude. However, the maximum value of δ_{FREF} which can be used (the placard value) is a function of airspeed. Since, for trim, it is necessary that $C_L \approx W/\bar{q}S_w$, the maximum value of δ_{FREF} is a function of aircraft weight. The values of $\dot{E}_T$ were calculated using maximum and minimum aircraft weights as discussed earlier. The placard flaps for the minimum weight were used for these tables and are the maximum that will be encountered. For heavier weights the maximum allowable δ_{FREF} will be reduced, resulting in turn in the reduction of the maximum magnitude of negative energy rate achievable. Interpolation on δ_{FREF} is used to adjust $\dot{E}_T$ to a value achievable for the actual aircraft weight.

Calculation of Energy-Rate Tables - If we assume that we have a desired flightpath angle and airspeed rate, we wish to determine whether the desired $\dot{E}_n$ can be achieved at the current flight conditions, and if so, to determine the corresponding required control settings for flaps, angle of attack, and thrust. Sets of tabular data referred to as "energy-rate tables" have been generated for this purpose.

The first step in generating the energy-rate tables was to compute sets of static trim conditions for the longitudinal mode using the CDC 7600 simulation software of the QSRA. The simulation uses tabular data from wind tunnel experiments described in reference 5. The simulation was used to compute sets of tables of C_L and $\dot{E}_T$ versus α_w for constant values of C_T and flaps. Here C_T is defined as the total gross thrust for four engines divided by $\bar{q}S_w$. This operation produced sets of tables, examples of which are illustrated in graphical form in figure A2. Tables representing the various combinations of outboard flaps (δ_F), USB flaps (δ_{USB}), and C_T sufficient to cover the aircraft flight envelope were generated. Values of C_T and α_w used for the original wind tunnel data were also used in this calculation.

Note that the flight control system is designed so that δ_{USB} is constrained to 0° unless $\delta_F = 59°$. Hence, δ_F and δ_{USB} may be regarded as a single control δ_{FREF}. Also note that it is assumed that the spoilers are biased from 0° to 10° proportionally to the value of δ_{USB} between 0° and 30°. As will be discussed later, the data indicate that it may be necessary to increase the spoiler bias in order to obtain sufficiently negative values of $\dot{E}_n$.

For the synthesis process, it is necessary that C_L be an independent variable, and it was necessary to "invert" the trim data using linear interpolation. Also, since there is one more control than necessary to trim the aircraft, some criterion must be used to eliminate the redundancy, even in the case of manual operation. Furthermore, the elimination process must be implemented on the computer if a reference flightpath is to be synthesized. The criterion chosen for the initial application to the QSRA is the minimization of fuel. A set of energy-rate tables were generated using the minimum-fuel criterion by finding, for specified combinations of C_L and C_T, the value of δ_{FREF} for which $\dot{E}_T$ is maximum. The minimum feasible value of $\dot{E}_n$ was also found, assuming that $C_{TMIN} = 0$ and with the constraint that $0 \le \alpha_w \le 15°$. Placard values of δ_{FREF} and C_{TMAX} were computed for an aircraft weight of 40,000 lb. Note that when C_L is calculated for the interpolation of the C_L table described in the section on speed-altitude synthesis, the value of γ_a in equation (A10) was set to zero. This was done to reduce computation time, but if more precision is required, iteration would be necessary.

The results of these computations in figure A3 show $\dot{E}_T$ as a function of C_L for different values of C_T. The upper dashed line is the contour of the maximum allowable value of C_T resulting from the constraint that the corrected engine core speed, $N_2/\sqrt{\theta_2}$, be less than or equal to 96%. This computation was made assuming $\delta_{AMB} = 1$ (sea level on a standard day). δ_{AMB} only rarely exceeds unity, but decreases exponentially with increasing altitude. C_{TMAX} may be further reduced as the result of the constraint that the engine exhaust gas temperature not exceed 920° C.

The lower dashed curve is for the minimum value of $\dot{E}_T$ obtainable with the spoiler values specified earlier and no minimum constraint on C_T. For values of C_L greater than that ($C_L = 2.4$) at the intersection of the lower dashed line and the $C_T = 0$ contour, the value of $\dot{E}_n$ is constrained by $\alpha_w = 15°$. At lower values of C_L, the constraint is the result of the flap placards. The two dashed curves, together with the vertical lines at the maximum and minimum values of C_L, represent an outer limit to the operational envelope of the aircraft. The maximum value of $C_L = 7$ results in minimum equivalent airspeeds of 53 kt and 63 kt for aircraft weights of 40,000 lb and 56,000 lb, respectively. The minimum value of C_L corresponds to the maximum equivalent airspeed of 160 kt and an aircraft weight of 40,000 lb. The minimum value of C_L will increase with aircraft weight.

Figures A3(b) and A3(c) show the values of α_w and δ_{FREF}, respectively, corresponding to the values of $\dot{E}_T$ in figure A3(a). The rather erratic nature of these curves resulted in the addition of a number of intermediate values of δ_{FREF} to the trim data before computing the energy-rate tables finally used, which are shown in figure A1.

Figure A4(a) shows curves of $\dot{E}_T$ versus C_L obtained by interpolation of data of the type used for figure A3. The upper three solid curves are for C_{TMAX} at values of δ_{AMB} corresponding to pressure altitudes of sea level, 10,000 ft, and 20,000 ft. The values of $\dot{E}_T$ shown are the maximum obtainable with those values of C_T. The lower two solid curves are for the maximum $\dot{E}_T$ obtainable using the minimum allowable value of C_T ($N_2/\sqrt{\theta_2} = 78\%$) at sea level and 10,000 ft. The two dashed curves are the minimum values of $\dot{E}_n$ obtainable with the minimum values of C_T. The dotted curve is the minimum $\dot{E}_T$ obtainable with C_{TMIN} set to 0. Note that in contrast to figure A1 discussed in the beginning of this appendix, minimum aircraft weight (40,000 lb) was used for all of these curves. This choice simplifies the following discussion. However, the data actually used in the program are represented by figure A1. At the higher values of C_L, all of the five lower curves merge into a single curve determined by the constraints on α_w and δ_{FREF}.

Figures A4(b), A4(c), and A4(d) show the corresponding values of α_w, δ_{FREF}, and C_T, respectively. In all of the maximum $\dot{E}_T$ cases (solid curves), α_w rises linearly with C_L until δ_{FREF} changes from 0% to 30%. At this point, α_w decreases to a lower value and then increases linearly until it reaches 15° (the maximum allowable value). Some of the curves have a break point and decrease in slope near $\alpha_w = 15°$. This change in slope could be eliminated by finding the exact value of C_L for which α_w attains 15°. Also, δ_{FREF} tends to remain at 30% until α_w reaches 15°. Similar relationships exist for the minimum $\dot{E}_T$ curves (dashed lines), but are complicated by the flap placards and by the nature of the trim data at high values of δ_{USB}.

Figure A4(d) shows the thrust coefficients which correspond to the data for figure A3(a,b,c). There are only five curves since both the minimum and maximum energy-rate data are plotted for C_{TMIN} at sea level and 10,000 ft. At lower values of C_L, the values of C_T are linear functions of C_L. The changes in slope at the higher values of C_L are caused when the limits on δ_{FREF} and α_W are encountered.

It can be seen from figure A4(a) that the descent/deceleration capability of the QSRA is rather limited. For $C_L > 2.0$, the minimum value of $\dot{E}_T$ at sea level has an average value of about -0.15. For higher weights, the minimum value of $\dot{E}_T$ may be larger in magnitude depending on the flap placards. However, it is desirable to increase the descent/deceleration capability, particularly at the lower weights and smaller value of C_L. One possible method of improving the descent/deceleration capability was investigated, and the results are presented in figure A5. Figures A5(a) and A5(b) show the minimum $\dot{E}_T$ curves for C_{TMIN} (δ_{AMB} = 1) and C_{TMIN} (δ_{AMB} = 0.687) from figure A4(a) as solid lines. The dashed curves are the result of increasing the spoiler bias by 8° from the nominal for all values of C_L. (The nominal spoiler bias increases linearly with USB flaps at the rate of one-third of a degree per degree of USB to a maximum spoiler bias of 10°.) This change produces a significant effect on the minimum $\dot{E}_T$ for $C_L \leq 2.0$. The effectiveness of the spoilers in producing more negative values of $\dot{E}_T$ is reduced with increasing δ_{USB} and to a lesser extent with increasing C_T.

It is apparent from the results in figure A5 that this increase in spoiler deflection is not effective in producing more negative values of $\dot{E}_n$ much beyond C_L = 2.0 (i.e., for equivalent airspeeds less than about 100 kt). (It has been suggested by NASA personnel that even larger increases in spoiler deflection are feasible and may produce desirable results. Further study of the problem is needed.)

Engine Speed Constraints on Thrust Coefficient

The thrust coefficient, C_T, is constrained to a maximum value C_{TMAX}, which requires that the corrected engine core speed, $N_2/\sqrt{\theta_2}$, not exceed 96% rpm while a lower limit, C_{TMIN}, is established by the requirement that $N_2/\sqrt{\theta_2} \geq 78\%$ rpm. The values of the resulting limits on T_G/δ_{AMB}, where T_G is the gross thrust for four engines, are given in table A2.

Mach number is defined as the ratio of true airspeed, V_T, to the speed of sound, a. By definition of V_{EQ}, the equivalent airspeed

$$V_T = V_{EQ}\sqrt{\frac{\rho_o}{\rho}} \tag{A13}$$

where ρ is the actual density and ρ_o is the sea level density of the standard atmosphere (ref. 6). It can be shown $\rho/\rho_o = \delta_{AMB}/\theta_{AMB}$ where θ_{AMB} is the ratio of the ambient absolute temperature to the standard value at sea level.

It can also be shown that

$$a/a_o = \sqrt{\theta_{AMB}} \tag{A14}$$

where a_o is the speed of sound at sea level in the standard atmosphere. Substituting equations (A13) and (A14) into the definition of Mach number, M, gives

$$M = \frac{V_{EQ}}{a_o} \frac{1}{\sqrt{\theta_{AMB}}} \tag{A15}$$

Linear interpolation on Mach number is used to find T_{GMAX}/δ_{AMB} and T_{GMIN}/δ_{AMB}, which are then multiplied by $\delta_{AMB}/\bar{q}S_w$ to give C_{TMAX} and C_{TMIN}.

Calculation of Limit on C_T Due to Exhaust Gas Temperature Limit of 920° C

The data used for these calculations were obtained from CDC 7600 simulation tables TMGT1(HPBLC=0), TMBT2(HPBLC=5), and TMGT3(HPBLC=10), where high-pressure boundary-layer control (HPBLC) is the percentage of cold thrust air bled from the engines to be blown over the leading edge and the ailerons for boundary layer control. These are tables of $MGT/\theta_2^{0.881}$ versus $N_1/\sqrt{\theta_2}$ and M, where MGT is the measured (exhaust) gas temperature, M is the Mach number, N_1 is the fan speed (in % rpm), and θ_2 is defined by $\theta_2 = (1.0 + 0.2M^2)T_{AMB}/T_O$. Here T_{AMB} is the ambient absolute temperature and T_O is the standard value of T_{AMB} at sea level, or we can define $T_{AMB} = T_O + \Delta T$. By using these tables it is possible for a given value of θ_2 to find the value of $N_1/\sqrt{\theta_2}$ for which MGT = 920° C. When this was done for values of ΔT in the range $-30° \text{ C} \leq \Delta T \leq 30° \text{ C}$ and for $0 \leq M \leq 0.3$, it was found that Mach number has a negligible effect on the value of $N_1/\sqrt{\theta_2}$. That is, if we define N_{TMX} as the value of $N_1/\sqrt{\theta_2}$ for which MGT = 920° C, then

$$N_{TMX} \approx N_o + k\Delta T$$

where N_o and k are functions of HPBLC. A conservative approximation is given by

$$N_{TMX} = 94.0 - 0.78(\text{HPBLC}) - \Delta T[0.1667 + 0.00333(\text{HPBLC})] \tag{A16}$$

This result is plotted in figure A6 for the three values of HPBLC for which data are available. Note that N_{TMX} is strongly dependent on HPBLC. The Boeing math model report (ref. 5) states that HPBLC varies from 10% at STOL idle to 0% at high thrust values.

The value of HPBLC in the CDC 7600 simulation is the result of a set of calculations using the actual core speed N_2 (not $N_2/\sqrt{\theta_2}$). Given a value of N_2, the value of HPBLC is adjusted so that the temperature constraint is not violated unless $N_1/\sqrt{\theta_2}$ is greater than the maximum for HPBLC = 0, in which case HPBLC is set to 0. Note that HPBLC is not necessarily adjusted to its allowable maximum for the given $N_1/\sqrt{\theta_2}$, but never exceeds it. Therefore, the maximum $N_1/\sqrt{\theta_2}$ for $MGT \leq 920°$ C can be taken as the value for HPBLC = 0, that is,

$$N_1/\sqrt{\theta_2} = 94.0 - \Delta T/6.0 \tag{A17}$$

The corresponding value of T_G/δ_{AMB} can be found in table A3 and multiplied by $\delta_{AMB}/\bar{q}S_W$ to get the maximum value of thrust coefficient, C_{TT}, which satisfies the temperature constraint. Then C_{TMAX} is set to the minimum of its original value (for which $N_2/\sqrt{\theta_2} \leq 96\%$) and C_{TT}.

APPENDIX B

DERIVATION AND USE OF CLOSED-FORM EQUATIONS FOR SPEED-ALTITUDE PROFILE

In order to determine the aircraft's capability to achieve a desired flightpath angle during a predetermined altitude change, a set of closed-form equations has been developed which calculate the altitude changes during changes in γ and/or V. When γ changes, its maximum magnitude is subject to the constraint that $|\dot{\gamma}| = k_1/V_T$, where V_T is the true airspeed and k_1 is an input normal acceleration. Note that if speed and altitude change in opposite directions, the total change in energy is minimized by requiring that the change in energy caused by speed change and that caused by altitude change have a fixed ratio which will cause them to be completed simultaneously. Four equations are used in the calculation of these altitude changes: one for V and h changing in the same direction, one for V constant while γ changes, one for γ constant and V changing, and one for V and h changing in opposite directions. These equations are applied in sequence to the intervals of the trajectory between successive pairs of waypoints during which the altitude changes.

<u>Case 1: V and h change: same sign</u>

We assume

$$V = V_0 + k_2 t \tag{B1}$$

$$\dot{\gamma} = k_1/V \tag{B2}$$

$$\dot{h} = V \sin \gamma \tag{B3}$$

From equations (B1) and (B2)

$$\dot{\gamma} = \frac{k_1}{V_0 + k_2 t} \tag{B4}$$

$$\int_{\gamma_0}^{\gamma} d\gamma = k_1 \int_0^{\tau} \frac{dt}{V_0 + k_2 t} \tag{B5}$$

Integrating equation (B5) gives

$$\gamma - \gamma_0 = \frac{k_1}{k_2} \ln(V_0 + k_2 t)\Big|_0^{\tau} \tag{B6}$$

or

$$\gamma - \gamma_0 = \frac{k_1}{k_2} \ln\left(\frac{V_0 + k_2 \tau}{V_0}\right) \tag{B7}$$

Let $u = \gamma - \gamma_0$. We have

$$u = \frac{k_1}{k_2} \ln\left(1 + \frac{k_2}{V_0} \tau\right) \tag{B8}$$

Inverting equation (B8)

$$\tau = \frac{V_0}{k_2} \left[e^{(k_2 u/k_1)} - 1\right] \tag{B9}$$

and differentiating from equation (B9)

$$dt = \frac{V_0}{k_1} e^{(k_2 u/k_1)} du \tag{B10}$$

Substituting equation (B9) into equation (B1) gives

$$V = V_0 e^{(k_2 u/k_1)} \tag{B11}$$

and substituting equations (B10) and (B11) into equation (B3) gives

$$dh = \frac{V_0^2}{k_1} e^{(2k_2 u/k_1)} \sin(\gamma_0 + u)du \tag{B12}$$

Let $V_0^2/k_1 = b$ and $2k_2/k_1 = a$ for convenience. Then

$$dh = b\, e^{au} \sin(\gamma_0 + u)du \tag{B13}$$

Using double angle formulas with (B13) gives

$$dh = b\, e^{au}[\sin \gamma_0 \cos u + \cos \gamma_0 \sin u]du$$

so that upon integration,

$$h - h_0 = b \left\{ \sin \gamma_0 [e^{au}(a \cos u + \sin u)] \frac{1}{1 + a^2} + \cos \gamma_0 [e^{au}(a \sin u + \cos u)] \frac{1}{1 + a^2} \right\} \Bigg|_0^u$$

or

$$\Delta h = h - h_0 = \frac{b}{1 + a^2} \{[a \sin(u + \gamma_0) - \cos(u + \gamma_0)]e^{au} - [a \sin \gamma_0 - \cos \gamma_0]\} \tag{B14}$$

Substituting $\gamma - \gamma_0$ for u in equation (B14) gives

$$\Delta h = \frac{b}{1 + a^2} [e^{a(\gamma - \gamma_0)}(a \sin \gamma - \cos \gamma) - (a \sin \gamma_0 - \cos \gamma_0)] \tag{B15}$$

Factoring $e^{-a\gamma_0}$ from equation (B15) gives

$$\Delta h = \frac{b\ e^{-a\gamma_0}}{1 + a^2} \left[e^{a\gamma}(a \sin \gamma - \cos \gamma) - e^{a\gamma_0}(a \sin \gamma_0 - \cos \gamma_0)\right] \tag{B16}$$

where Δh is the altitude change while changing γ and V.

Case 2: V constant, h changing

In this case we desire to specify V_{EQ} instead of V_T because it is equivalent airspeed which will be held constant. A good approximation for the altitudes under consideration is

$$V_T = V_{EQ}(1 + Kh)$$

where $K = 0.16\times10^{-4}\ ft^{-1}$ and h is in feet.

From equation (B2)

$$\dot{\gamma} = \frac{k_1}{V_T} = \frac{k_1}{V_{EQ}(1 + Kh)} \tag{B17}$$

$$\dot{h} = V_T \sin \gamma = V_{EQ}(1 + Kh)\sin \gamma \tag{B18}$$

From equations (B17) and (B18)

$$\frac{dh}{d\gamma} = \frac{[V_{EQ}(1 + Kh)]^2}{k_1} \sin \gamma$$

so that

$$\frac{k_1\ dh}{V_{EQ}^2(1 + Kh)^2} = \sin \gamma\ d\gamma$$

or

$$\frac{k_1}{V_{EQ}^2} \int_{h_0}^{h} \frac{dh}{(1 + Kh)^2} = \int_{\gamma_0}^{\gamma} \sin \gamma\ d\gamma \tag{B19}$$

Integrating equation (B19) gives

$$\frac{k_1}{KV_{EQ}^2} \left[\frac{1}{1 + Kh_0} - \frac{1}{1 + Kh}\right] = \cos \gamma_0 - \cos \gamma \tag{B20}$$

Solving equation (B20) for h results in

$$h = \frac{1}{k}\left[\frac{k_1(1 + Kh_0)}{-K(1 + Kh_0)V_{EQ}^2(\cos\gamma_0 - \cos\gamma) + k_1} - 1\right] \tag{B21}$$

From which it follows that

$$\Delta h = h - h_0 = \frac{(1 + Kh_0)^2 V_{EQ}^2(\cos\gamma_0 - \cos\gamma)}{k_1 - K(1 + Kh_0)V_{EQ}^2(\cos\gamma_0 - \cos\gamma)} \tag{B22}$$

Case 3: γ constant, V changing

From equations (B1) and (B3),

$$\dot{h} = (V_0 + k_2 t)\sin\gamma_0$$

$$\dot{V} = k_2$$

$$dh = \frac{V}{k_2}\sin\gamma_0 \, dV \tag{B23}$$

Integrating equation (B23) gives

$$\Delta h = h - h_0 = \left(\frac{V^2 - V_0^2}{2k_2}\right)\sin\gamma_0$$

Case 4: V and h changing in opposite directions

In order to minimize the total change in energy (and thus minimize $|\dot{E}_n|$), we desire the altitude and speed changes to be accomplished simultaneously for this case. We define the aircraft energy E as

$$E = h + \frac{V^2}{2g} \tag{B24}$$

Therefore,

$$\Delta E_h = h - h_0 = \Delta h \tag{B25a}$$

$$\Delta E_V = \frac{V^2 - V_0^2}{2g} \tag{B25b}$$

where ΔE_h is the change in energy from altitude change, and ΔE_V is the change in energy from velocity change. Differentiating equations (B25a) and (B25b),

$$\Delta\dot{E}_h = \dot{h} \tag{B26a}$$

$$\Delta\dot{E}_V = \frac{V\dot{V}}{g} \tag{B26b}$$

Define

$$k^* = \frac{\Delta E_v}{\Delta E_h} = \frac{\Delta \dot{E}_v}{\Delta \dot{E}_h} \tag{B27}$$

Then to satisfy the minimum total energy change condition, we want

$$\frac{V\dot{V}}{g\dot{h}} = k^* \tag{B28}$$

or, substituting $V \sin \gamma$ for $\dot{h}$,

$$\dot{V} = k^* g \sin \gamma \tag{B29}$$

or, defining $K_3 = gk^*$,

$$\dot{V} = K_3 \sin \gamma \tag{B30}$$

We want to restrict $\dot{\gamma}$ to $\dot{\gamma} = k_1/V$ (from eq. (32)), so that

$$\frac{dV}{d\gamma} = \frac{\dot{V}}{\dot{\gamma}} = \frac{k_3 \sin \gamma}{k_1/V} \tag{B31}$$

from which

$$\frac{dV}{V} = \frac{k_3}{k_1} \sin \gamma \; d\gamma \tag{B32}$$

and, integrating equation (B32)

$$\int_0^{\tau} \frac{dV}{V} = -\frac{k_3}{k_1} \cos \gamma \Big|_0^{\gamma}$$

$$ln \frac{V}{V_0} = \frac{k_3}{k_1} (\cos \gamma_0 - \cos \gamma) \tag{B33}$$

$$V = V_0 \; e^{(k_3/k_1)(\cos\gamma_0 - \cos\gamma)}$$

$$\frac{dh}{dV} = \frac{V \sin \gamma}{k_3 \sin \gamma} = \frac{V}{k_3} \tag{B34}$$

and, integrating equation (B34)

$$\Delta h = h - h_0 = \frac{1}{k_3}\left(\frac{V^2 - V_0^2}{2}\right)$$

Computer Implementation of Closed-Form Equations

The closed-form equations developed in this section are implemented in the computer program subroutines INTEG and VGMALT described in appendix C. There are two sections in INTEG which solve the equations for: (1) Case 4, where the speed and altitude changes called for are of opposite signs, and (2) Cases 1, 2, and 3.

Case 4 is solved in a simple iterative loop. Since the velocity-altitude relationship is known in this case throughout the interval, it is possible to determine the altitude changes during the required changes in γ at both ends of the interval in closed form.

After this is done it is determined whether the sum of these altitude changes exceeds the total altitude change desired in the trajectory; if so, γ_C is limited to its old value multiplied by the ratio of the total altitude change desired over the sum of the individual altitude changes, and the computation is iterated.

It is possible that the altitude-velocity relationship may not be solved in one calculation at the end of the trajectory for Cases 1, 2, and 3, since finding the velocity at the beginning of the final pitch maneuver may require an iteration process. Therefore, the process used for these cases is somewhat different from that for Case 4.

At the beginning of the closed-form process for Cases 1, 2, and 3 it is determined whether or not there is to be a velocity change during the interval. If not, program execution skips directly to the constant equivalent airspeed portion of the logic. If there is a velocity change, the subroutine VGMALT is called.

The first step in VGMALT is to solve equation (B9) for the time, t_γ, required to achieve γ_C and then to solve equation (B1) for the time, t_V, required to achieve the desired speed change. If $t_V < t_\gamma$, equation (8) (with $\tau = t_V$) is used to compute u, the change in γ, and if $t_V > t_\gamma$, u is set to $\gamma_C - \gamma_0$. Equation (B16) is then used to compute the corresponding altitude change, Δh, which is stored in DELHG if the γ change is completed first and in DELHV if the speed changed is completed first.

If the speed change is completed first, program execution continues to the constant equivalent airspeed portion of the closed-form algorithm, where equation (B22) is used to compute and store in DELHG the remaining altitude change to achieve the commanded γ (if no velocity change is called for during the trajectory, this altitude change will be the total Δh from the initial to the commanded γ). The values of DELHG and DELHV (which are zero if there is no speed change) are summed to compute the total altitude change, DHTOT, required to achieve the commanded γ. The logic of this paragraph is skipped if the γ change is completed first; in the latter case DHTOT is simply set to DELHG.

We have now computed the altitude change during the beginning parts of the trajectory (Δh) from the start of the trajectory to P_1 (see fig. B1). In order to compute the altitude change during the final portion of the interval, we must first compute the velocity at the beginning of the final pitchover maneuver at P_2 in figure B1. If the aircraft completed the velocity change before the γ change in the initial portion (prior to P_1) of the interval, the velocity at P_2 will simply be the equivalent airspeed at the end of the interval. Otherwise, V_{EQ} for the pitchover altitude at P_2 must be computed with an iterative process. The velocity at P_2 is initially set to the true airspeed at the end of the flightpath. The procedure for determining altitude changes in the previous paragraphs is then executed, resulting in an initial estimate for the altitude change from P_2 to the end of the flightpath. This altitude change estimate is used to compute a new initial velocity by subtracting the altitude-change estimates from the final altitude and determining the velocity at the resultant altitude. This velocity is determined by first calculating the altitude change needed for the aircraft to complete its required velocity change and then adding that altitude change to the altitude reached when γ_c is initially intercepted at P_1. If the resultant altitude is less than the initial estimated altitude, the speed change has been achieved by the time the pitchover maneuver started at point P_2, and no new computation is necessary. If the resultant altitude exceeds the initial estimate, the velocity at the initial estimated altitude is computed using the formula

$$V_f = \sqrt{2k_2 \ \Delta h/|\sin \gamma_c| + V_i^2}$$

and the altitude change computation process is iterated again. The process is considered complete when two successive altitude estimates differ by less than 1 ft.

We now have altitude-change values for both the initial and final portions of the flightpath (there is, of course, a constant flightpath angle in the middle portion of the flightpath in most cases). If, as with Case 4, the sum of the altitude changes for the initial and final parts of the interval total more than the entire altitude change desired during the interval, the value for the $\sin \gamma_c$ is reduced by multiplying by the ratio of the total altitude change desired over the sum of the initial and final altitude changes, and the resultant γ_c is used to recompute new values for the initial and final altitude changes.

When the computation of the sum of the initial and final altitude changes is completed, the altitude at the beginning of the final pitchover maneuver (ALTGAM) is computed by subtracting the final altitude change from the final altitude at the end of the interval. Thus, we now have usable values for the commanded value of the flightpath angle during the interval and the altitude at which the final pitchover maneuver must be initiated.

APPENDIX C

GENERAL DESCRIPTION OF THE QSRA ENERGY CONSERVATIVE GUIDANCE SYSTEM

The objective of the QSRA ECG system is to synthesize a flyable flightpath from the current aircraft states to some desired terminal states. Then, on command from the pilot, the system will generate the synthesized flightpath, in real time, and provide inputs to an automatic control system or flight director to enable the pilot to fly the aircraft along the synthesized path.

The guidance system is shown in block diagram form in figure C1. When the pilot engages the reference flightpath mode of the autopilot, the guidance executive initializes the guidance system. The pilot enters the capture waypoint number to start the synthesis computation. The synthesis algorithm first computes the horizontal path from the aircraft to the final waypoint and stores the results of this computation in the waypoint tables. The horizontal path is affected by the aircraft characteristics only in the magnitudes of the turning radii that may be used.

The speed-altitude profile is then found by integrating the equations of motion along the horizontal path. This is the most time-consuming part of the synthesis and the one in which energy management plays a dominant role. At each point at which a change in speed, altitude, or course begins or ends (referred to as a command point), a row of data is stored in the command table. An example command table is given in table C1. Each row in the table contains sufficient information to initialize integration in the forward direction to the next command point. Note than IVH = 0 signifies a null point and the row is skipped. As soon as the synthesis of one complete flightpath (both speed-altitude and horizontal profiles) is completed, another one is started unless the pilot engages the track mode. In the track mode, the synthesized reference flightpath is integrated forward in real time from command point to command point, and the appropriate information is generated for the flight director and the stability and control augmentation system (SCAS).

All of the operations shown in figure C1 which are inside the dashed lines must be done in "foreground"; that is, these computations have the highest priority and must be completed each computation cycle. All other computations, including most of the real-time reference flightpath generation, have lower priority and can be a background computation, wherein computations are allowed to be interrupted in one cycle and completed in subsequent cycles.

The horizontal flightpath synthesis is illustrated in figure C2. The path consists of a fixed portion specified by stored waypoints and a capture portion shown by the dashed lines. Waypoints are generally used only at the beginnings and ends of turns and at the end of the flightpath. Between each pair of waypoints airspeed, altitude, or both may change. The speed-altitude profile synthesis causes the speed and the altitude changes to terminate at various waypoints. Therefore, it may be necessary to insert additional waypoints in order to have the changes terminate where desired.

The horizontal capture flightpath takes the aircraft from its current position to one of the fixed waypoints designated by the pilot as the capture waypoint, including touchdown. The complete synthesis of an approach flightpath for the Augmentor Wing program requires from 6 to 8 sec (most of it for computing the speed-altitude profile), so it was necessary to extrapolate ahead from P_1 to P_2 (fig. C2) to provide computation time. This extrapolation was done assuming straight, constant-speed flight. The pilots, however, continually captured from turns, thus causing large initial errors. Therefore, the capture algorithm (subroutines HRZCAP and NEWPSI) was modified to allow capture from turns and from non-zero flightpath angles. The algorithm has also been modified to allow capture paths consisting of three circular arcs in addition to the turn-straight-turn paths for improved close-in path generation.

If the aircraft deviates too far from the reference (as in case of ATC vector), the pilot can disengage and recapture the fixed flightpath at a suitable waypoint. (The pilots have expressed an interest in recapturing between waypoints, but this is not included in the present implementation.) A number of other options are possible for use of the capture algorithm including holding patterns, path stretching, and go-around. Their feasibility depends on the computation time for the speed-altitude profile and the development of a suitable method for the pilot to control the system.

The speed-altitude profile is found by integrating the equations of motion forward from the aircraft along a portion of the flightpath and then backward from the final point to the point where forward integration ended. This procedure is explained in the text for a simple approach flightpath. Airport-to-airport paths would use forward integration to a waypoint near the destination runway and then backward from touchdown. This forward/backward procedure ensures the ability to reach the desired end conditions, provided the switch-over point is a sufficient distance from the final point.

Synthesis of Horizontal Path

The fixed portion of the horizontal path is specified by input constants for the cartesian coordinates; radius of turn; and maximum, minimum, and nominal equivalent airspeeds (ref. 6). The guidance system (subroutine TWOD) starts with the final waypoint and calculates the course at the preceding waypoint, the angle turned through, and the arc length or straight-line distance traversed. Then it iterates in a similar manner from waypoint to waypoint until it reaches the capture waypoint. This computation is done only once after each selection of a capture waypoint by the pilot. The capture path must be continually updated as the aircraft moves until the pilot activates the track mode.

The generation of the capture path (subroutine HRZCAP) is discussed in detail in reference 2. The resulting capture path may consist of a circular arc, followed by a straight-line segment, followed by a second circular arc, or it may be made up of three circular arcs. All of the information about the horizontal path needed for subsequent computations is stored in the waypoint tables for both the capture and fixed portions (see table C2). The first three elements of each table are used for the capture flightpath and subsequent ones are used for the fixed path. Only the numbers of the fixed waypoints are displayed to the pilot, and these numbers are reduced by three from the indices of the waypoint tables.

Speed-Altitude Profile Synthesis

An overall description of the technique is given here. The derivations of equations, a description of the sources, and manipulation of aero/propulsion data were given in appendix A.

In order to assure an acceptably flyable flightpath, certain constraints must be satisfied. These can be divided into three categories:

1. Operational constraints: maximum and minimum aerodynamic flightpath angles, maximum and minimum airspeed rates, maximum magnitude of normal acceleration, and maximum bank angle. These are input constants and may be modified by the pilot through the keyboard.

2. Geometric constraint: maximum magnitude of flightpath angle rate, changing from the initial value of γ to the commanded γ (γ_c) during the altitude change between two waypoints. If this is not possible because of γ_c being too large (fig. B1), γ_c is reduced until a sufficiently small value is found, and the altitude at which the final pitchover maneuver begins (h_γ) is computed and stored.

3. Aircraft and engine constraints: the result of limited capability of the aircraft and engines, including safety constraints. As an example, a flightpath angle meeting the constraints in (1) and (2) may not be within the flight envelope of the aircraft for a particular flight condition.

The speed-altitude profile synthesis is illustrated in block diagram form in figure C3. The speed-altitude synthesis executive (subroutine VHTSYN) transfers data for two adjacent waypoints from the waypoint tables into the synthesis algorithm (subroutine INTEG). In the discussion of the synthesis, these will be referred to as the current and next waypoints regardless of the direction of integration. Thus, for backward integration, waypoint N is the current waypoint while N-1 is the next one.

Closed-Form Equations

After the initialization in INTEG, a test is made to determine whether there is a change in the altitude between the current and next waypoints. If so, starting with an initial value of γ_c, at the maximum operational constraint discussed earlier, iteration is used to find a γ_c for which the change from the initial value of γ to γ_c and then to the final γ can be made during the specified altitude change between the waypoints (fig. B1). The altitude h_γ at which the pitchover to the final γ begins is also stored.

The next step in the synthesis is to integrate the equations of motion, usually backward in time, in order to establish the speed, altitude, and heading as functions of distance along the reference flightpath. Since the γ achieved may be limited in subroutine STPINT and not reach the γ_c computed in the closed-form solutions, the pitchover altitude is recomputed shortly before the altitude, computed by integration, reaches it. The same closed-form equations are used, but γ_c is replaced by the actual achieved value of γ, and the revised value of ALTGAM is stored for use in NOMTRJ if the integration is being carried out forward in time.

If the integration is backward in time, as is the case with most of the synthesis, the value of ALTGAM obtained from the closed-form equations will not be appropriate for the real-time (forward integration) reference flightpath computed in subroutine NOMTRJ. This can be seen from figure B1. If integration is backward from left to right, the pitchover should begin at P_2, while for forward integration (from right to left), the pitchover altitude is that at P_1. Again, the aircraft may not actually be able to achieve γ_c, so when the backward integration reaches the altitude computed for P_1 by the closed-form solution, the closed-form computation is repeated using the value of γ actually achieved. This value is stored for use in the real-time computation in subroutine NOMTRJ. The resulting γ_c is only a geometrical limit on $|\gamma|$, however, and the aircraft may be incapable of achieving it because of aircraft and/or engine constraints. For this reason, as h_γ is approached during the integration, it is recomputed using the current value of γ. There is a separate part of subroutine INTEG which computes γ_c and h_γ for this latter case.

The derivatives of the closed-form equations and a further discussion of their use are given in appendix B.

Real-Time Reference Generation

The real-time reference generation is illustrated in block diagram form in figure C4. The algorithm is divided into two phases. The first (subroutine NOMTRJ) essentially repeats the fast-time integration (but not the closed-form calculations) done in the synthesis. In this case, however, the integration is all done forward in time. The integration between successive command points is initialized from the command table. Large integration step sizes (1 or 2 sec) are used as in the synthesis. In the flight program the integration is done in background. The resulting data are stored in the 15 × 6 array, RDERIV. Each column of RDERIV corresponds to the end of one of the long integration steps. When a command point is reached, the step size is adjusted to the distance to the command point. At the command point the speed, altitude, and heading are set to the values stored in the command table.

The final step in the real-time reference generation is the integration in real time between the columns of RDERIV (entry NOMTR2). Distance is used as the independent variable, and in the flight program, the step size is set to the projection of the distance traveled by the aircraft in one frame time (currently 0.1 sec) projected on the reference path. When the distance corresponding to one of the columns of RDERIV is passed, the step size is reduced to the exact value needed and the aircraft states are corrected to the values stored in RDERIV. The remainder of the small integration step is added to the one immediately following. The horizontal cartesian coordinates are generated only in this final real-time computation, and at waypoints they are corrected to the values in the waypoint tables generated by the horizontal-path synthesis.

At some command points the synthesis may call for a step change in $\dot{V}_a/g$, which may in turn require step changes in flaps and, if $|\sin\gamma + \dot{V}_a/g|$ exceeds the limits on $\dot{E}_n$, in γ_a. These step changes are smoothed out by computing perturbations in speed, altitude, flaps, and γ_a to be added to the values from the tables for a lead distance on each side of the command point (see fig. C5). The perturbations are computed by assuming linear changes in γ_a, $\dot{V}_a/g$, and flaps over the distances needed, such that for each variable, half of the step change is achieved at the command point.

The Carrier Landing Modifications

The program has been modified to account for straight, constant-speed motion of the aircraft carrier. This is accomplished by adding a velocity which is equal in magnitude and opposite in direction to the ship velocity to the estimated winds. This is done in subroutine WINDAT for all the tabulated values of estimated winds.

This procedure results in the aircraft motion in the basic program being defined relative to the moving, ship-fixed coordinate system. As a result, the inertial flightpath angle γ_I is relative to the ship-fixed system. However, it appears desirable to limit the flightpath angle, γ_{IE}, with respect to the Earth-fixed inertial system. If we define $\bar{V}_{IE}$ as the velocity of the aircraft with respect to the Earth-fixed system, $\bar{V}_I$ as the velocity with respect to the ship-fixed system, and $\bar{V}_a$ as the true airspeed vector, then

$$V_{IE} \sin \gamma_{IE} = V_I \sin \gamma_I = V_a \sin \gamma_a \tag{C1}$$

where γ_a is the aerodynamic flightpath angle. From equation (C1),

$$\sin \gamma_a = \frac{V_{IE}}{V_a} \sin \gamma_{IE} \tag{C2}$$

Equation (C2) is used to compute the limits on $\sin \gamma_a$ from the limits on $\sin \gamma_{IE}$, which are input constants.

Now define the velocity vectors. The first set are new definitions of variables in the basic program.

$\bar{V}_a$ true airspeed vector (no change)

$\bar{V}_w$ velocity of the wind with respect to the ship (used to be with respect to Earth)

$\bar{V}_I$ velocity of aircraft with respect to ship (used to be with respect to Earth)

New variables are:

$\bar{V}_{SH}$ velocity of ship with respect to Earth

$\bar{V}_{wE}$ velocity of wind with respect to Earth (input estimated values)

$\bar{V}_{IE}$ velocity of aircraft with respect to Earth

The following are relationships beweeen the vectors

$$\left.\begin{aligned} \bar{V}_w &= \bar{V}_{wE} - \bar{V}_{SH} \\ \bar{V}_I &= \bar{V}_{IE} - \bar{V}_{SH} \end{aligned}\right\} \tag{C3}$$

or

$$\bar{V}_{IE} = \bar{V}_I + \bar{V}_{SH} \tag{C4}$$

From eqation (C4)

$$V_{IE} = \sqrt{V_I^2 + 2V_I V_{SH} \cos(HR) + V_{SH}^2} \tag{C5}$$

where HR is the course of the aircraft with respect to the ship.

REFERENCES

1. Erzberger, H.; and McLean, J. D.: Fuel-Conservative Guidance System for Powered-Lift Aircraft. Journal of Guidance and Control, vol. 4, no. 3, May 1981, pp. 253-261.

2. McLean, John D.: A New Algorithm for Horizontal Capture Trajectories. NASA TM-81186, 1980.

3. Erzberger, H.; and Lee, H. Q.: Constrained Optimum Trajectories with Specified Range. J. Aircraft, vol. 3, no. 8, Mar. 1980, pp. 78-85.

4. Stevens, V. C.; Riddle, D. W.; Martin, J. L.; and Innis, R. C.: Powered-Lift STOL Aircraft Shipboard Operations; A Comparison of Simulation, Land-Based and Sea Trial Results for the QSRA. AIAA/SETP/SFTE/SAE/IEEE/ITEA 1st Flight Testing Conference, Las Vegas, Nev., Nov. 11-13, 1981.

5. Flora, Clarence C.; Nicol, Laura E.; Marley, Arley C.; Middleton, Robin; Schaer, Donald K; and Vincent, James H.: Quiet Short-Haul Research Aircraft Phase II Flight Simulation Mathematical Model — Final Report. NASA CR-152197, 1979.

6. Kayton, Fried: Avionics Navigation Systems. John Wiley and Sons, 1969.

TABLE 1.- WAYPOINTS FOR PATH NO. 1

Waypoint No.	EPSLN	X, ft	Y, ft	Z, ft	Turn radius, ft	Nominal airspeed, kt	Maximum airspeed, kt
1	1	-59311	52166	-2000	0	140	160
2	1	-57030	50160	-2000	0	140	160
3	1	-52864	44869	-2000	9258	140	160
4	1	-41767	12440	-1200	0	140	160
5	1	-35745	7164	-1200	8033	140	160
6	1	-26127	5236	-1200	0	80	90
7	1	-17872	3582	-1200	0	65	75
8	1	0	0	-60	0	65	75

TABLE 2.- WAYPOINTS FOR PATH NO. 2

Waypoint No.	EPSLN	X, ft	Y, ft	Z, ft	Turn radius, ft	Nominal airspeed, kt	Maximum airspeed, kt
1	1	-59311	52166	-2000	0	140	160
2	1	-57030	50160	-2000	0	140	160
3	1	-52864	44869	-2000	9258	140	160
4	1	-41767	12440	-1200	0	140	160
5	1	-35745	7164	-1200	8033	140	160
6	1	-17872	3582	-1200	0	65	75
7	1	0	0	-60	0	65	75

TABLE 3.- WAYPOINTS FOR PATH NO. 3

Waypoint No.	EPSLN	X, ft	Y, ft	Z, ft	Turn radius, ft	Nominal airspeed, kt	Maximum airspeed, kt
1	1	-17872	3582	-1200	0	65	75
2	1	0	0	-60	0	65	75

TABLE 4.- WAYPOINTS FOR PATH NO. 4

Waypoint No.	EPSLN	X, ft	Y, ft	Z, ft	Turn radius, ft	Nominal airspeed, kt	Maximum airspeed, kt
1	1	-5842	1171	-919	0	65	75
2	1	0	0	-60	0	65	75

TABLE 5.- WAYPOINTS FOR PATH NO. 5

Waypoint No.	EPSLN	X, ft	Y, ft	Z, ft	Turn radius, ft	Nominal airspeed, kt	Maximum airspeed, kt
1	1	-2974	596	-919	0	65	75
2	1	0	0	-60	0	65	75

TABLE 6.- FLIGHTPATH RESULTS SUMMARY

Flight-path	Distance flown, ft	Flight time, sec	Fuel used, lb
1	95,062	747	1148
2	95,062	701	1080
3	88,254	676	1070
4	85,999	529	685
5	96,314	442	552

TABLE A1.- ENGINE PARAMETERS

Index	Gross thrust	Ambient pressure ratio	$\dot{E}_T$ constraint	Aircraft weight
1	Maximum	1.000	Maximum	Minimum
2	Maximum	.688	Maximum	Minimum
3	Maximum	.459	Maximum	Minimum
4	Minimum	1.0	Maximum	Maximum
5	Minimum	.688	Maximum	Maximum
6	Minimum	1.0	Minimum	Maximum
7	Minimum	.688	Minimum	Maximum

TABLE A2.- LIMITS ON GROSS THRUST DUE TO LIMITS ON ENGINE CORE SPEED

Mach no.	T_{GMAX}/δ_{AMB}, lb	T_{GMIN}/δ_{AMB}, lb
0	25,400	8,200
.1	25,400	8,200
.2	27,000	9,100
.3	29,520	10,900

TABLE A3.- T_G/δ_{AMB} VERSUS $N_1/\sqrt{\theta_2}$ AND MACH NO. (ONE ENGINE)

$N_1/\sqrt{\theta_2}$	M = 0	M = 0.1	M = 0.2	M = 0.3
80	4416	4539	4824	5235
82	4700	4823	5094	5507
84	4984	5108	5364	5839
86	5268	5392	5659	6172
88	5559	5697	5981	6504
90	5878	6014	6303	6837
92	6197	6332	6625	7167
94	6516	6650	6947	7499

TABLE C1.- SAMPLE COMMAND TABLE WITH COMPUTER-VARIABLE DEFINITIONS

IWPT	IVH	KCOR	T	D	GAMMA	VADTG	FLAPS	PHID	ALTS	VIASS	DLPHI	DLFAC
1	5	1	298.9	50000.0	0.00	0.00	0.00	0.00	500.00	236.60	47794	48252
1	0	4	288.9	47793.9	0.00		0.00		0.00	0.00	47794	48252
1	0	0	288.9	47793.9	0.00		0.00		0.00	0.00	47794	48252
1	0	0	288.9	47793.9	-0.04		0.00		0.00	0.00	47794	48252
2	2	0	288.9	47793.9	0.03		-59.00		500.00	236.60	39696	40797
2	0	1	249.1	39695.6	0.00		0.00		500.00	202.80	39696	39696
2	5	1	249.1	39695.6	0.00		0.00		500.00	202.80	14739	14739
2	1	1	115.4	14738.6	0.01	-0.04	65.97		500.00	202.80	9516	10552
3	0	0	84.6	9516.0	0.00	0 00	0.00		0.00	0.00		9516
3	0	0										
3	0	0										
3	0	0										
8	0	0										
8	0	0										
8	3	0			-0.05		0.66		996.76	169.00	8405	8705
8	1	1	77.5	8404.8	0.05	-0.03	-12.41		917.17	169.00	3800	3919
9	0	0	40.6	3800.0	0.00	0.00	0.00		0.00	0.00	3800	3800
9	0	0	40.6	3800.0	0.00	0.00	0.00		0.00	0.00	3800	3800
9	0	0	40.6	3800.0	0.00	0.00	0.00		0.00	0.00	3800	3800
9	3	0	40.6	3800.0	0.00	0.00	0.00		600.35	111.54	0	0

Variable definitions:

IWPT Waypoint number

IVH Defined quantity (in INTEG) showing type of flightpath change:
- 0 - null point, no change in state
- 1 - speed and altitude changing
- 2 - speed only changing
- 3 - altitude only changing
- 4 - constant speed level turn
- 5 - constant speed, straight and level flight

KCOR Flag used to correct integrated path to correspond to horizontal capture path

T Time to go to touchdown

D Distance to touchdown

GAMMA Aerodynamic flightpath angle

VADTG Airspeed rate in g's

FLAPS Sum of outboard and USB flap settings

PHID Bank angle at command point

ALTS Altitude at command point

VIASS Indicated airspeed at command point

DLPHI Distance at which roll command changes (includes lead distance)

DLFAC Distance at which flaps and $\dot{V}_a/g$ change (includes lead distance)

TABLE C2.- SAMPLE WAYPOINT TABLE WITH COMPUTER-VARIABLE DEFINITIONS

	XP	YP	DELD	D	R	H	XQ	YQ	TURN	VNOM	VMAX	VMIN
1	-47794.0	0.0	0.0	0.0	0.0	0.0000	-47794.0	0.0	0.0000	120.0000	160.0000	140.0000
2	-9516.0	0.0	0.0	38277.9	0.0	0.0000	-9516.0	0.0	0.0000	120.0000	160.0000	140.0000
3	-9516.0	0.0	0.0	0.0	3111.9	0.0000	-9516.0	0.0	0.0000	100.0000	100.0000	0.0000
4	0.0	0.0	0.0	0.0	0.0	0.0000	5484.0	-9500.0	0.0000	140.0000	160.0000	0.0000
5	5484.2	-9499.9	7330.3	0.0	7000.0	2.0944	-578.0	-6000.0	1.0472	100.0000	100.0000	0.0000
6	-9516.0	-6000.0	0.0	8938.0	0.0	3.1416	-9516.0	-6000.0	0.0000	100.0000	100.0000	0.0000
7	-9516.0	-6000.0	9424.8	0.0	3000.0	3.1416	-9516.0	0.0	-3.1416	100.0000	100.0000	0.0000
8	-3800.0	0.0	0.0	5716.0	0.0	0.0000	-3800.0	0.0	0.0000	66.0000	75.0000	0.0000
9	0.0	0.0	0.0	3800.0	0.0	0.0000	0.0	0.0	0.0000	66.0000	75.0000	0.0000
10						0.0						

(Note: the following part of the waypoint table appears with the command table printout after the trajectory synthesis)

IWPT	ALTGAM	GAMC	EPSLN
1	500.00	0.0000	1.0000
2	905.90	0.1184	1.0000
3	500.00	-0.1115	0.0000
4	0.00	0.0000	1.0000
5	0.00	0.0000	1.0000
6	0.00	0.0000	1.0000
7	0.00	0.0000	1.0000
8	616.43	-0.1115	1.0000
9	173.29	-0.1109	1.0000
10	0.00	0.0000	0.0000
11	0.00	0.0000	0.0000
12	0.00	0.0000	0.0000

Variable Definitions:

(XP, YP): Coordinates at beginning of turn
DELD: Arc length of turn
D: Straight-line distance from previous waypoint
R: Radius of turn (with waypoint at end of turn)
H: Heading at waypoint (point Q)
(XQ, YQ): Coordinates at end of turn
TURN: Angle turned through
VNOM: Nominal equivalent airspeed
VMAX: Maximum equivalent airspeed
VMIN: Minimum equivalent airspeed
ALTGAM: Pitchover altitude
GAMC: Commanded value of gamma for waypoint
EPSLN: Priority index for energy apportionment between $\dot{V}/g$ and γ:
$\varepsilon = 0.0$ priority on γ
$\varepsilon = 0.5$ equal priority between $\dot{V}/g$ and γ
$\varepsilon = 1.0$ priority on $\dot{V}/g$

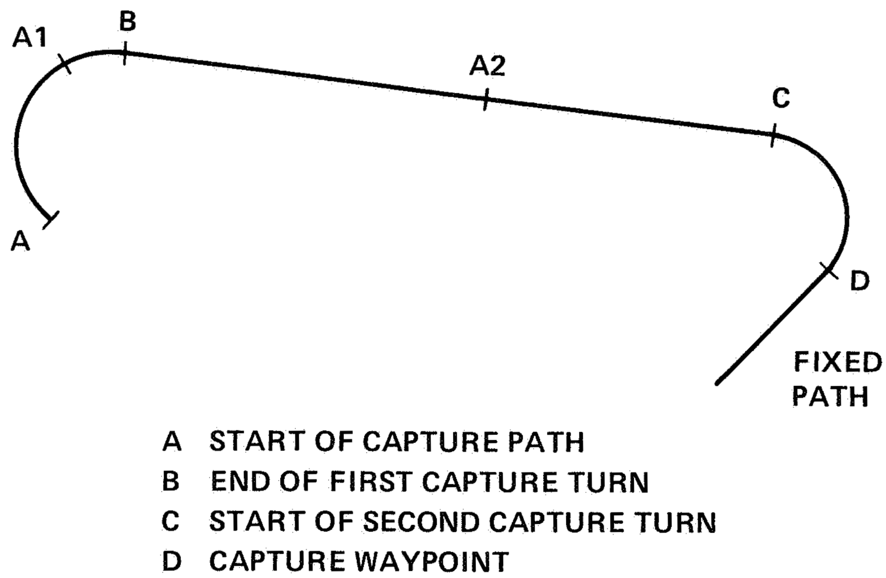

Figure 1.- Horizontal profile of capture trajectory.

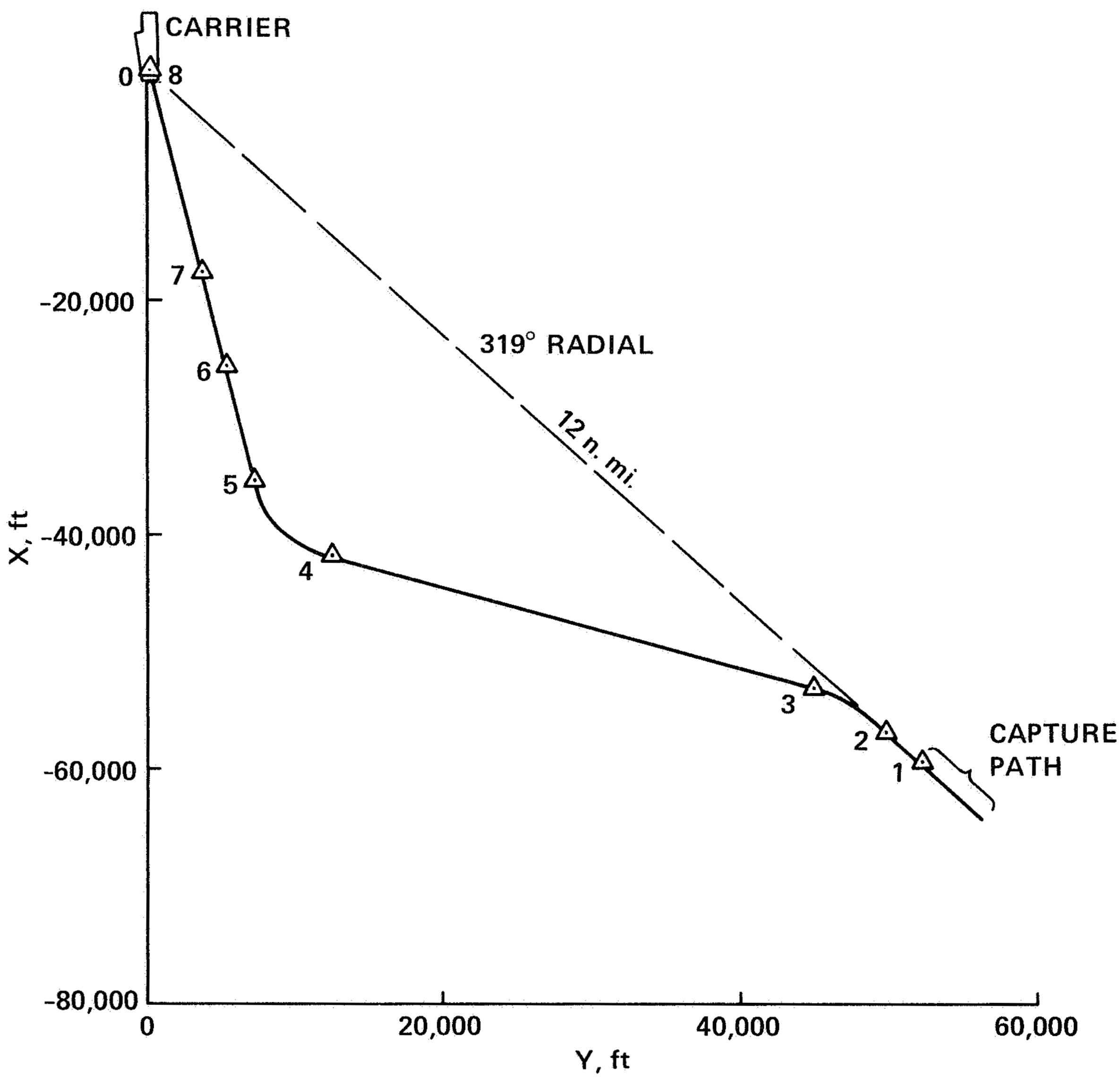

Figure 2.- Path No. 1 horizontal profile with waypoints.

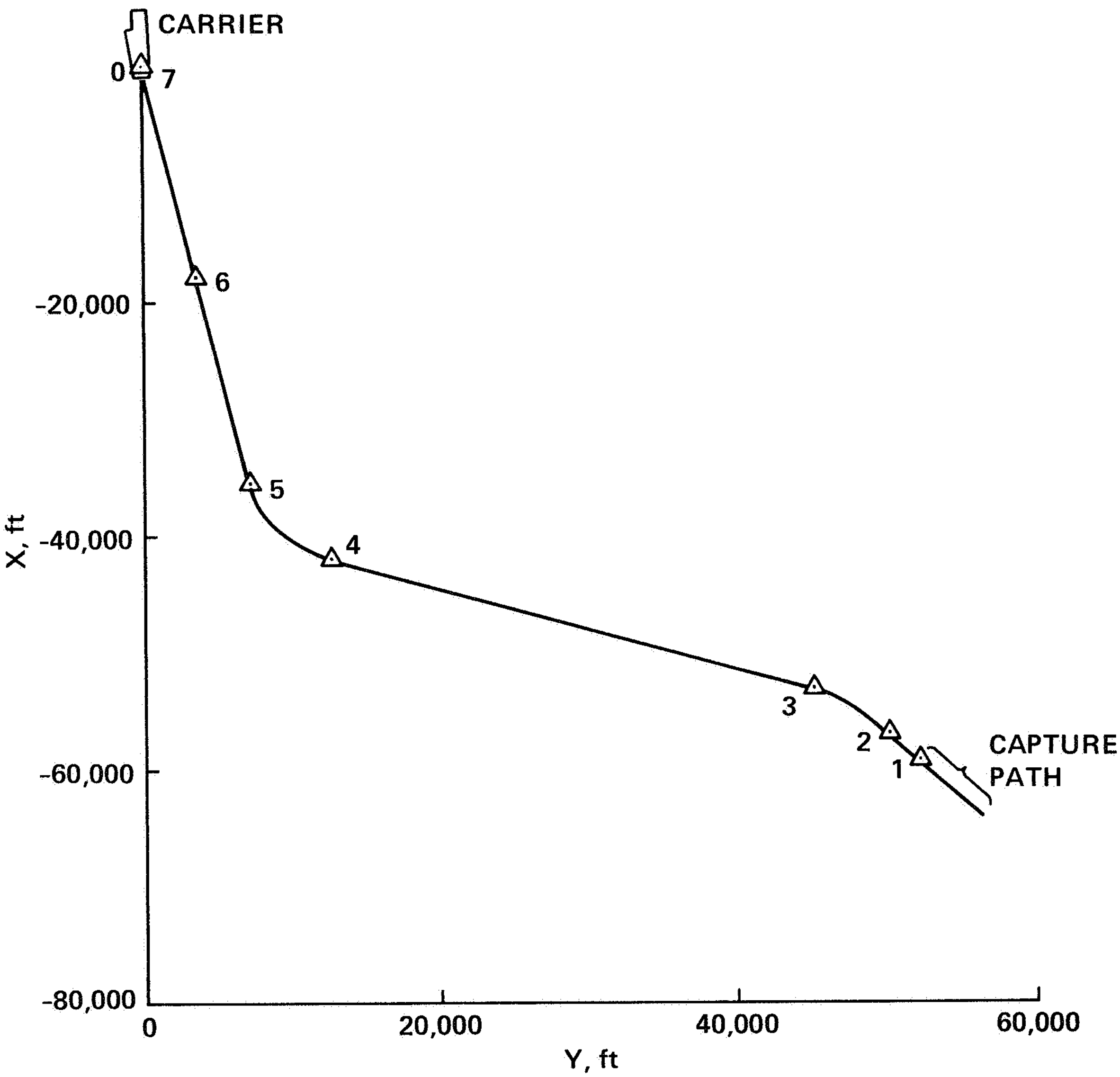

Figure 3.- Path No. 2 horizontal profile with waypoints.

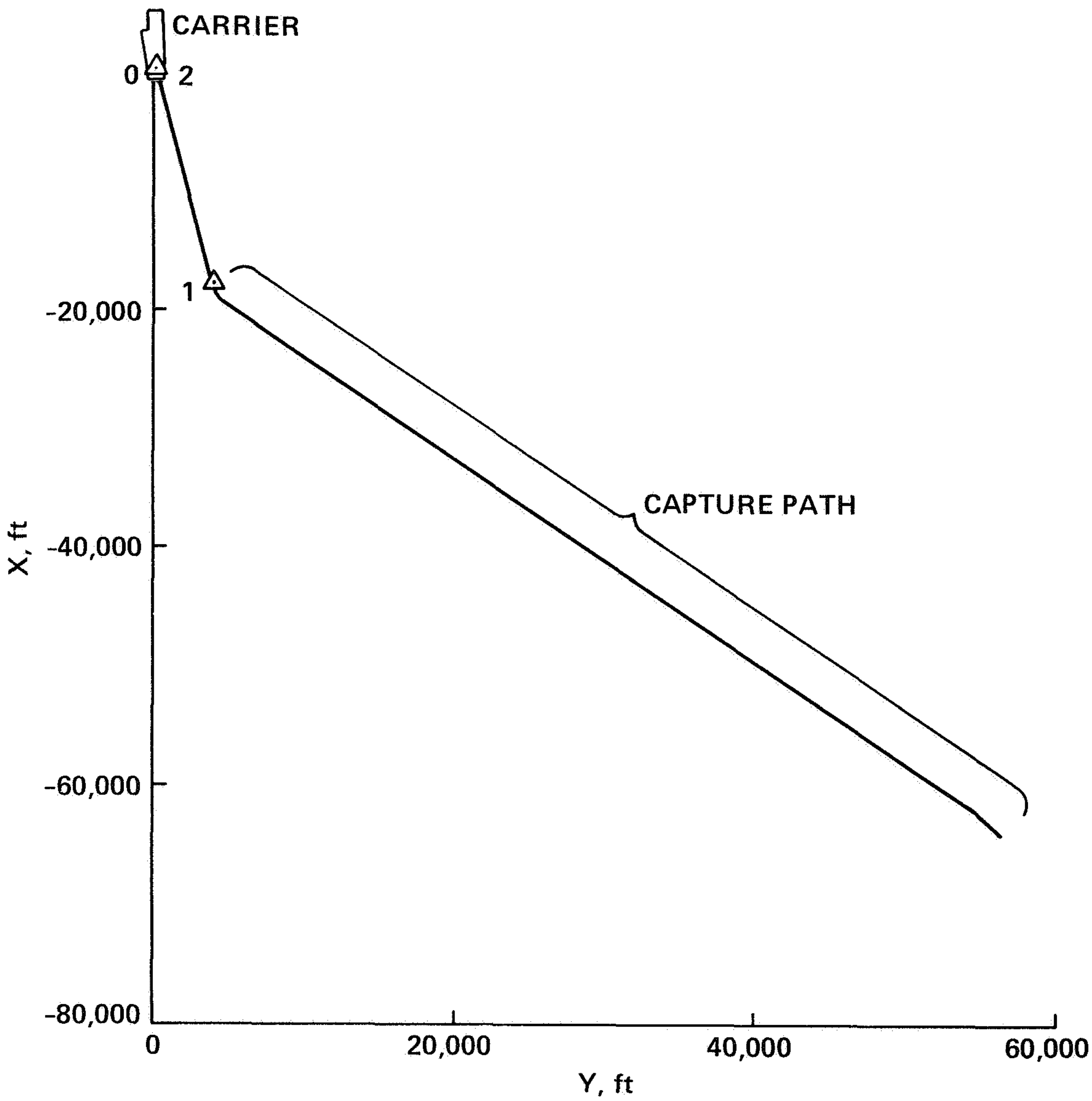

Figure 4.- Path No. 3 horizontal profile with waypoints.

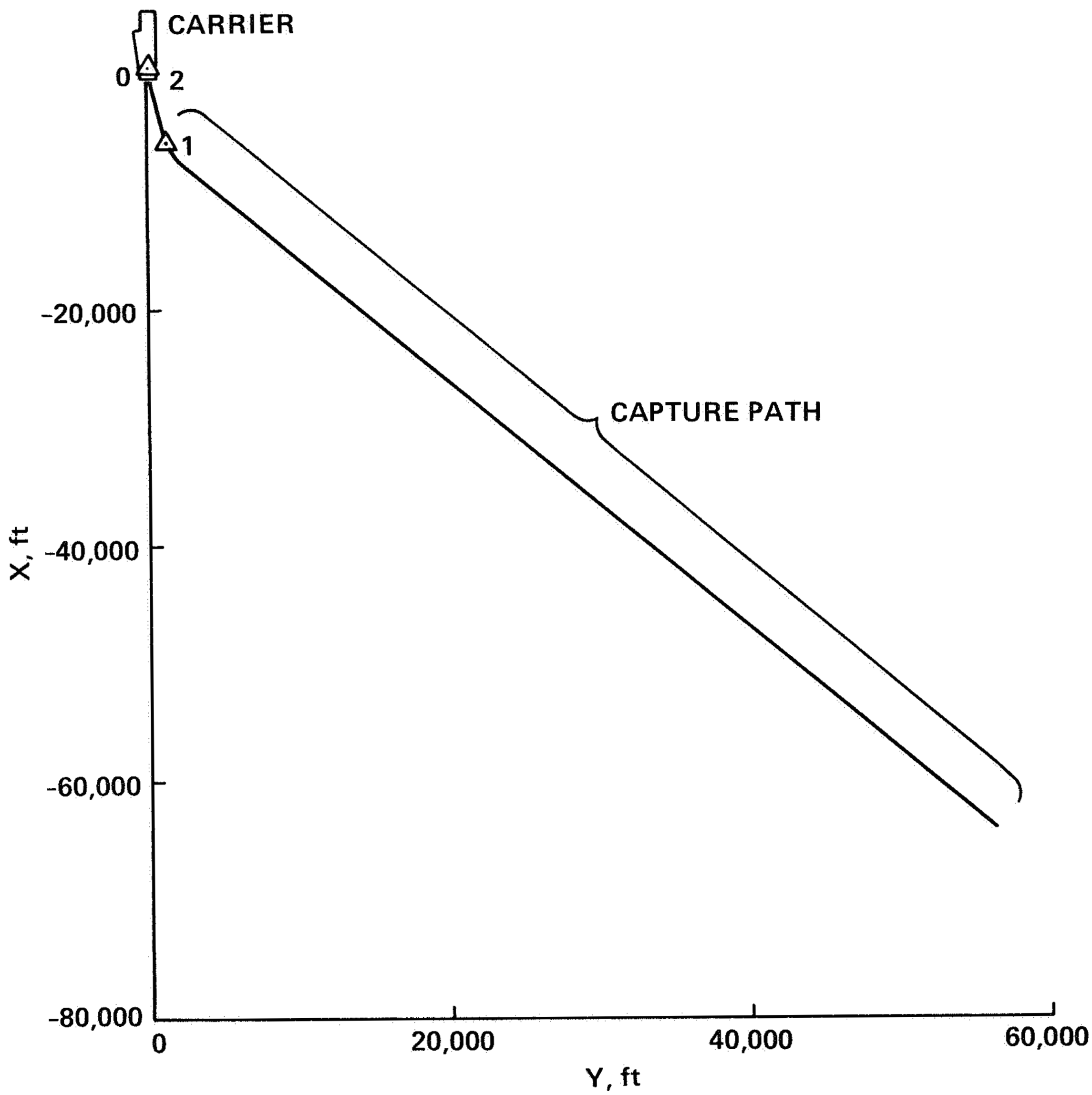

Figure 5.- Path No. 4 horizontal profile with waypoints.

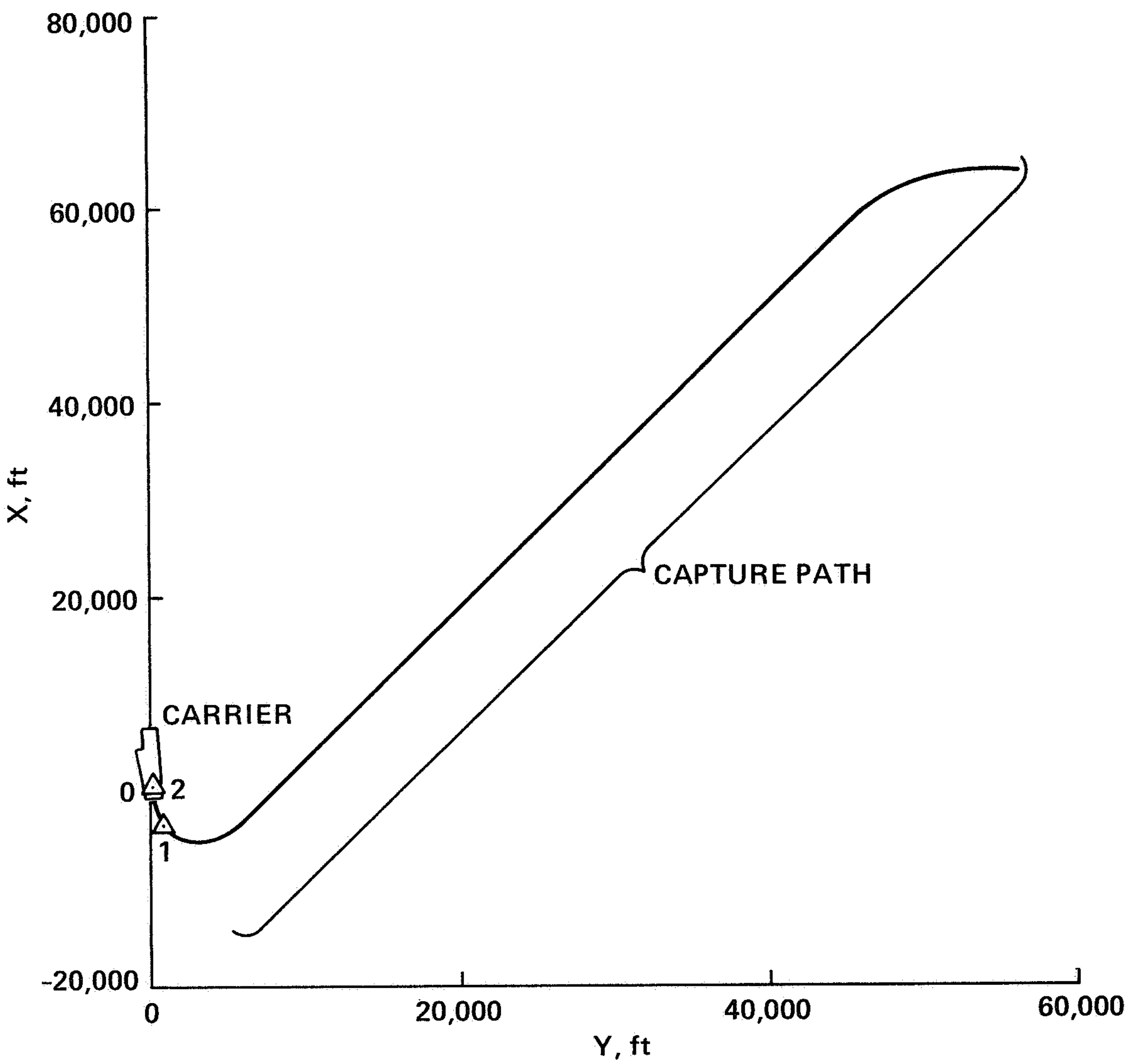

Figure 6.- Path No. 5 horizontal profile with waypoints.

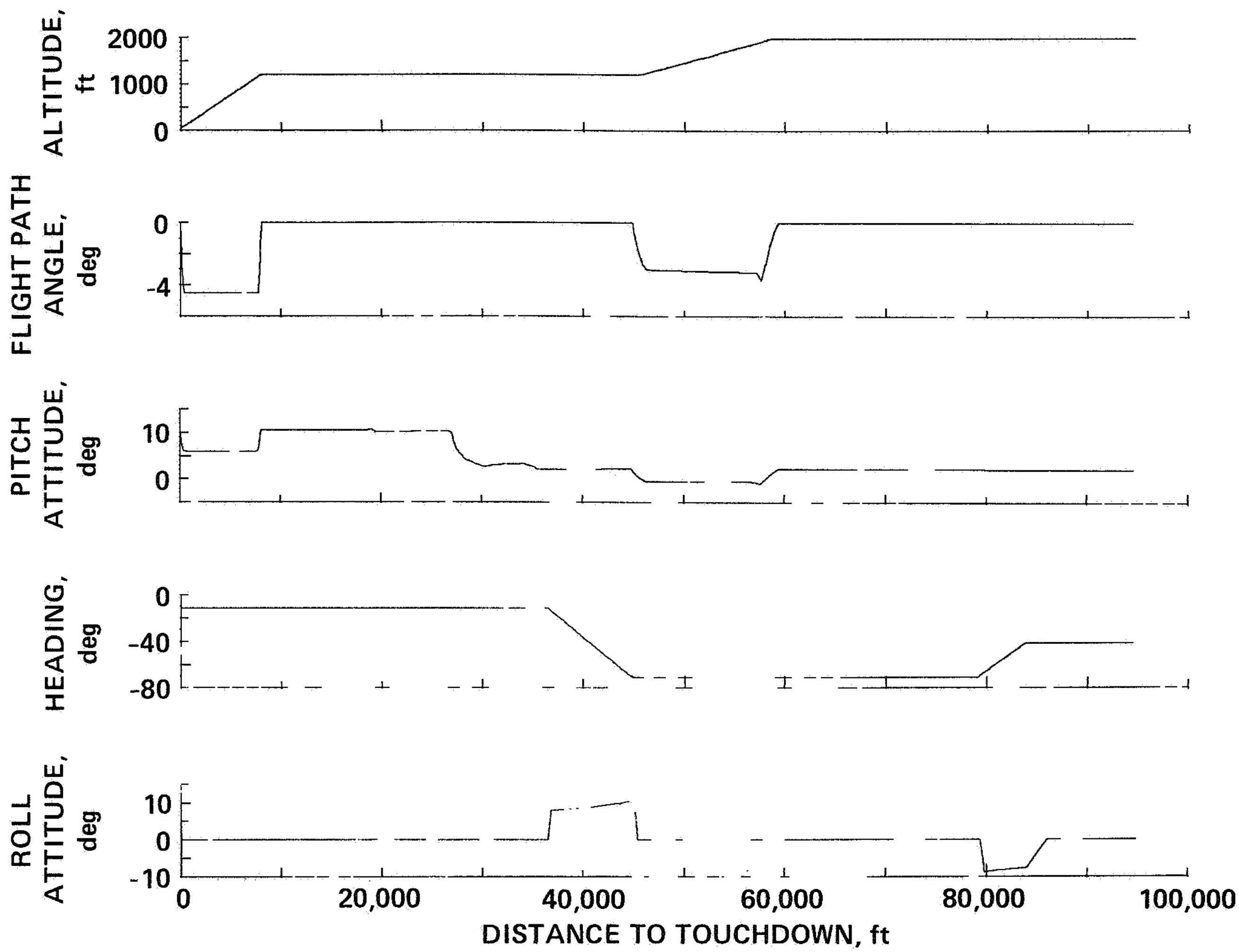

Figure 7.- Synthesized data for Path No. 1.

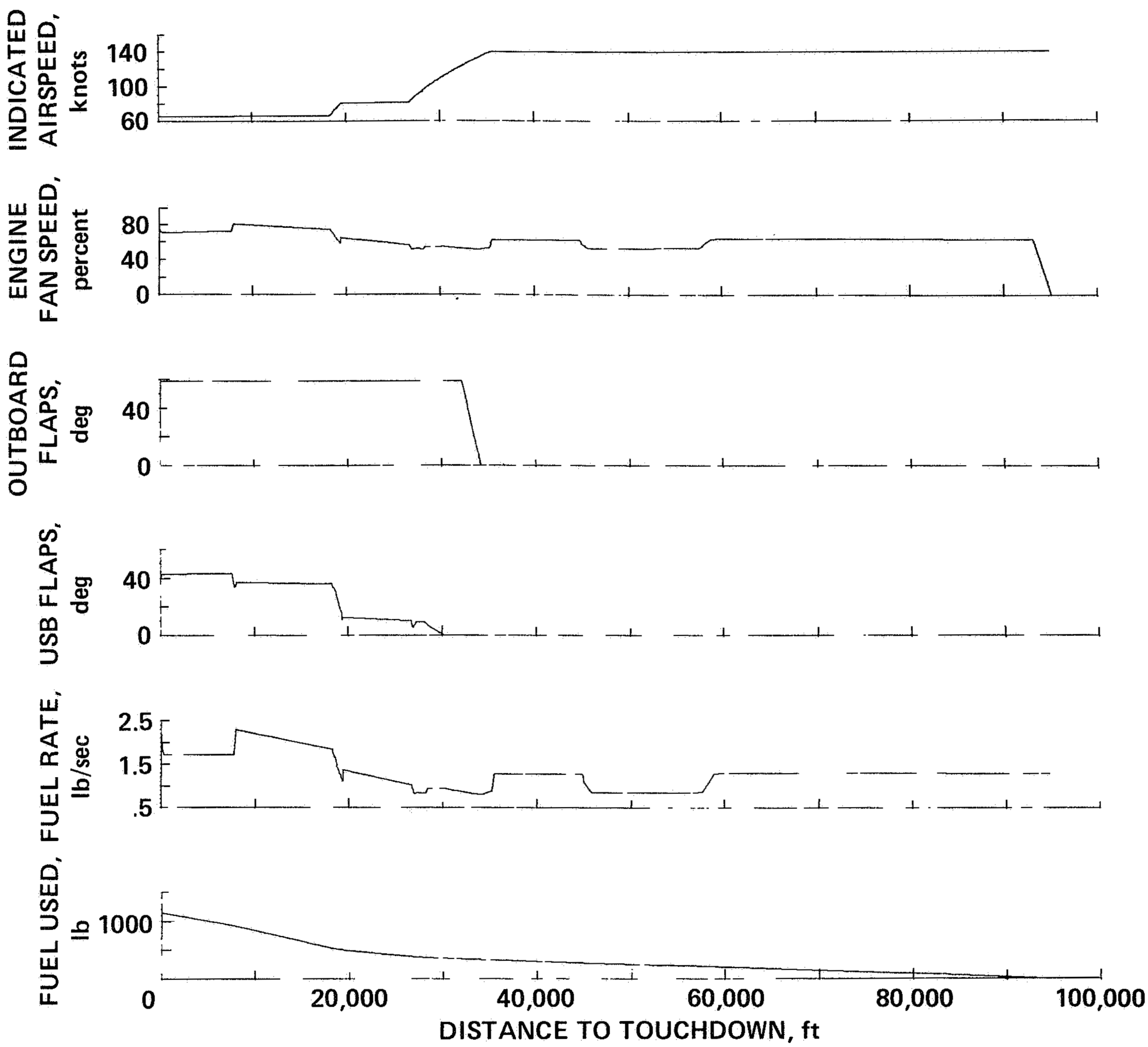

Figure 7.- Concluded.

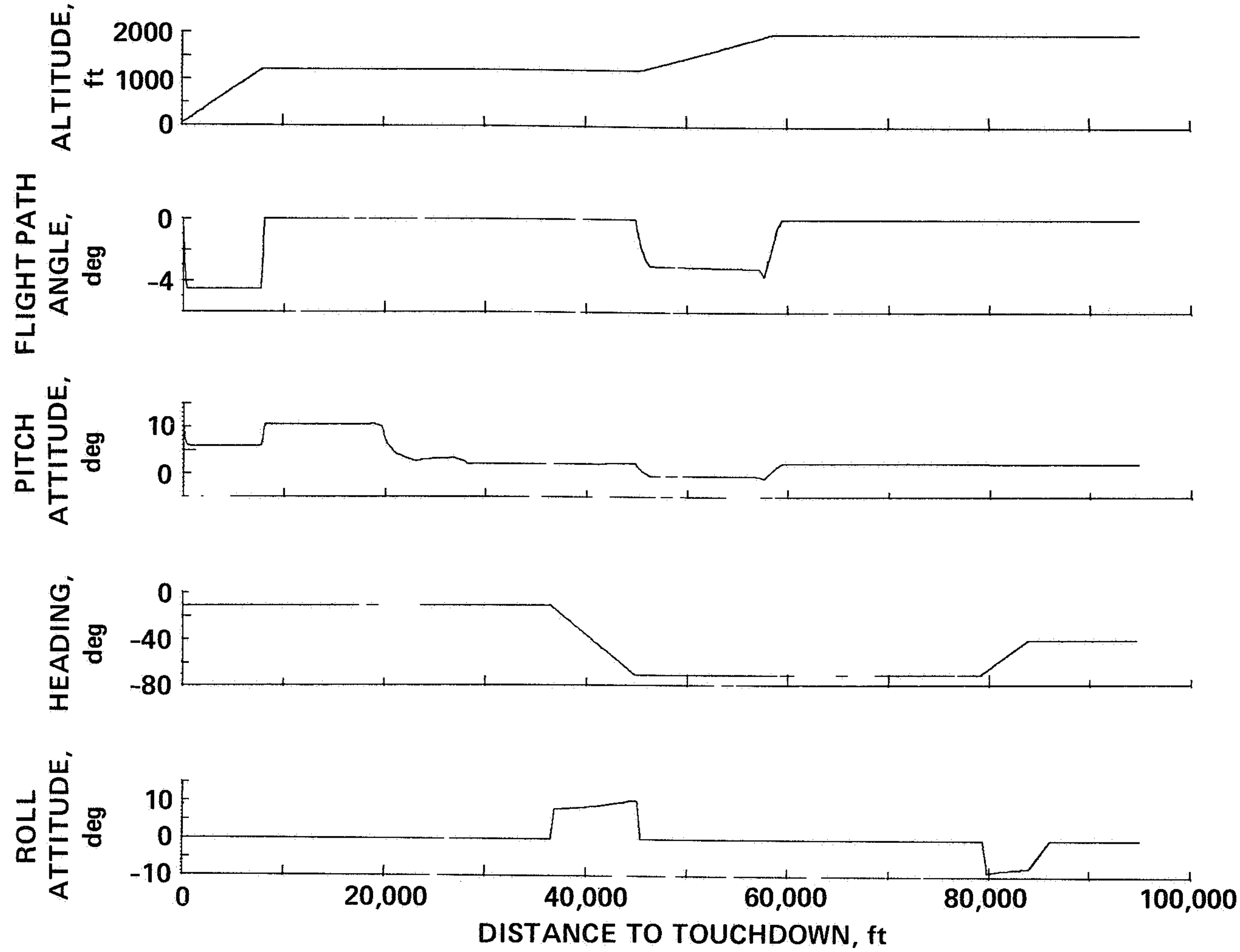

Figure 8.- Synthesized data for Path No. 2.

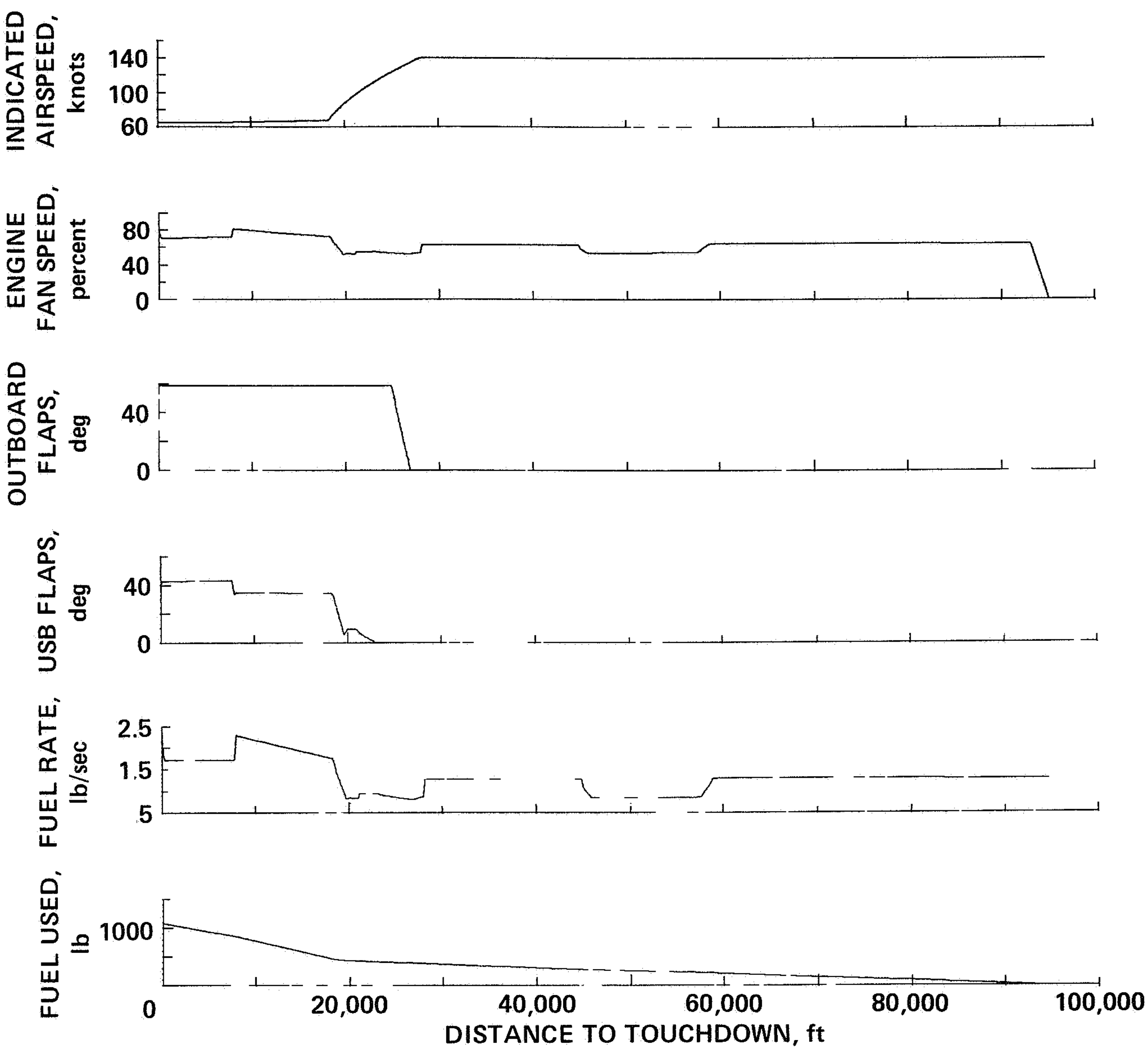

Figure 8.- Concluded.

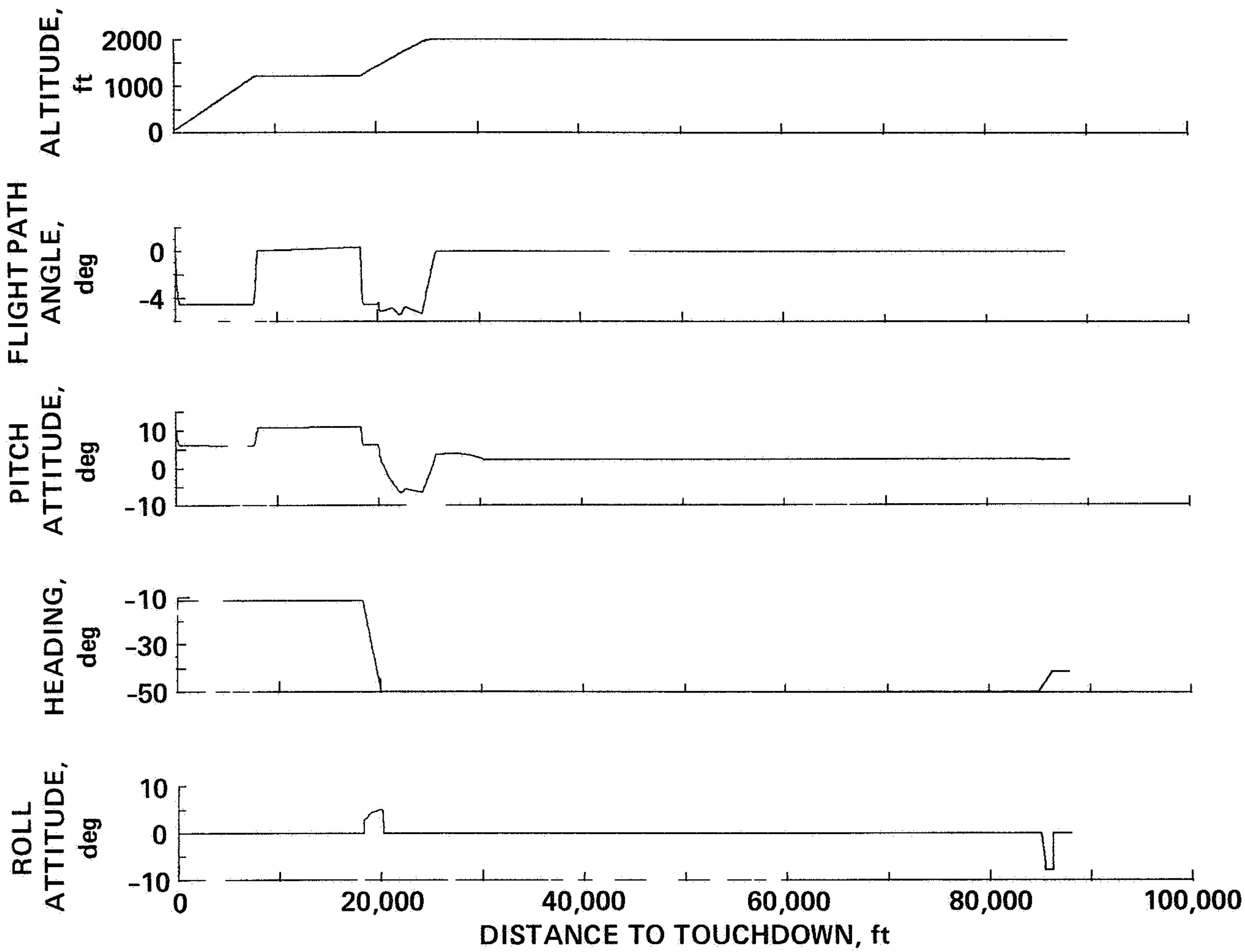

Figure 9.- Synthesized data for Path No. 3.

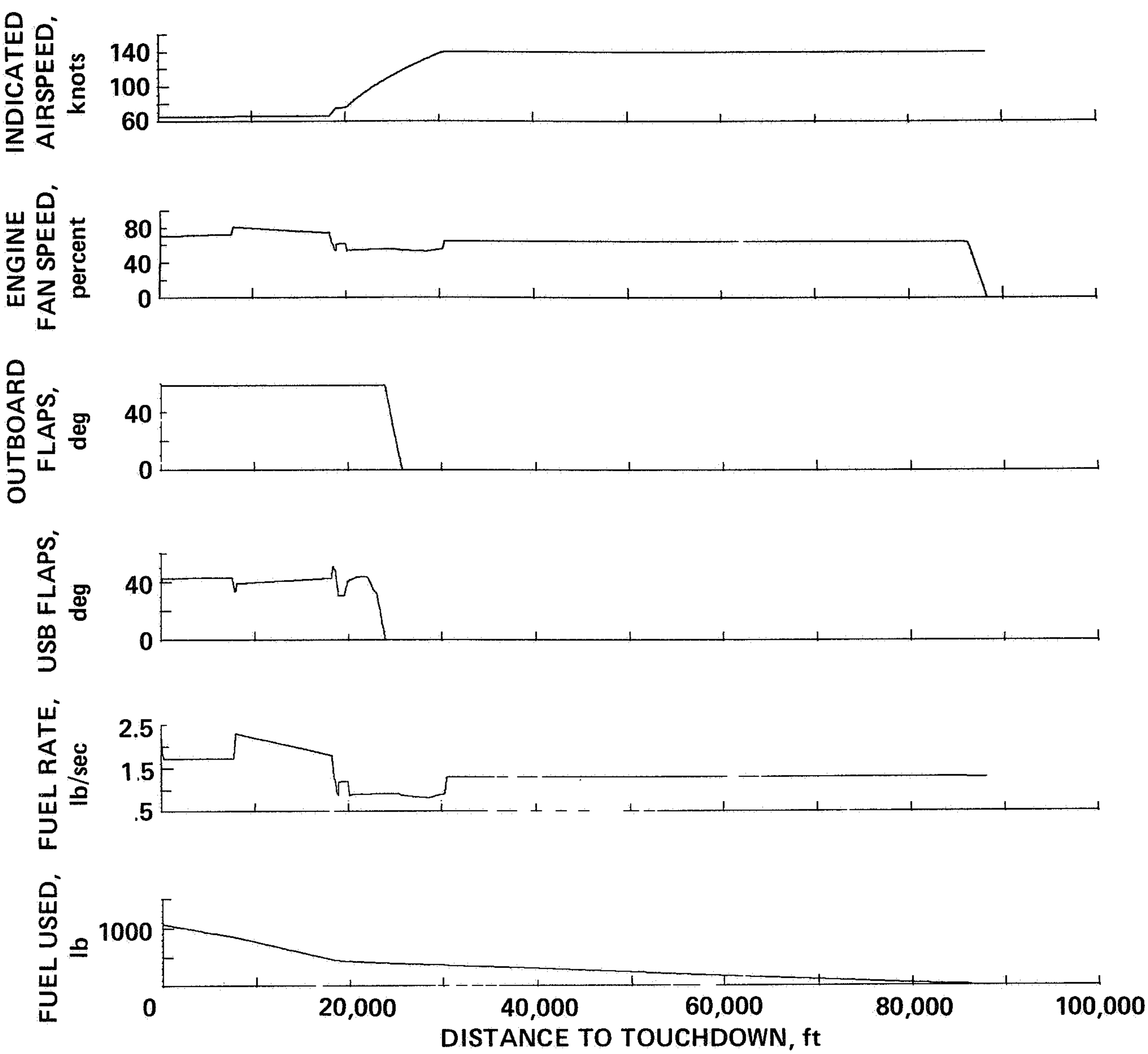

Figure 9.- Concluded.

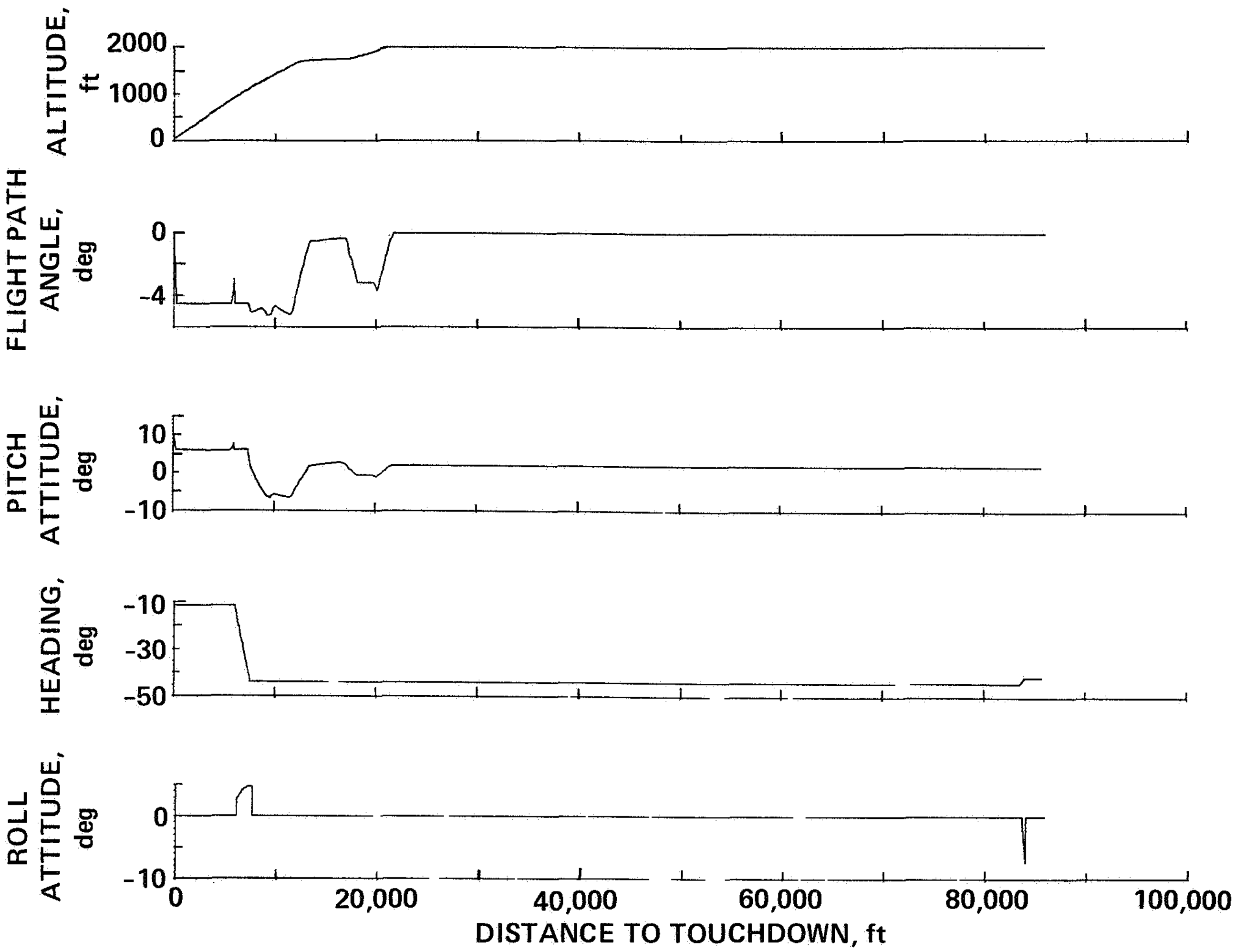

Figure 10.- Synthesized data for Path No. 4.

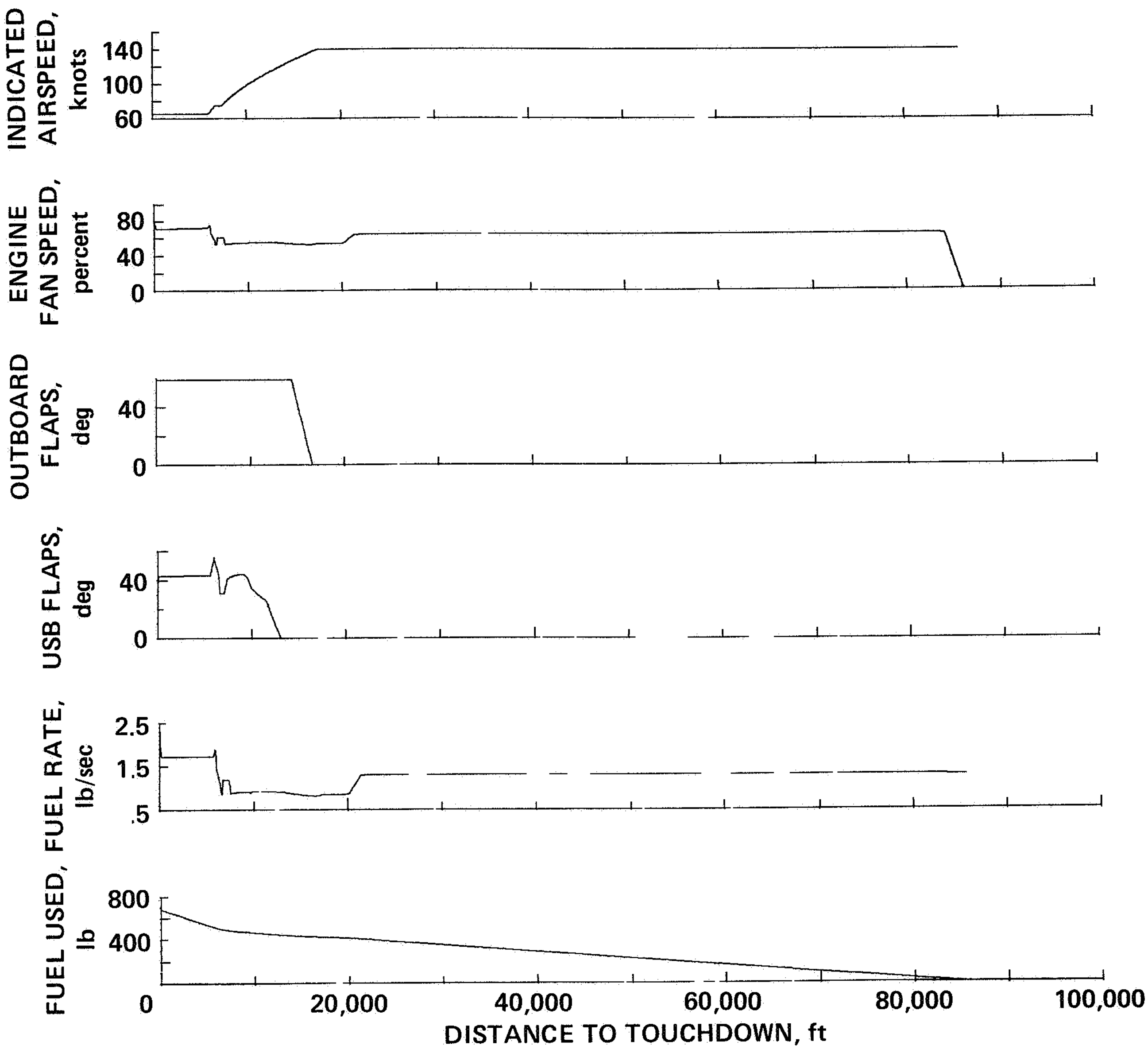

Figure 10.- Concluded.

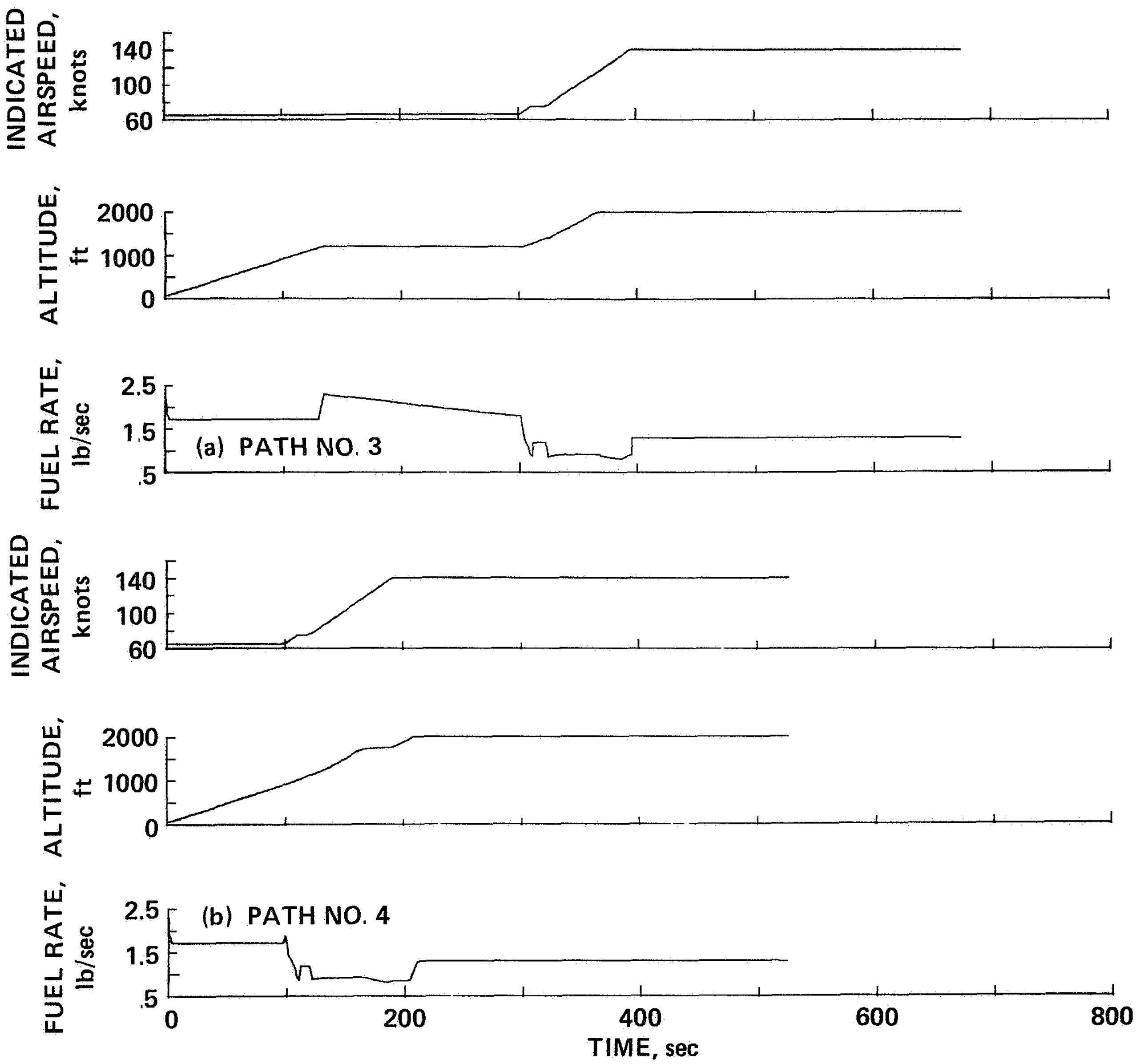

Figure 11.- Fuel usage comparison.

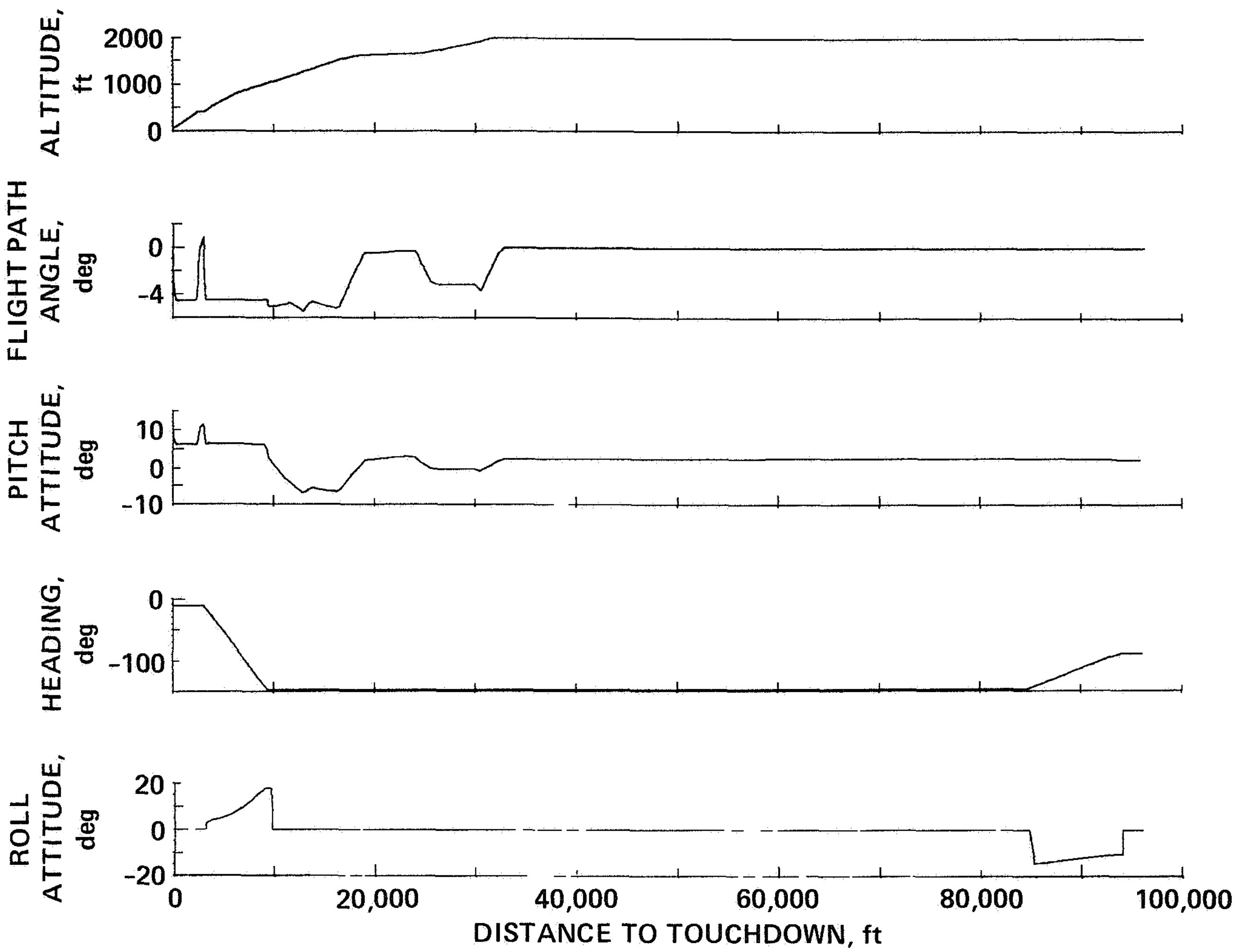

Figure 12.- Synthesized data for Path No. 5.

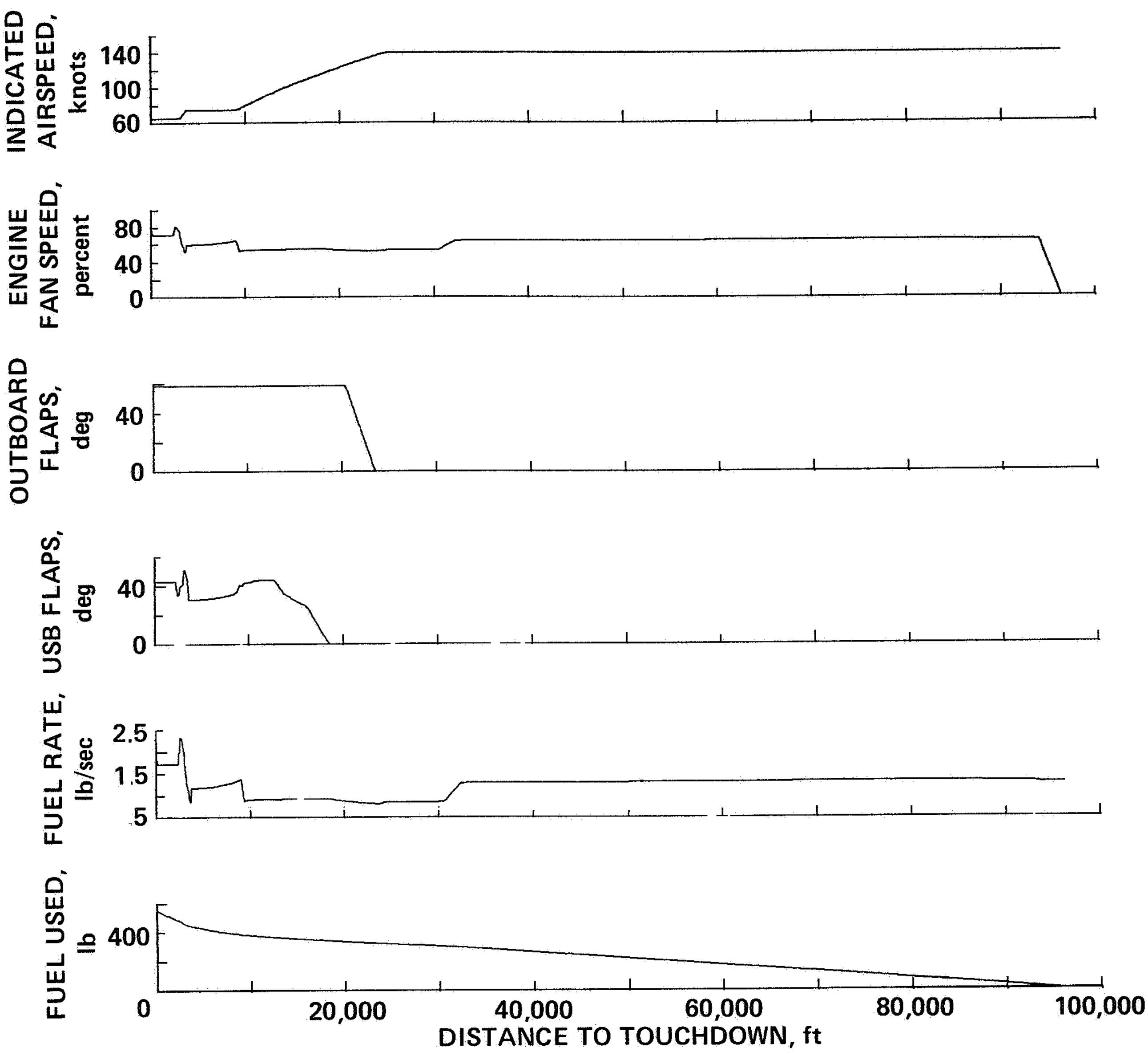

Figure 12.- Concluded.

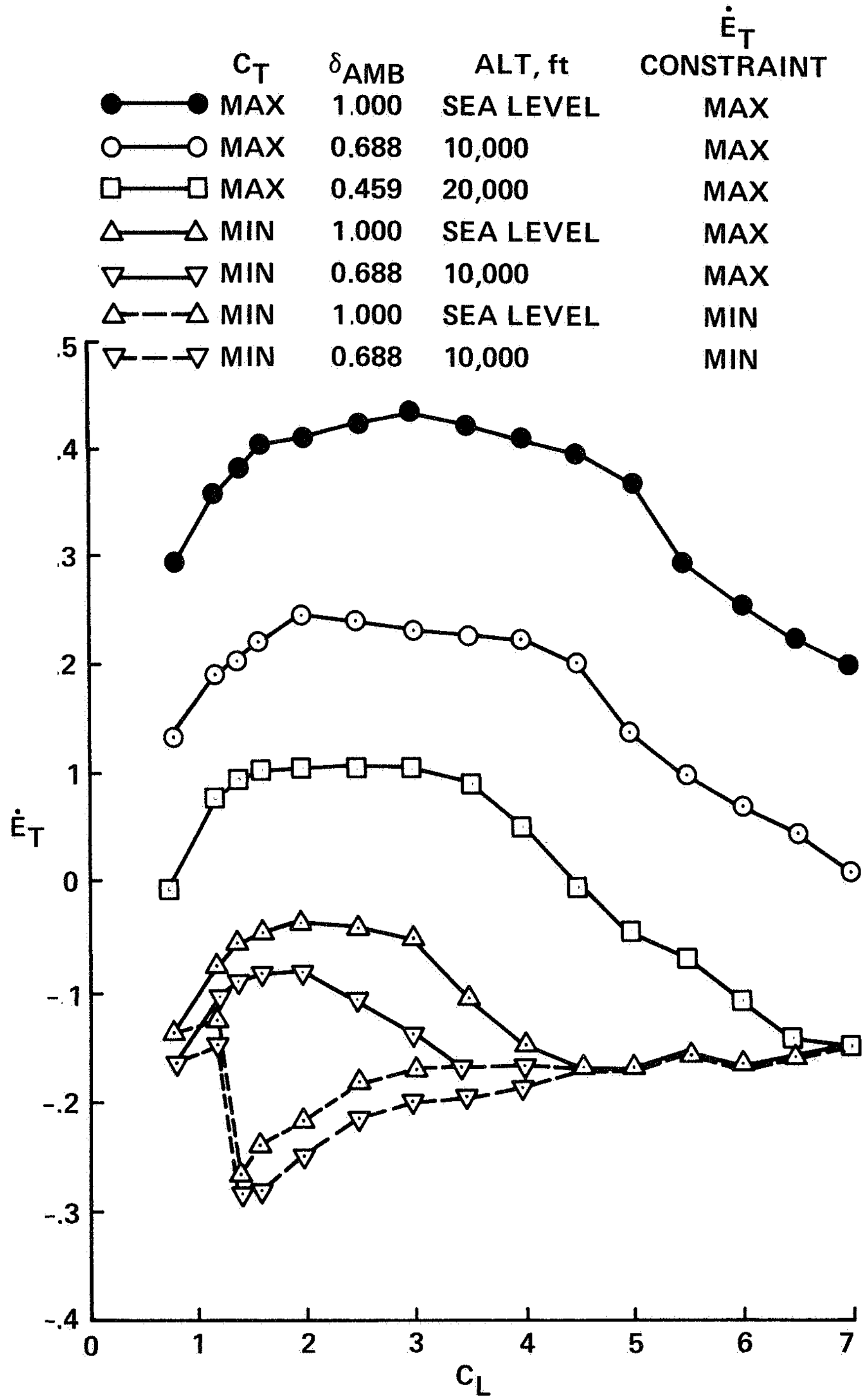

Figure A1.- Total energy rate ($\dot{E}_T$) versus lift coefficient (C_L).

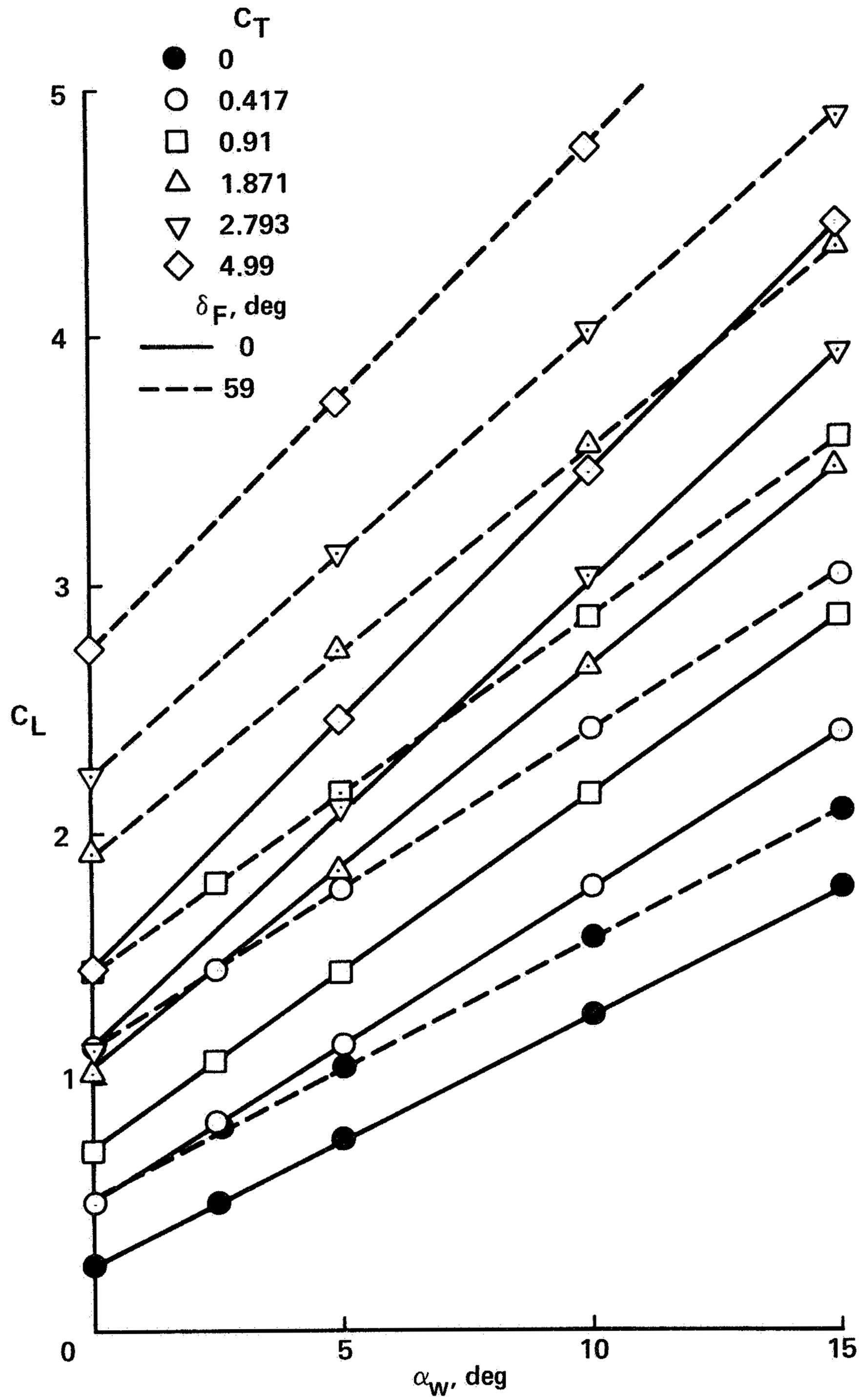

(a) Lift coefficient (C_L) versus wing angle of attack (α_w).

Figure A2.- Constant thrust coefficient (C_T).

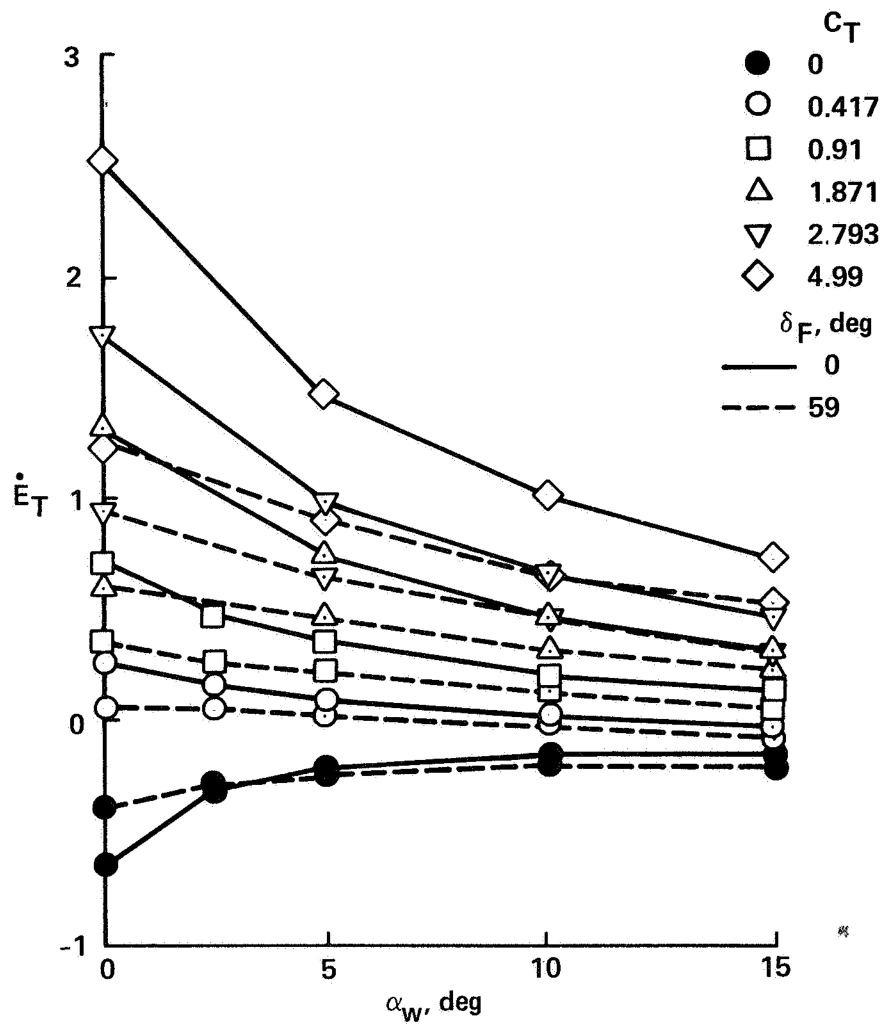

(b) Total energy rate ($\dot{E}_T$) versus wing angle of attack (α_w).

Figure A2.- Concluded.

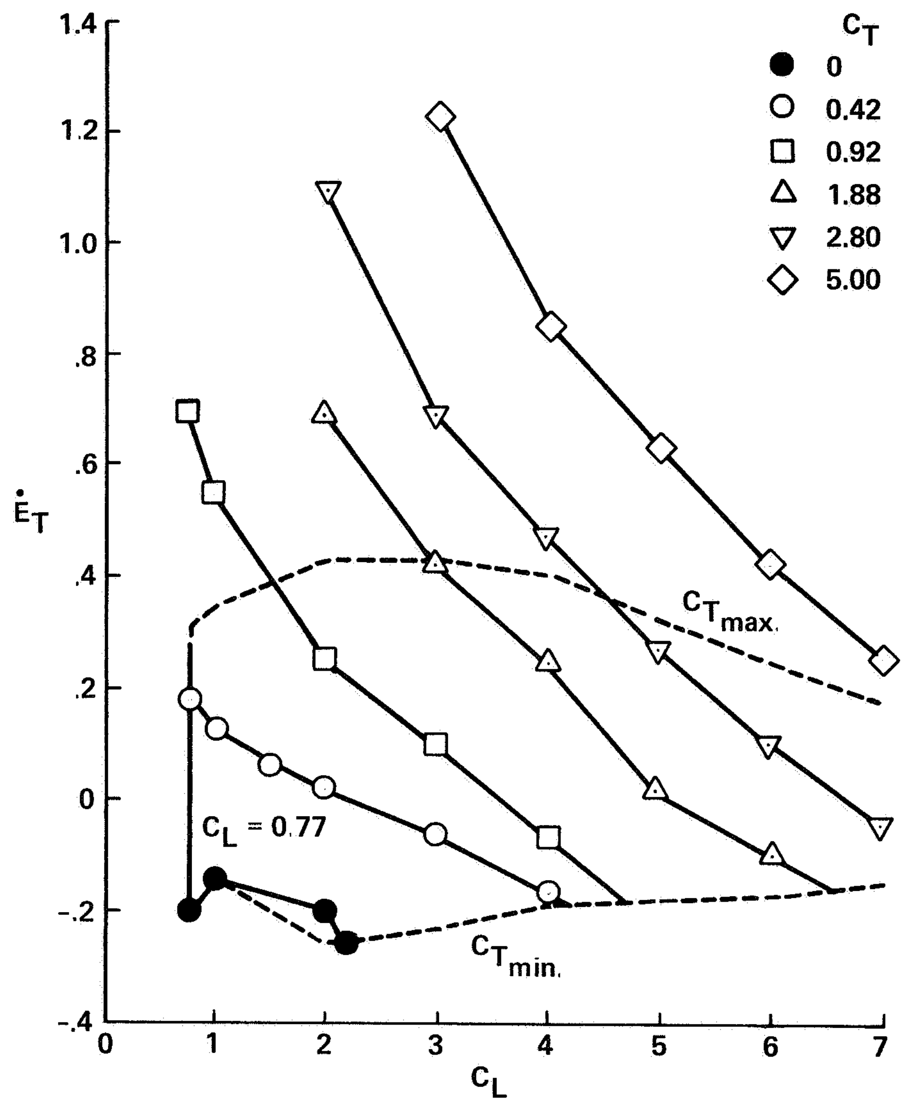

(a) Total energy rate ($\dot{E}_T$) versus lift coefficient (C_L).

Figure A3.- Constant thrust coefficient (C_T).

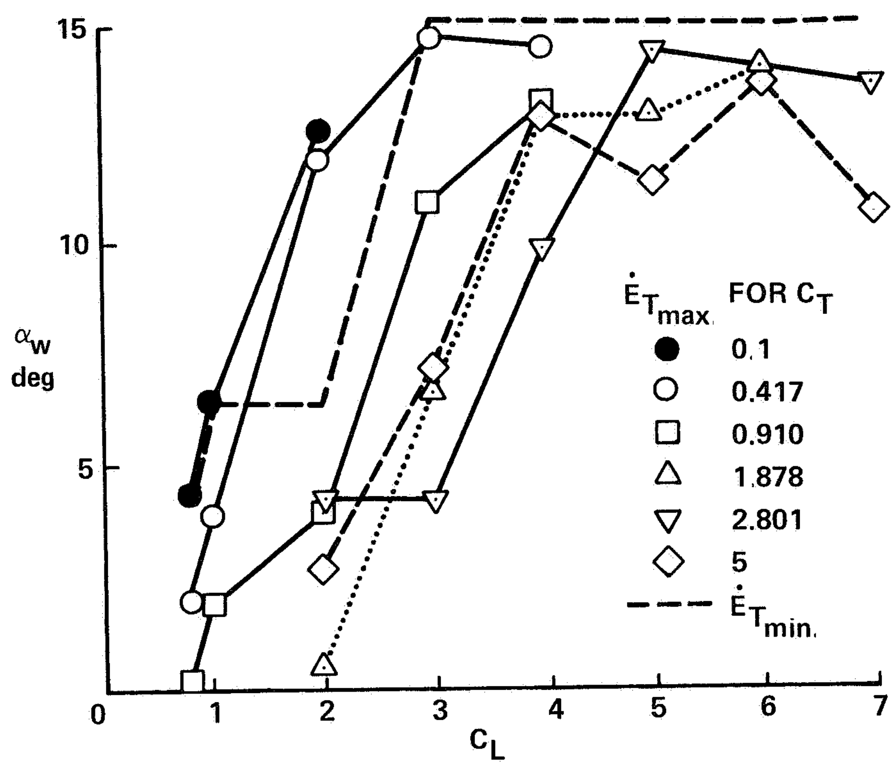

(b) Wing angle of attack (α_w) versus lift coefficient (C_L).

Figure A3.- Continued.

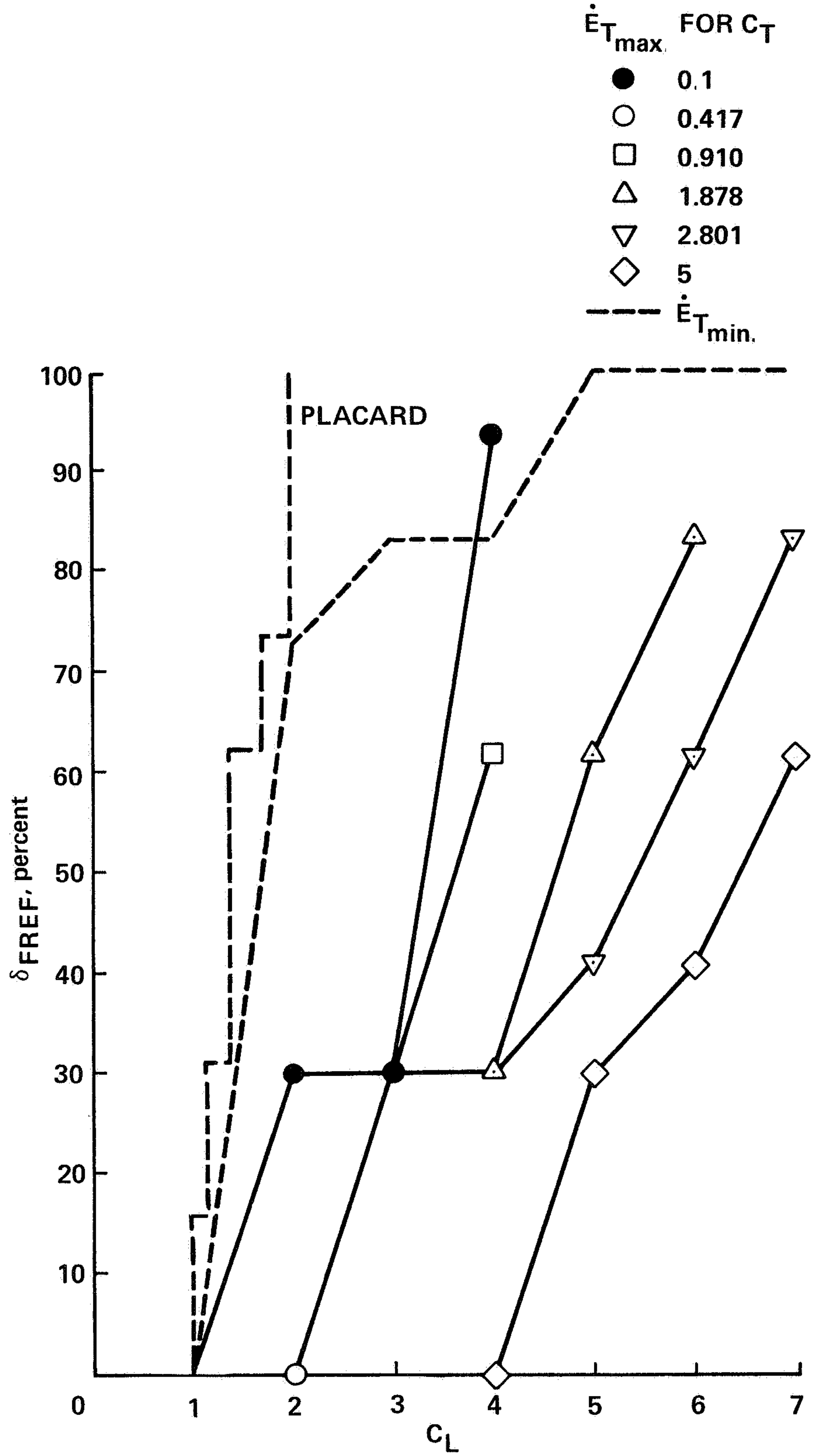

(c) Flap setting (δ_{FREF}) versus lift coefficient (C_L).

Figure A3.- Concluded.

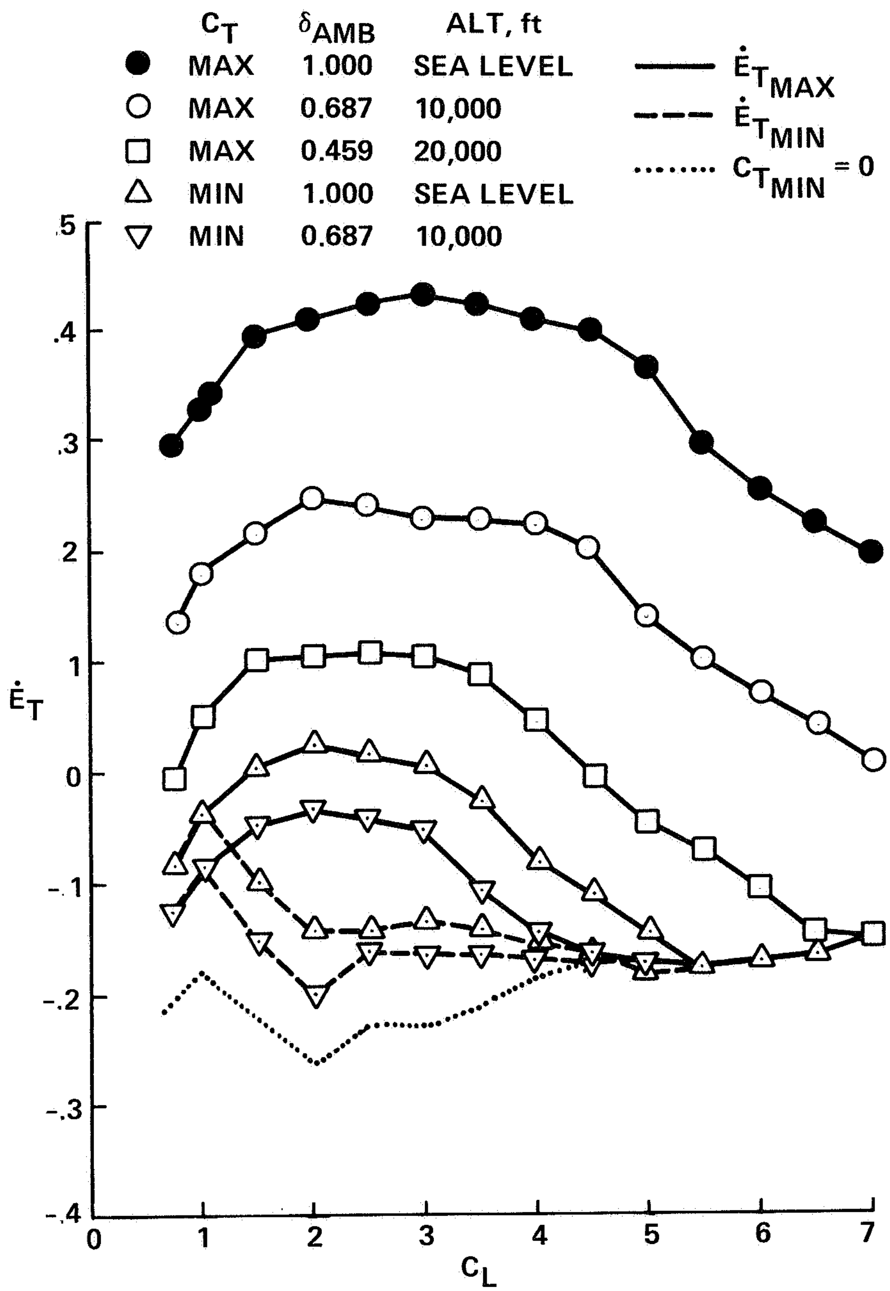

(a) Total energy rate ($\dot{E}_T$) versus lift coefficient (C_L).

Figure A4.- Constant thrust coefficient (C_T).

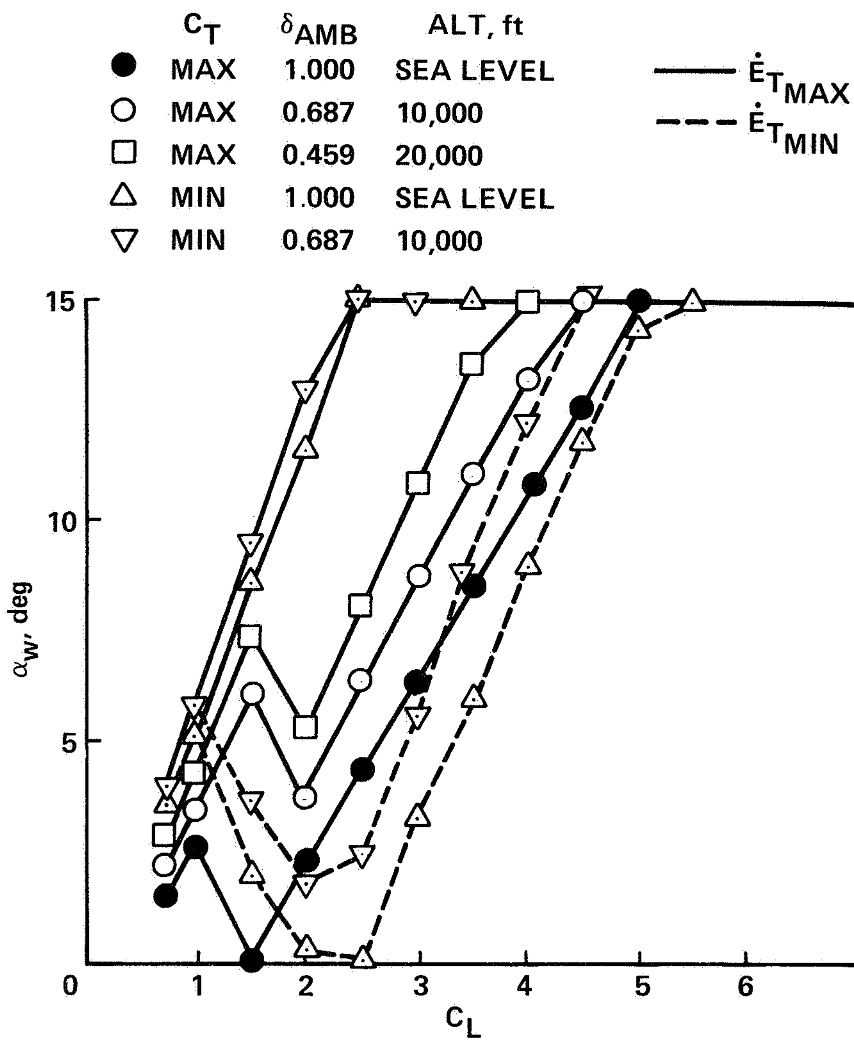

(b) Wing angle of attack (α_w) versus lift coefficient (C_L).

Figure A4.- Continued.

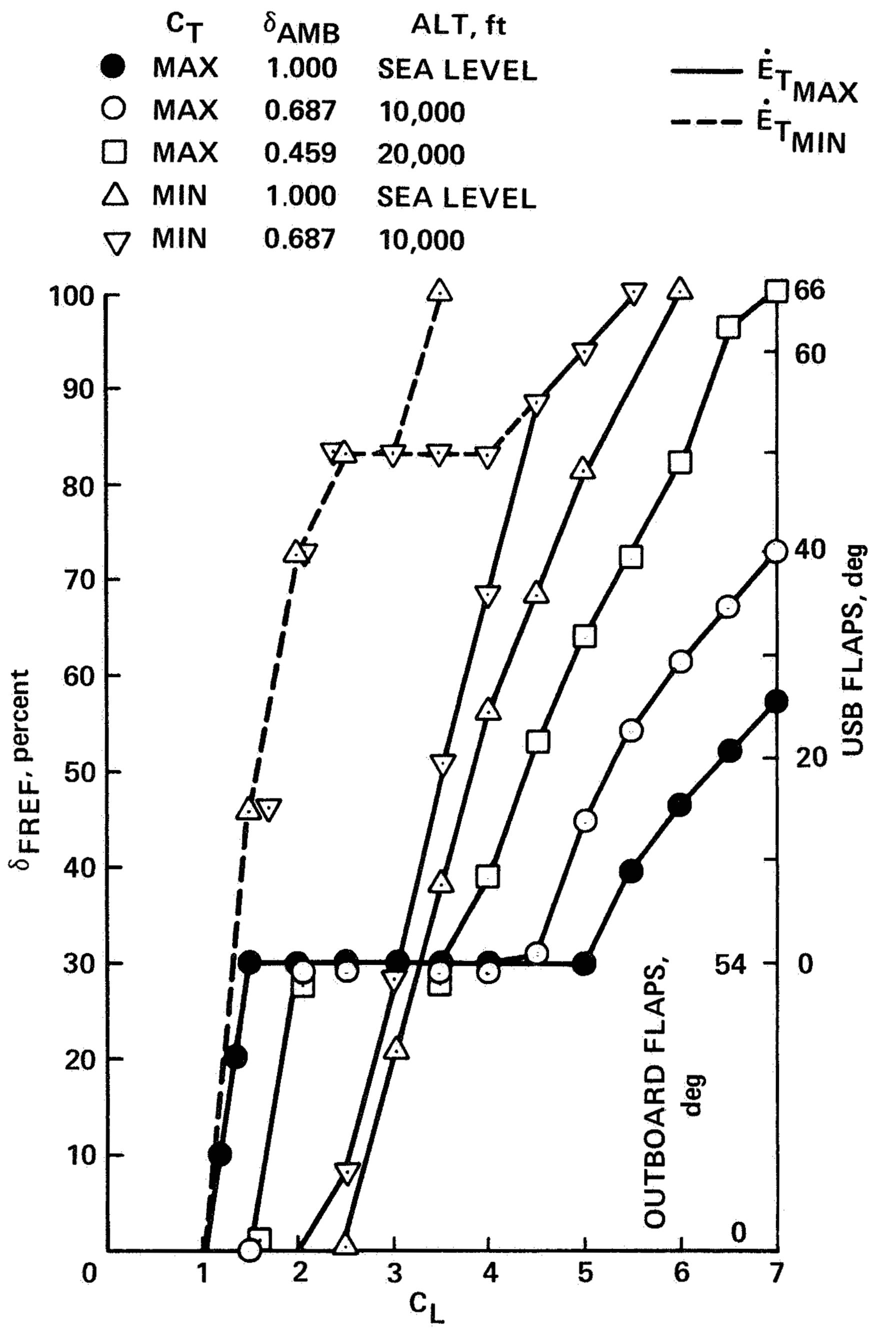

(c) Flap setting (δ_{FREF}) versus lift coefficient (C_L).

Figure A4.- Continued.

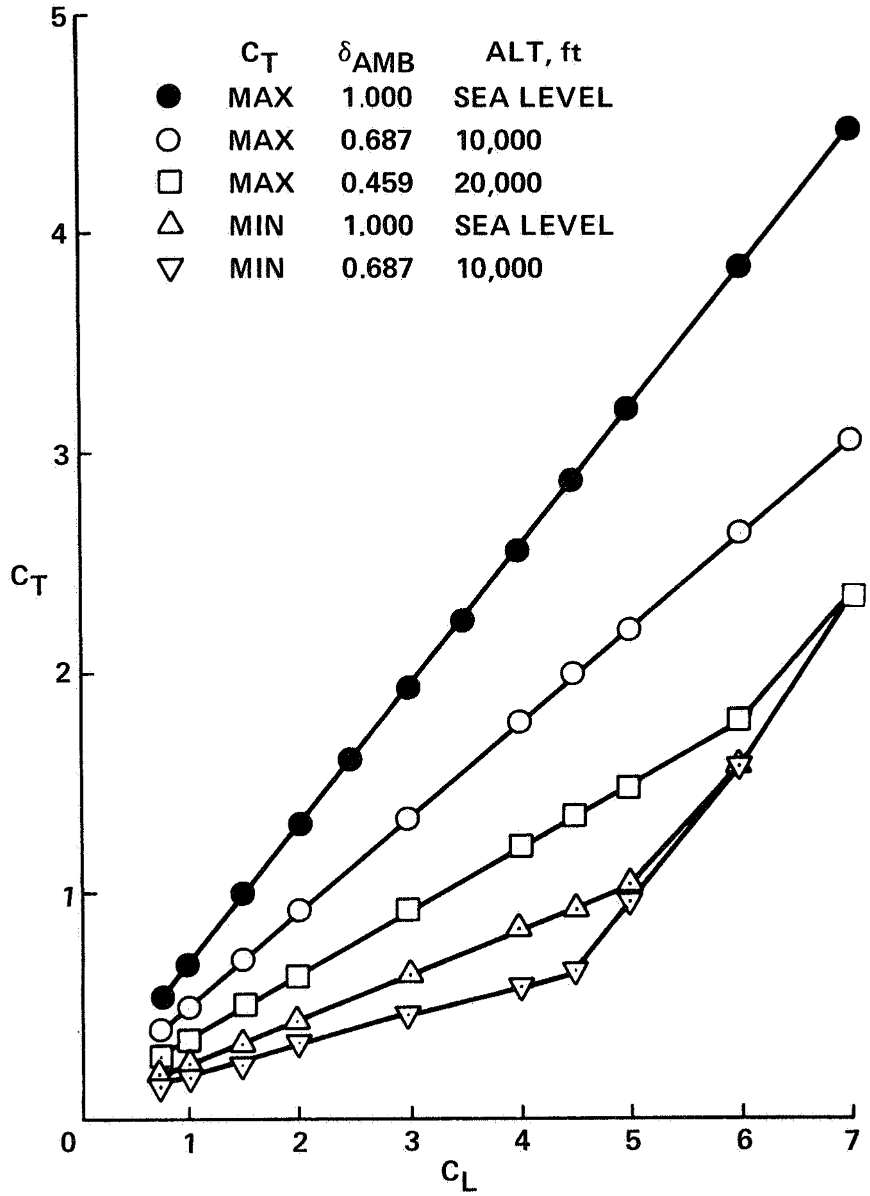

(d) Thrust coefficient (C_T) versus lift coefficient (C_L).

Figure A4.- Concluded.

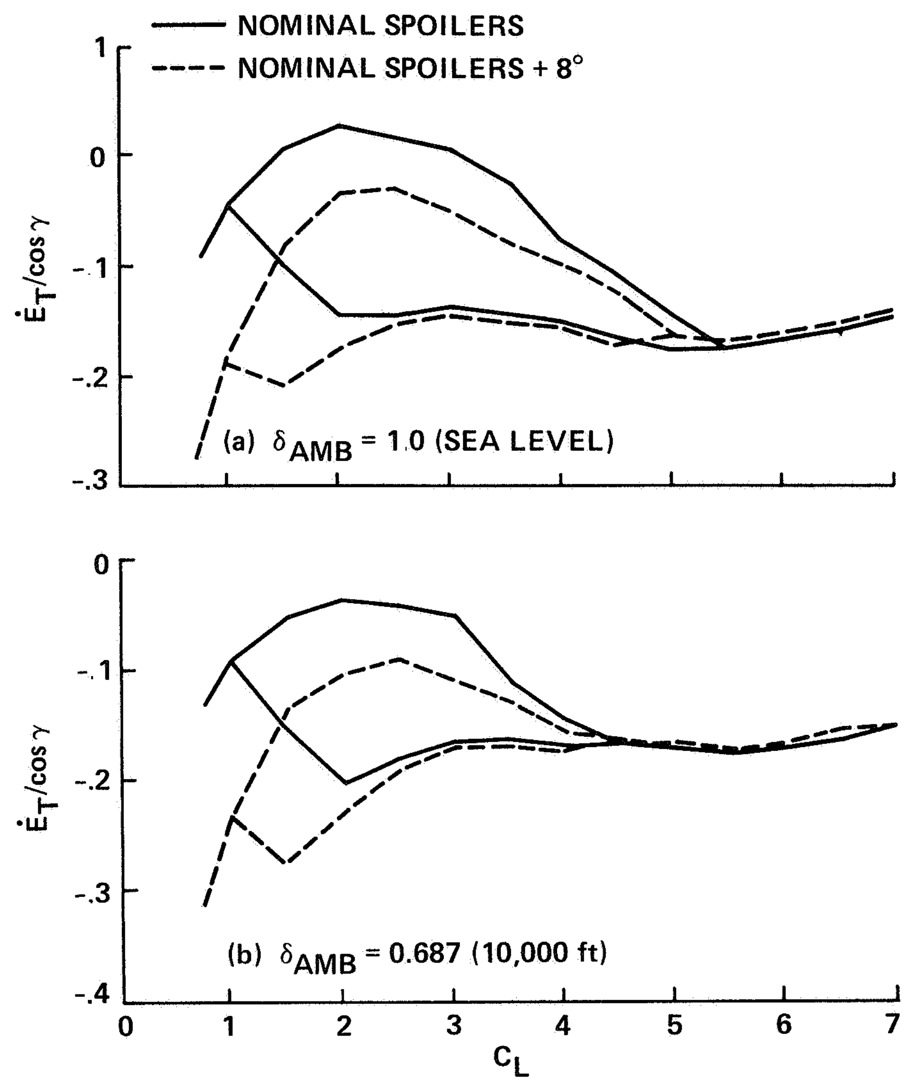

Figure A5.- Effects of spoilers on minimum total energy rate ($\dot{E}_T$) for low values of lift coefficient (C_L). (a) δ_{AMB} = 1.0 (sea level); (b) δ_{AMB} = 0.687 (10,000 ft).

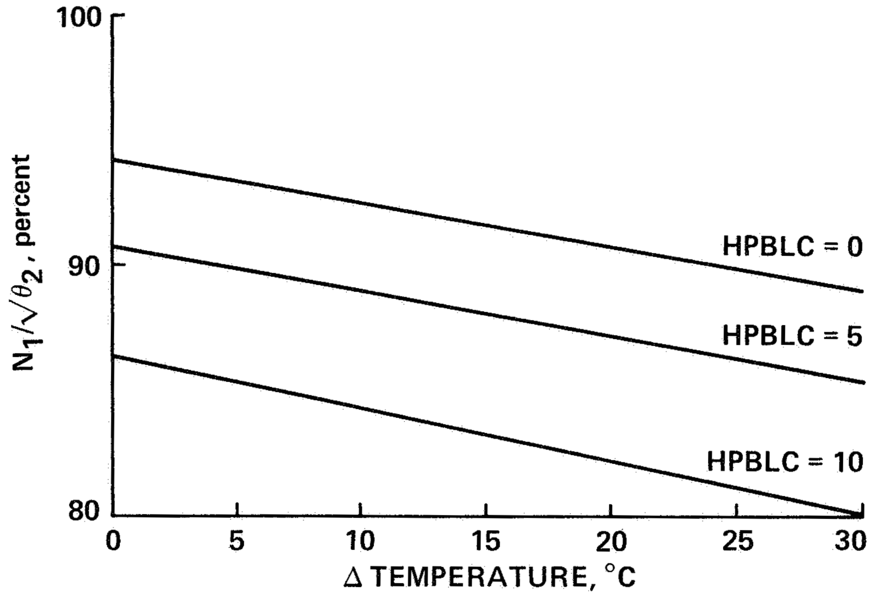

Figure A6.- Corrected engine fan speed ($N_1/\sqrt{\theta_2}$) for exhaust gas temperature (MGT) of 920° C versus temperature change (ΔT).

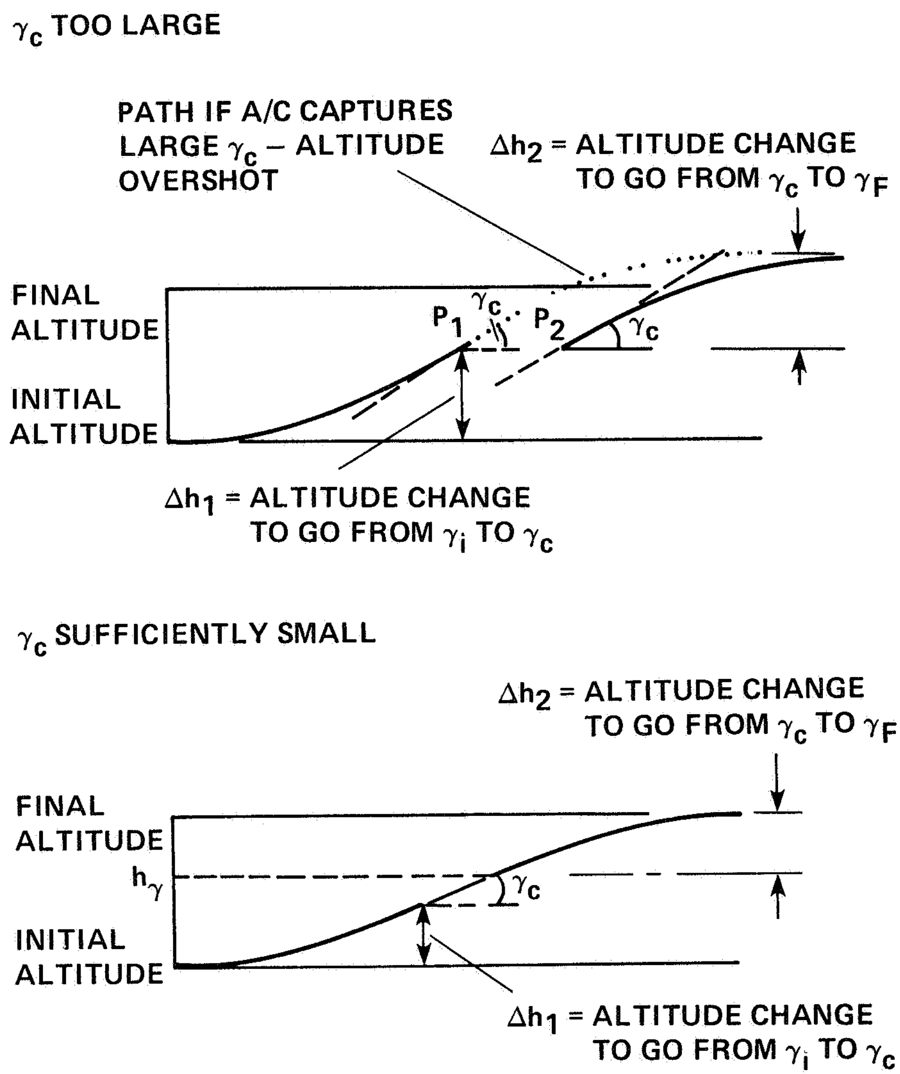

Figure B1.- Closed-form solutions illustration.

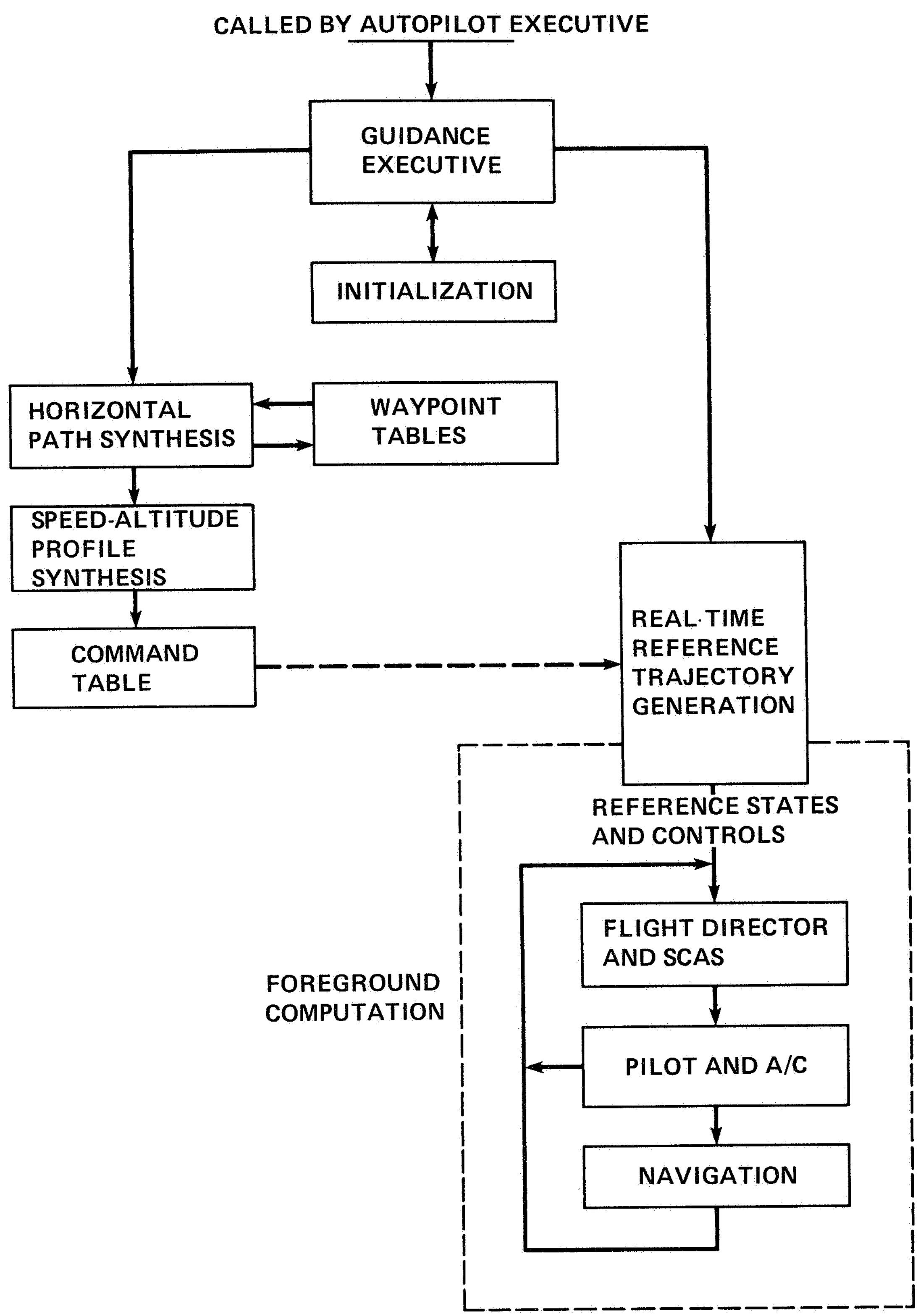

Figure C1.- QSRA ECG guidance system.

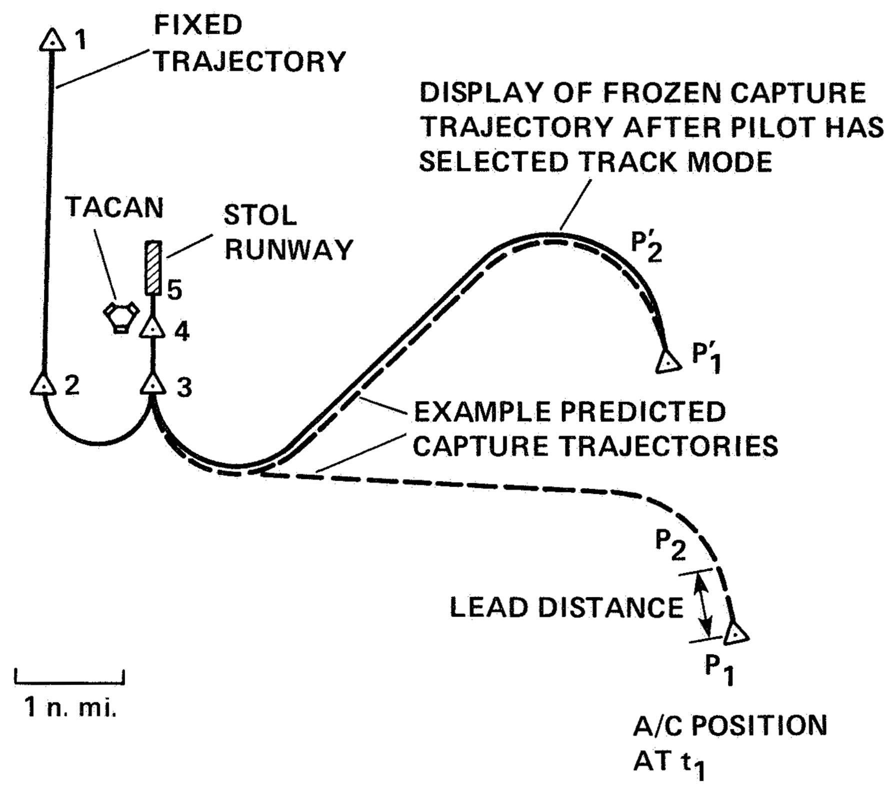

Figure C2.- Horizontal flightpaths displayed on cockpit map display.

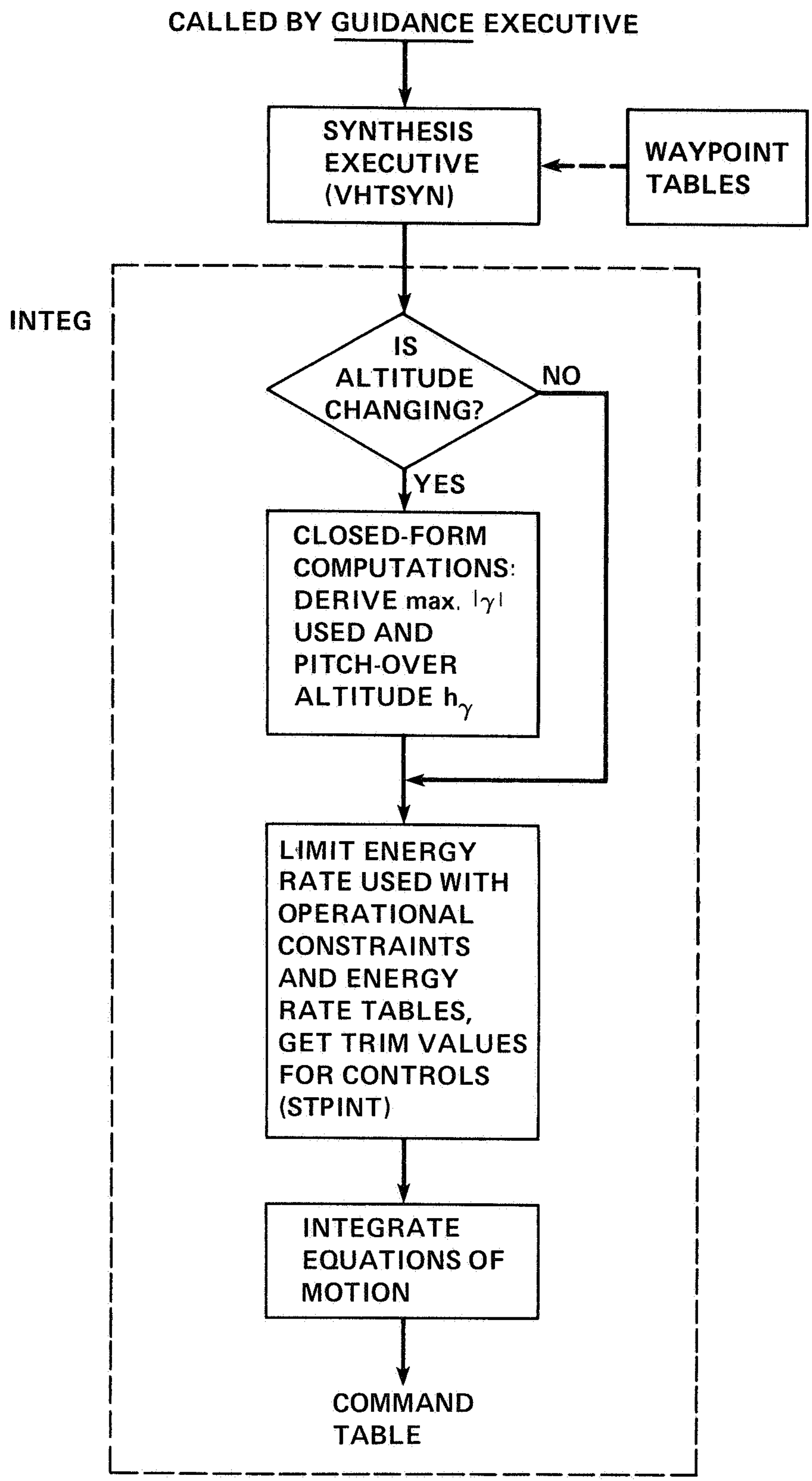

Figure C3.- Speed-altitude profile synthesis.

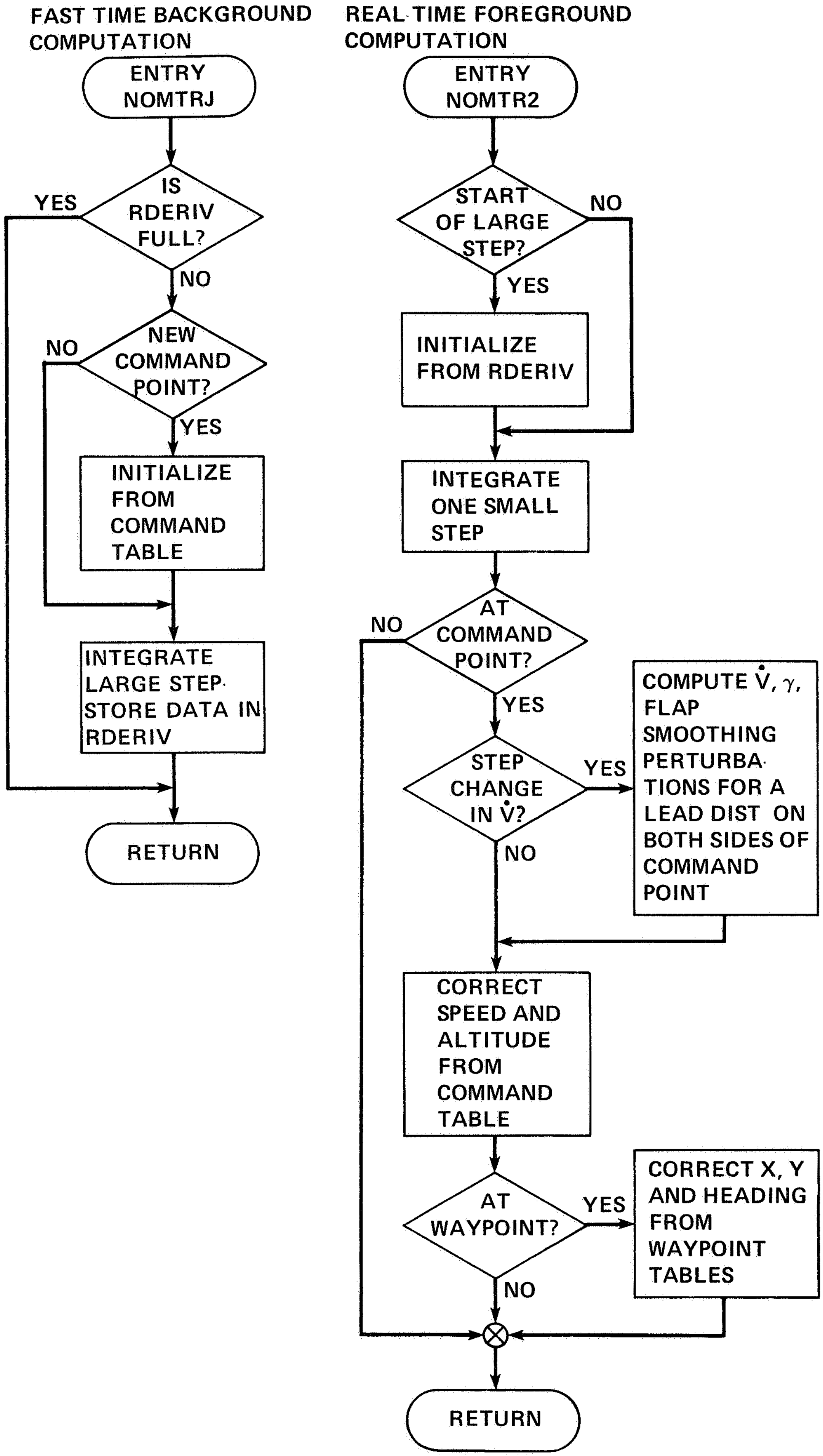

Figure C4.- Real-time reference generation.

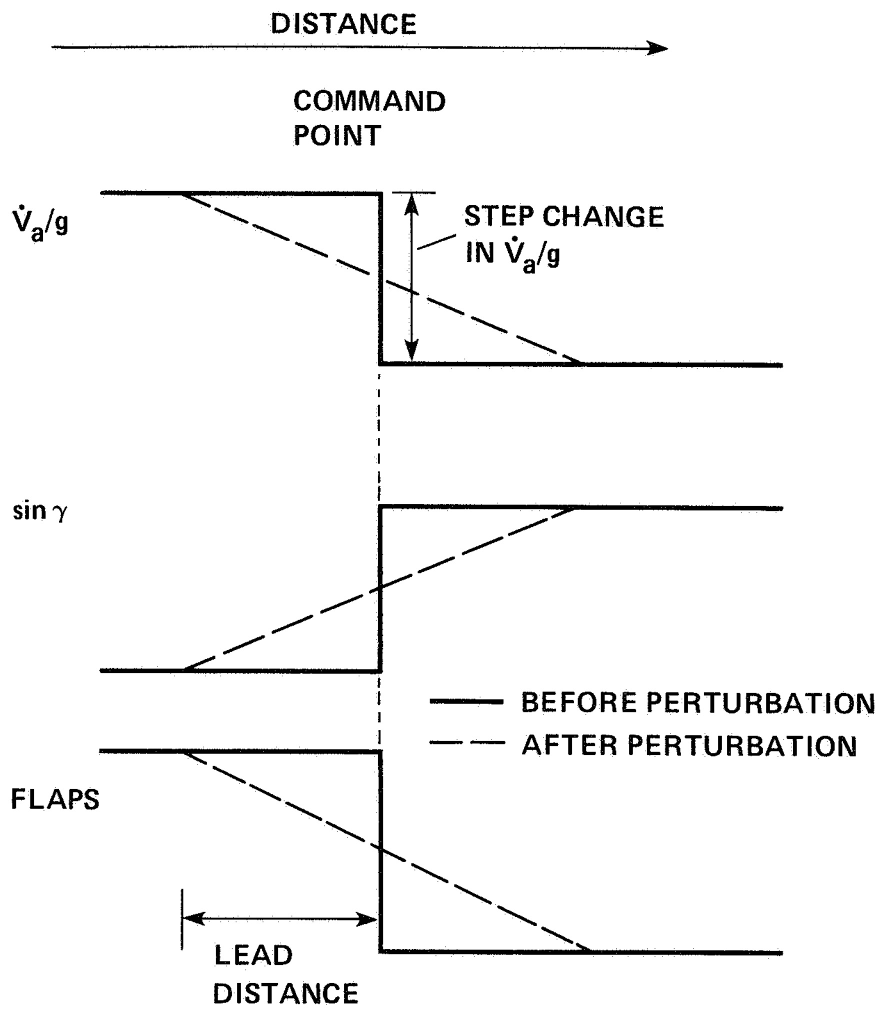

Figure C5.- Perturbations in $\dot{V}_a/g$, γ, and flaps resulting from step changes in $\dot{V}_a/g$.

1. Report No.	2. Government Accession No.	3. Recipient's Catalog No.
NASA TM-85971		

4. Title and Subtitle

FUEL CONSERVATIVE GUIDANCE CONCEPT FOR SHIPBOARD LANDING OF POWERED-LIFT AIRCRAFT

5. Report Date

July 1984

6. Performing Organization Code

7. Author(s)

David N. Warner, Jr. and Leonard A. McGee (Ames Research Center), and John D. McLean and Gregory K. Schmidt (Analytical Mechanics Associates, Inc., Mountain View, Calif.)

8. Performing Organization Report No.

A-9783

9. Performing Organization Name and Address

Ames Research Center
Moffett Field, CA 94035

10. Work Unit No.

T-3309

11. Contract or Grant No.

12. Sponsoring Agency Name and Address

National Aeronautics and Space Administration
Washington, DC 20546

13. Type of Report and Period Covered

Technical Memorandum

14. Sponsoring Agency Code

532-01-11

15. Supplementary Notes

Point of Contact: David N Warner, Jr., Ames Research Center, MS 210-9, Ames Research Center, Moffett Field, CA 94035 (415) 965-5443 or FTS 448-5443

16. Abstract

A simulation study was undertaken to investigate the application of Energy Conservative Guidance (ECG) software, developed at NASA Ames Research Center, to improve the time and fuel efficiency of powered-lift airplanes operating from aircraft carriers at sea. The ECG software system consists of a set of algorithms whose coefficients and parameter limits are those of the Quiet Short-Haul Research Aircraft (QSRA) When a flightpath is indicated by a set of initial conditions for the aircraft and a set of positional waypoints with associated airspeeds, the ECG software synthesizes the necessary guidance commands to optimize fuel and time along the specified path. A major feature of the ECG system is the ability to synthesize a trajectory that will allow the aircraft to capture the specified path at any waypoint with the desired heading and airspeed from an arbitrary set of initial conditions In this study, five paths were identified and studied. The first path closely follows the manual approach procedures specified in the U S. Navy CV NATOPS MANUAL for prop and turboprop aircraft using tactical air navigation aid (TACAN) as the major area navigation aid. Each of the four remaining paths were established to successively remove the manual restrictions from the path. These paths demonstrate the ECG system's ability to save flight time and fuel by more efficiently managing the aircraft's capabilities

Results of this simulation study show that when restrictions on the approach flightpath imposed for manual operation are removed completely, fuel consumption during the approach was reduced by as much as 49% (610 lb fuel) and the time required to fly the flightpath was reduced by as much as 41% (5 min). When it is possible to remove only a portion of the operational constraints, somewhat lesser, but still significant, savings in both fuel and time were realized using the ECG synthesis software. Savings due to ECG were produced by (1) shortening the total flight time; (2) keeping the airspeed high as long as possible to minimize time spent flying in a regime in which more engine thrust is required for lift to aid the aerodynamic lift; (3) minimizing time spent flying at constant altitude at slow airspeeds; and (4) synthesizing a path from any location for a direct approach to landing without entering a holding pattern or other fixed approach path.

17. Key Words (Suggested by Author(s))	18. Distribution Statement
Guidance Aircraft Fuel conservation STOL Powered-lift	Unlimited Subject Category: 08

19. Security Classif. (of this report)	20. Security Classif. (of this page)	21. No. of Pages	22. Price*
Unclassified	Unclassified	75	A04

*For sale by the National Technical Information Service, Springfield, Virginia 22161